AN OPTIMUM RADIATION CRYOSTAT FOR INFRARED DETECTOR COOLING ON EARTH ORBITING SATELLITES

By

VICTOR JOHN ANSELMO

Bachelor of Science
University of Maryland
College Park, Maryland
1963

Master of Science
Southern Methodist University
Dallas, Texas
1966

Submitted to the Faculty of the Graduate College
of the Oklahoma State University
in partial fulfillment of the requirements
for the Degree of
DOCTOR OF PHILOSOPHY
May, 1971

AN OPTIMUM RADIATION CRYOSTAT FOR INFRARED DETECTOR COOLING ON EARTH ORBITING SATELLITES

Thesis Approved:

J. A. Weibelt
Thesis Adviser

Ronald L Panton

Jay G Porterfield

J E Bose

D Dunham
Dean of the Graduate College

PREFACE

The primary objective of this study has been the thermal design and optimization of a radiation cryostat for cooling infrared detectors on earth orbiting satellites. The development of the basic geometrical philosophy for the optimum system was established by preliminary consideration of various passive cryostat systems and later by analytic techniques. The final design and optimization consisted in the establishment of a thermal model of the cryostat which produced a set of four nonlinear algebraic equations in terms of twelve system parameters. The analytical techniques were verified by test data and the final design was supported by a digital computer grid search optimization routine. An extensive parametric sensitivity analysis was conducted which verified the optimum design parameters.

I would like to express my appreciation for the assistance and guidance given me by the members of my advisory committee: Professor John Wiebelt, my major professor and thesis advser, and Professors Ronald Panton, Jim Bose, and J. G. Porterfield.

Further, I would like to offer my thanks to Miss Velda Davis for her excellent typing and Mr. Eldon Hardy for his superior drafting work.

Last, but of most importance, I would like to express my deep appreciation to my wife, Mary Catherine, and my family whose encouragement, sacrifice, and dedication have been an invaluable contribution to the success of my studies.

TABLE OF CONTENTS

LIST OF TABLES

LIST OF FIGURES

LIST OF SYMBOLS

a	- Geometric parameter - FT (see Figure 37)
a_e	- See Figure 43a
a_{ij}	- Variable coefficients defined in Equations (7-12) to (7-17)
A_{i-i_b}	- Conduction cross section surface area - FT^2 (see Equation (7-31))
A_i	- Area of surface i - FT^2
b	- Geometric parameter - FT (see Figure 37)
c	- Geometric parameter - FT (see Figure 37)
d	- Geometric parameter - FT (see Figure 43b)
E_i	- Emissive power of surface i ($BTU/HR-FT^2$)
F_{i-j}	- Geometric shape factor from surface i to surface j (dimensionless)
$F_{i-j(k,l,\ldots,n)}$	- Geometric shape factor from surface i to surface j with a specular reflection in surfaces k, l, ..., n (dimensionless)
G_i	- Irradiation of surface i ($BTU/HR-FT^2$)
h	- Geometric parameter (inches) (see Figure 43b)
	- Geometric parameter (see Figure 1)
H	- Variable defined by Equation (A-2)
	- Enclosure height (inches)
J_i	- Radiosity of surface i ($BTU/HR-FT^2$)

k_a - Proportionality coefficient (see Equation (8-5))

k^* - Proportionality coefficient (see Equation (8-9))

K_{ij} - Thermal conductance between surfaces i and j (BTU/HR-$^\circ$F)

K_{i-i_b} - See Equation (7-31)

P_i - Parameter as defined in Equation (7-41)

q_i - Radiative energy transfer from surface i (BTU/HR)

q_{i-j} - Radiative energy transfer between radiosity nodes i and j (BTU/HR)

$q_{i,cond}$ - Conducted energy (BTU/HR)

$q_{i,misc}$ - Parametric energy input to surfaces (BTU/HR)

q_{i-i_b} - See Equation (7-31)

Q_1 - Parametric energy input to radiator (BTU/HR)

Q_2 - Parametric energy input to sides (BTU/HR)

Q_3 - Parametric energy input to reflector (BTU/HR)

$\dot{Q}_E$ - Internal heating (see Figure 2)

Q_P - Incident flux from earth (BTU/HR-FT^2)

Q_{PR} - Albedo (BTU/HR-FT^2)

Q_s - Direct solar flux (BTU/HR-FT^2)

Q_{solar} - Direct solar flux plus albedo (BTU/HR-FT^2)

Q_{IR} - Total incident infrared flux (BTU/HR-FT^2)

r_e - Earth disc radius (see Figure 43a)

r - Geometric parameter (see Figure 49)

R - Thermal resistance (HR-$^\circ$F/BTU)

- Orbit radius from earth center (see Figure 1)

T - Absolute temperature ($^\circ$R)

- Insulation thickness (inches)

x	- Geometric parameter (see Figure 43b)

Greek Symbols

A_O	- Orbit altitude above earth (see Figure 49)
α	- Absorptance (dimensionless)
β	- Reflector angle (degrees)
β_{A_O}	- See Figure 43
ρ	- Reflectance (dimensionless)
	- Earth radius (see Figure 1)
τ	- Current time (hours)
τ_o	- Orbital period (hours)

Subscripts

B	- See Figure 1
e	- Refers to earth
IR	- Infrared spectrum
O	- Open side of enclosure
S	- Solar spectrum

CHAPTER I

INTRODUCTION

The development of infrared sensing detectors has accelerated in recent years. The unlimited potential of these devices for the purpose of earth resources and planetary exploration, meterology, and astronomical exploration has only begun to be realized. One problem that concerns a large percentage of these detectors is the requirement of very low operating temperatures. Three potential methods are available to the thermal designer to provide this necessary cooling during a space mission. First, a cryogen can be stored in dewars which serve the purpose of a heat sink. Second, active cooling devices, such as the mechanical cryostats, are available and are able to operate to very low temperatures, and finally a radiating device can be used to radiate energy to space and provide the necessary cooling.

If one considers some of the disadvantages of the first two methods, such as reliability, weight and operating life, the radiant cooling becomes an immediately-favored design. It is the purpose of this study to design such a passive cooling system for an earth-orbiting satellite, and to optimize this design.

CHAPTER II

LITERATURE SEARCH

Very little work has been done in the study of radiation cryostats. The works that have been published have proposed methods for obtaining cryogenic temperatures in thermally, non-severe orbits (1, 2). Both works have considered orbits in the ecliptic.

The publication of Fuschillo, Schultz and Gibson (1) considered three basic designs. The first was a cylinder of height h and radius r. The orbit of the cylinder was in the plane of the ecliptic and its axis was normal to its orbital plane. This situation is described in Figure 1.

Two thermal coating systems were considered for this cylinder. The first had a high emittance (absorptance) value for the top and bottom (ϵ_B, α_B) and low values for the sides (ϵ_W, α_W). The second utilized low α/ϵ values for the top and the bottom, (α_B/ϵ_B), and low ϵ_W and α_W.

The results of this parametric study are shown in Figure 2. The temperature of the cryostat was shown to decrease with decreasing h/r and increasing distance from earth where ρ/R is the number of earth radii of the orbit from the center of the earth. This decrease levels out at $\rho/R = 0.1$. A comparison at $\rho/R = 0.1$ was made between the $\alpha_B/\epsilon_B = 0.16/0.95$ and the $\alpha_B/\epsilon_B = 0.90/0.90$ cases which indicated an

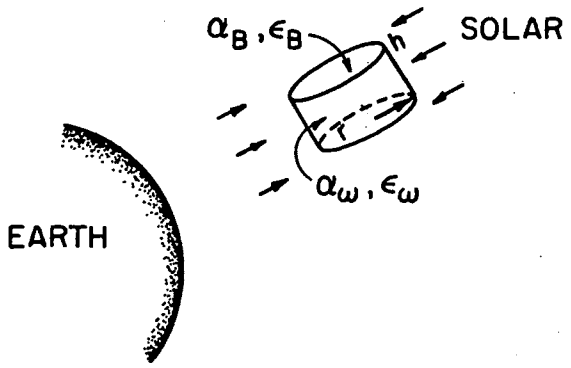

Figure 1. Cryostat Orbital Operation

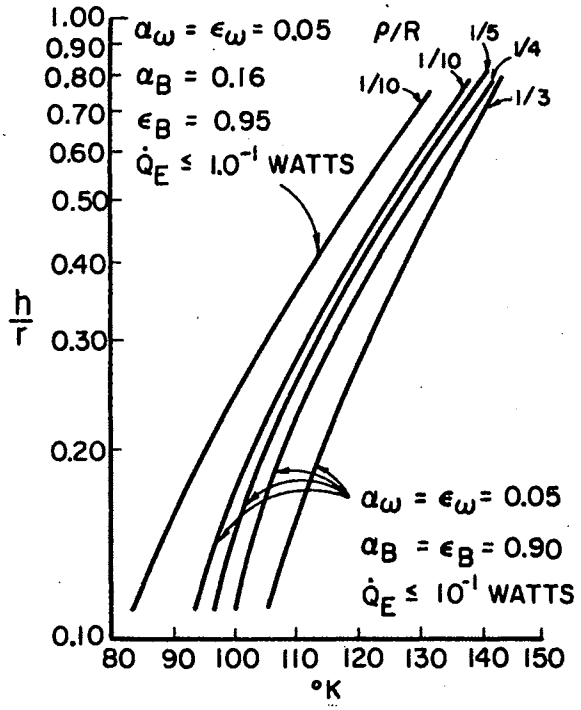

Figure 2. Cylinder Thermal Analysis

effective decrease in the cryostat temperature by using low values of α/ϵ. Internal power dissipation was shown to be less than 0.1 watt.

The second design considered is shown in Figure 3. It consisted of a circular disk within a toroid. The purpose of the toroid is to shield the disk from its environmental energy inputs, the earth and sun. The energy absorbed by the toroid on its side is re-radiated out of both the top and the sides of the toroid. The energy input to the disk consists of that received from the inner walls of the toroid, as well as through conduction from the toroid. In the analysis, the conductive inputs were neglected since it was believed that they could be practically limited to negligible quantities.

A design procedure was established for sizing the toroid and a parametric analysis was performed assuming a toroid temperature of 540° R and a circular orbit in the ecliptic of 12,000 statute miles. Using a disk internal power generation of 10 watts, the resulting calculated disk temperature was 275° R. For zero watts dissipation, the disk temperature was 225° R.

The third design which was considered was an adaptation of the toroid design. It is shown in Figure 4. An outer toroid structure is added to the design which serves the purpose of a thermal shield to the disk. The analysis of this design assumed that the outer toroid temperature was 540° R; the inner toroid was at 180° R, and the resulting calculated disk temperature was at 63° R. This assumed an internal power generation of less than one milliwatt, and an orbit of $\rho/R = 0.1$.

The thermal surface parameters were low ϵ_W, α_W and α_B/ϵ_B. The disk radius was 20 cm, but its height was not given.

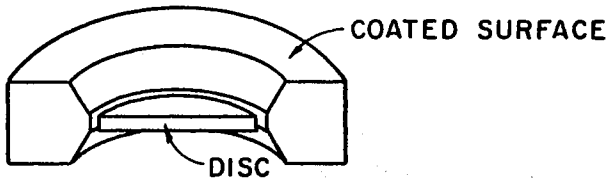

Figure 3. Disc-Toroid Cryostat

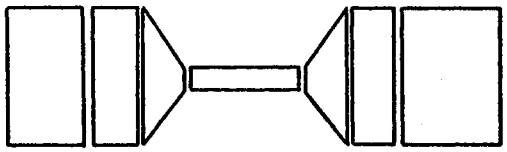

Figure 4. Double Toroid-Disc Cryostat

The second and most recently published work on radiation cryostats by Annable (2), January 1970, presents an approach to the design of radiant cooling in an earth ecliptic orbit. The approach is based on a highly specular cone channel to direct energy emission from a black patch (radiator) to space. The basic design is shown in Figure 5. The radiator is contained in an enclosure whose outward sloping, specularly reflecting and low ε walls were designed so that space is the only external source seen by the radiator. The cone, thereby, acts as a collimator for radiator emission.

The radiator is thermally attached to the cone walls and to space. The temperature of the cone is controlled by the low (α/ε) walls of the cone end which is thermally connected to the cone. This cone end is used to offset the high temperatures which would result from a relatively high (α/ε) surface exposed to solar inputs.

The cone is insulated from the spacecraft. In Figure 5 the cone is shown inserted into the spacecraft external lines. Thermal analysis was made assuming a typical Nimbus E orbit for 900 statute miles and using a 17.6 sq. cm. radiator area. The conductive heat input to the cone of 1,000 sq. cm. area was .165 watt. The resulting calculated cone temperature was 331° R. If the conductive input to the cone is reduced to zero, the calculated cone temperature would be 277° R. The radiator was thermally connected to the cone with the conductance of 9×10^{-5} watts per degree R, and assuming a Joule heat to the detector of 3×10^{-3} watts, the resulting radiator temperature was 331° R. The effective radiator cone emissivity of 0.0277 was used for this analysis.

Some radiant cooling devices are presently used in space. The high resolution IR radiometer (HRIR) flown on Nimbus I, II, and III contains

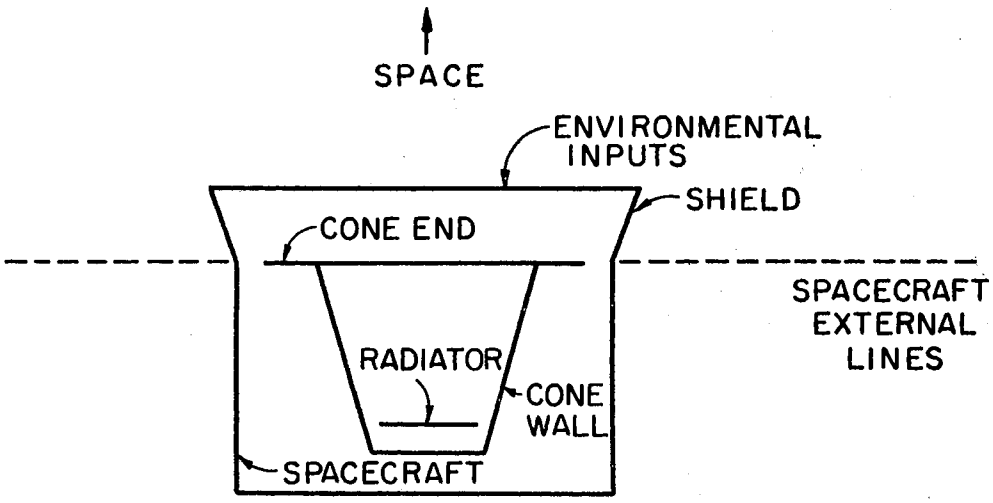

Figure 5. Cone Cryostat

a simple conical cooler that maintains a PbSe element at 360° R (3, 4). A filter wedge spectrometer designed for use on Nimbus D also contains a conical cooler designed to operate a PbSe element at 315° R (5, 6).

A feasibility model for very high resolution radiometer for the improved TOS spacecraft is designed to cool a HgCdTe detector to 153° R for a 1,100 km. orbit. This design proposes the use of a cone within a cone design.

Annable (2) points out in conclusion that specular reflection modeling techniques may be used with success in design, and that conical radiant cooling devices are useful for high altitude thermally, non-severe orbits such as a surface that is parallel to the orbital plane when the orbit is in the ecliptic.

Since the passive thermal control of a satellite system is totally dependent on the thermal radiation properties of the exterior surfaces, some consideration should be given to the important literature in this area.

Two reports that are basic in their considerations are presented by Christensen (7) and Greenberg (8).

Christensen discusses at length some of the past problems associated with thermal control in space, and establishes some basic requirements to thermal design in space. A year later, Greenberg presented the results of his investigations of second-generation thermal control surfaces and coatings. Of primary importance was the development of OSR, optical solar reflector, which is comprised of a fused silica substrate coated with silver. The silica surface is directly exposed to the incident irradiation. The silica transmits the solar energy which is 95%+ reflected by the silver surface. About 30 per

cent of the infrared energy is reflected by the silica and 70 per cent is absorbed. The infrared emittance is also about 70 per cent. Consequently OSR exhibits a low absorptance of solar spectrum energy and a high infrared emittance. This low α/ϵ ratio allows a room temperature or lower environment in direct solar irradiation. The data presented by Greenberg indicates that tailoring of the optical properties is possible for a wide range of thermal control experiments, and therefore, is a most valuable tool for space thermal design.

CHAPTER III

STATEMENT OF THE PROBLEM

This research project was initiated in order to design an optimized radiation cryostat for use on earth-orbiting satellites. This cryostat was to have a long life, high reliability, low weight and require no power. These requirements would allow indefinite time span missions and allow continuous scanning over the earth's surface for purposes of weather detection, agricultural surveying, military reconnaissance and numerous other missions.

Simple radiating devices and louver systems which may be used in non-severe thermal environments are presently available. It was the goal of this task to provide a system for the relatively severe thermal environment. This included consideration of a polar orbiting satellite at a minimum altitude with a radiating surface area that would be in a position to see direct solar irradiation for at least 50 per cent of its orbital period. The relative dimensions of the cryostat system should be optimized, as well as the thermal properties of the surfaces involved.

The design consisted of a preliminary study to define an approach to the optimum system, an orbit altitude definition, and finally, an optimization of the geometrical and thermal parameters.

CHAPTER IV

PRELIMINARY DESIGN CONSIDERATIONS

Initial consideration was given to a one-dimensional system as shown in Figure 6. This system consisted of a multilayer superinsulation base, one side of which was connected to a room temperature satellite. The other side was connected to an infrared detector, and finally to some cold plate or radiator which emits to space. The only heat inputs considered were the Joule dissipation by the detector, and that originating from the satellite.

The objectives of this simple model analysis were to determine the importance of the following effects:

1. The surface area required of the radiator.
2. The effective temperature of space.
3. The values of the thermal conductances between the satellite and the detector, and between the detector and the radiator.

The results of this study are shown in Figure 7 and indicate that with the equivalent of one inch of multilayer insulation, it would be possible to reach temperatures as low as 100° R with a radiator of one square foot area. It was further determined that if radiator temperatures as low as 100° R were considered, the effective temperature of space may vary between 0° R to 20° R without significant effect on the radiator temperature. This variation in effective space temperature is well above that reported in the literature. Finally, it was noted that

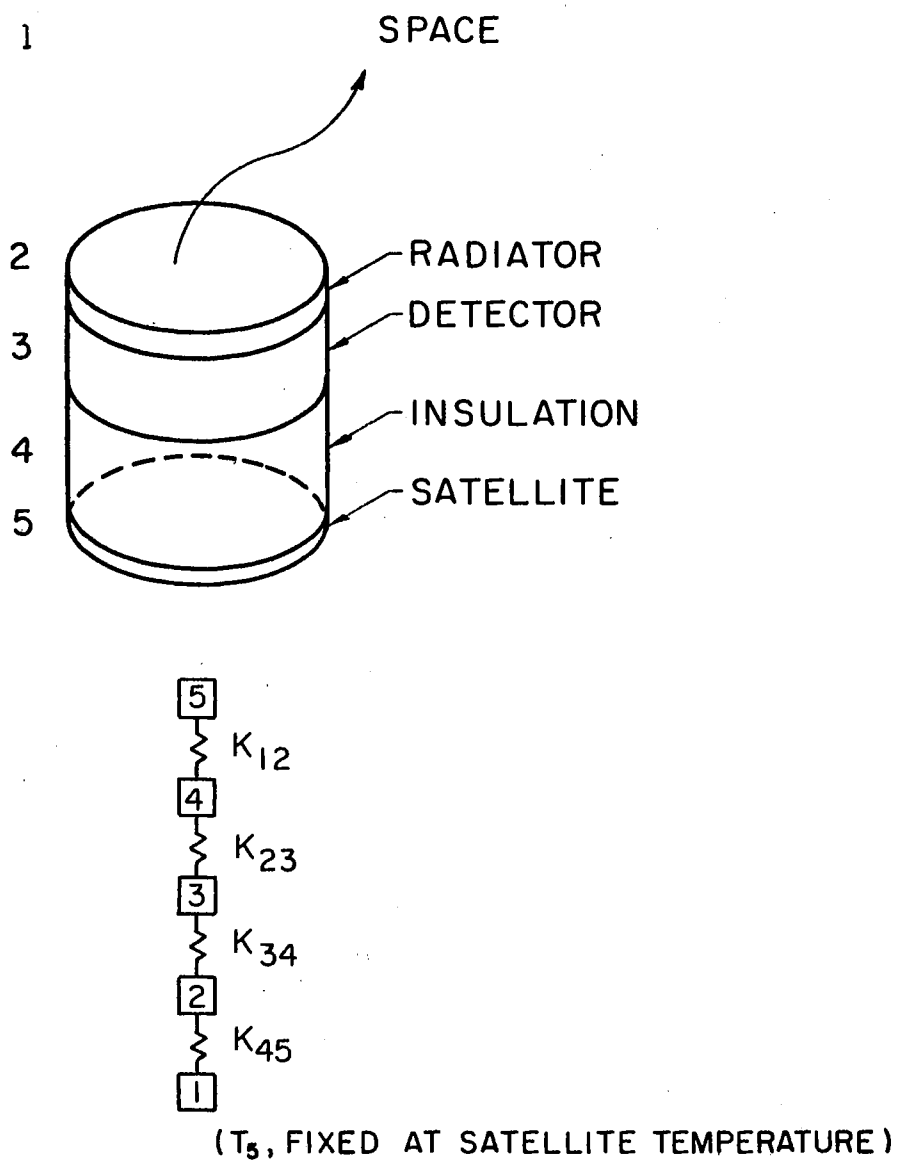

Figure 6. Thermal Model for Preliminary Study

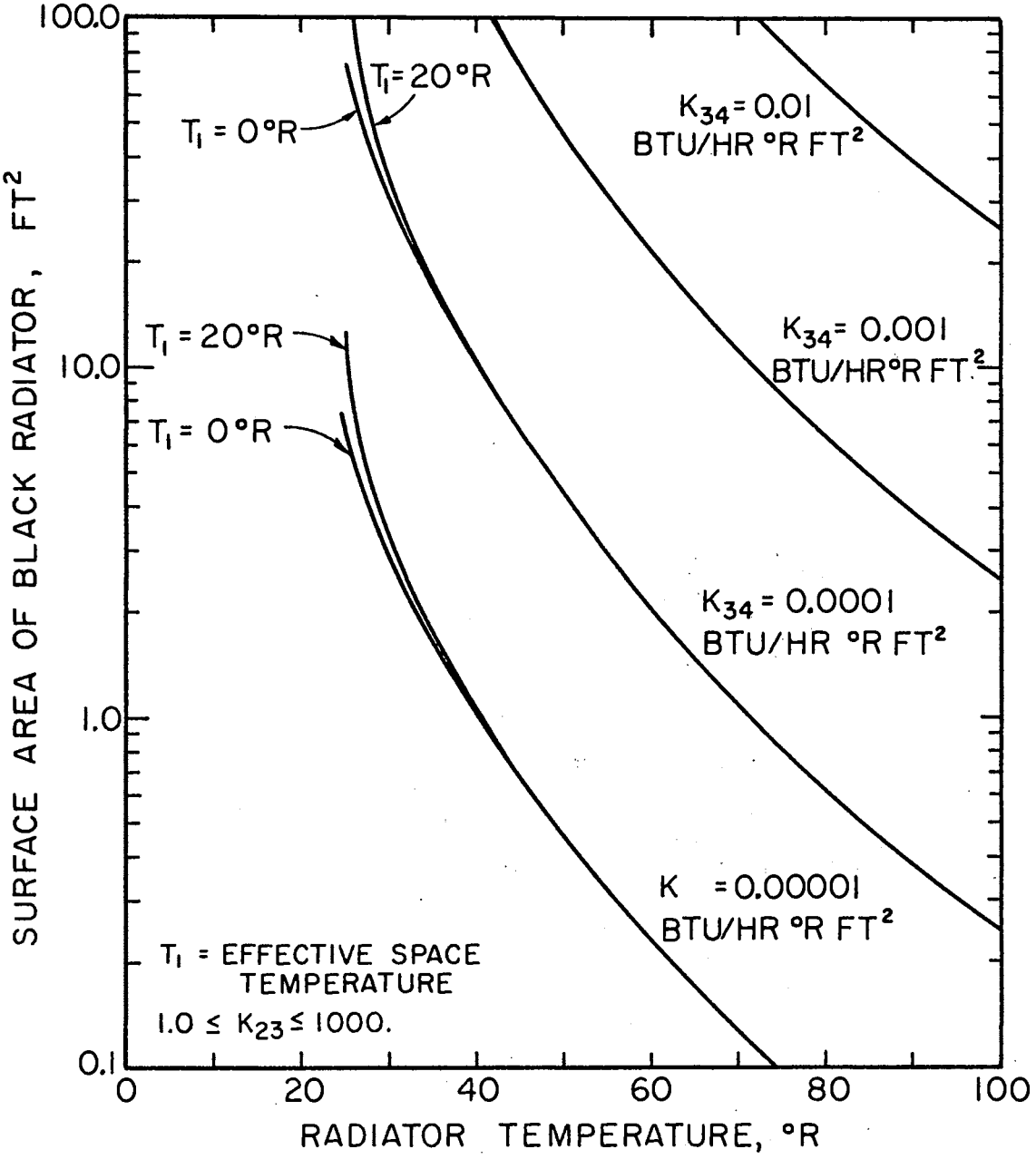

Figure 7. Thermal Analysis for Simplified Cryostat System

with as little as one inch of multilayer insulation between the satellite and the detector, the thermal conductance between the detector and the radiator could be as low as 1 BTU/HR-$^{\circ}$ R. This is based on a cross-sectional area of one square foot and does not affect an important increase in the detector temperature. This magnitude of conductance would be typical of an insulator and, consequently, there should be no problems in thermally connecting the radiator and the detector.

Because of these points, the following simplifications were assumed for the remainder of the analysis:

1. The effective temperature of space was assumed to be absolute zero.
2. The presence of the detector, as well as its temperature, was assumed to be equivalent to that of the radiator.
3. A reasonable thermal connection was made with a relatively warm satellite to insure proper thermal isolation of the detector and radiator from the satellite.

A more definite type of conducting scheme between the radiator and the satellite was then proposed. The scheme is shown in Figure 8. It consists of a series of thin aluminum foil cups, separated by dexiglas insulators. This scheme would allow the energy which would be conducted from the satellite to be short-circuited away from the radiator to a separate heat leak radiator that could operate at a slightly higher temperature. A radiator system, as shown in Figure 9, was then considered. This shielding system was arranged such that it would be just large enough to avoid any input to the radiator directly from the earth. It was further assumed that the spacecraft could be rotated around the spacecraft-earth axis such that the sun would never strike the radiator surface. With these assumptions, the shield would be irradiated by

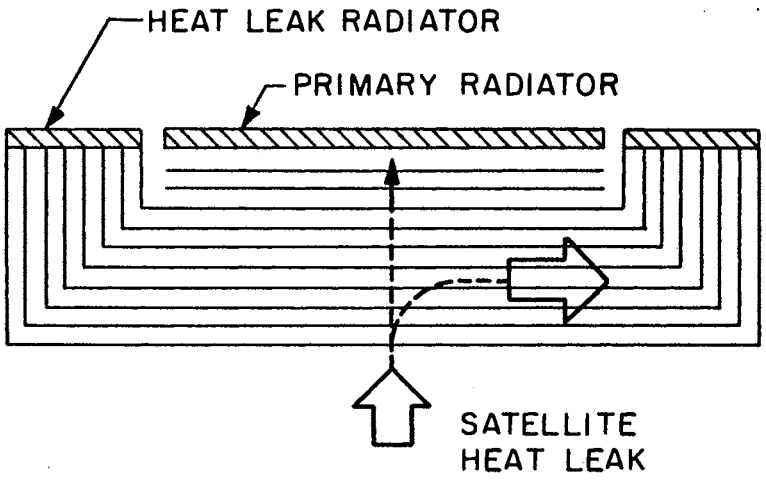

Figure 8. Radiator Insulating Scheme

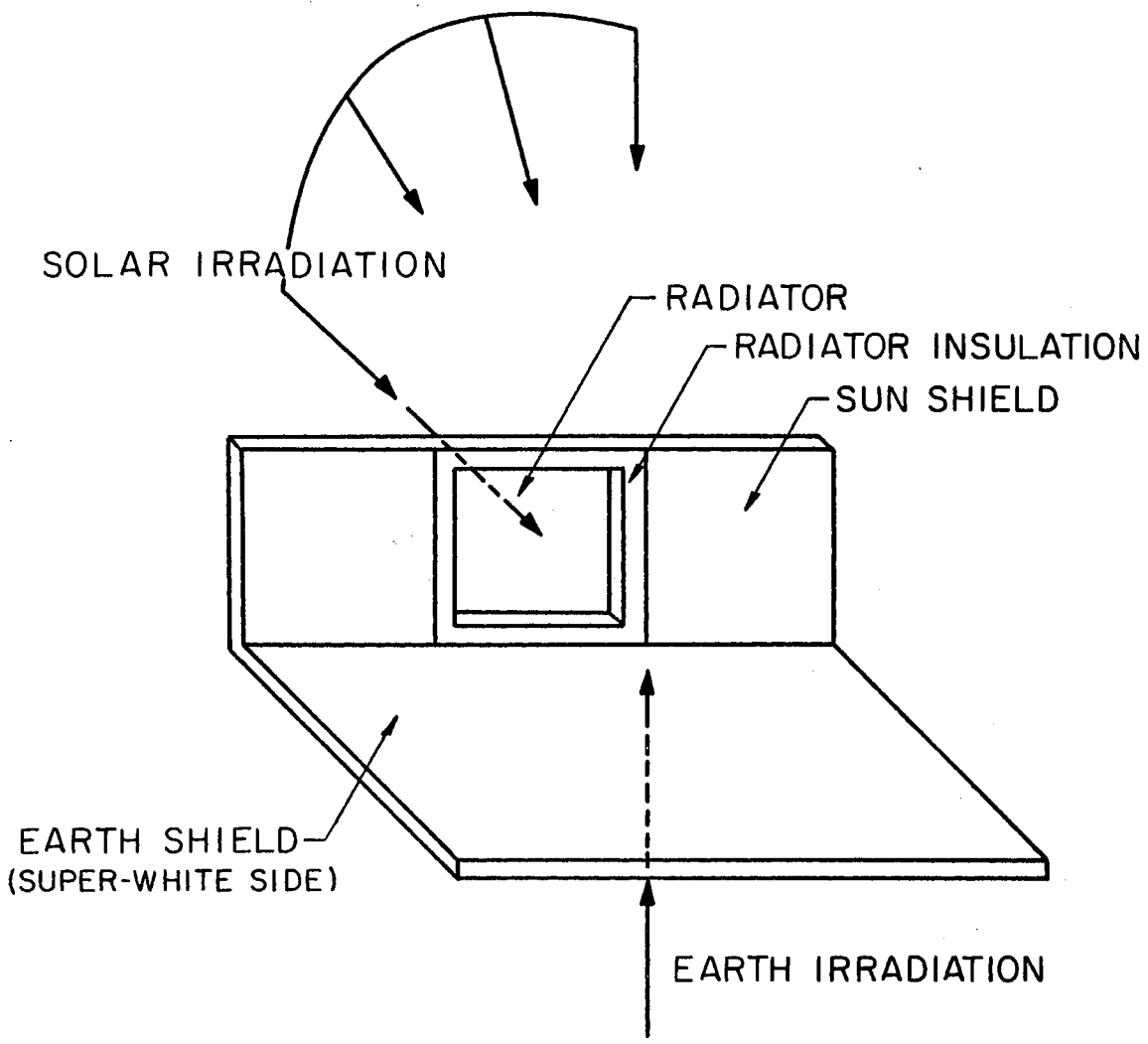

Figure 9. Earth Shield Configuration

energy from the earth emission or earth albedo on the bottom and would be irradiated on top by the sun with varying intensity, depending on the location of the spacecraft in orbit. The two vertical shields next to the radiator surface would see a portion of the earth's albedo, but would not see the sun at any time. These two vertical shields were assumed to be insulated on the back.

After this system was formulated, the necessary input parameters for a transient heat transfer analysis were determined. The radiator surface was assumed to be insulated with two inches of the multilayer superinsulation wrapped around the radiator surface in a manner which allows the short circuiting of energy from the spacecraft, as previously described in Figure 9. The energy input to the radiator consisted of energy by conduction from a 520° R spacecraft through two inches of superinsulation and radiant energy input from this shield which would be warmed by the sun. This energy would be lost from the radiator by radiation to space in approximately one-half of the total solid angle over the radiating plate. A 300 statute mile circular orbit was considered.

The results of this analysis are shown in Figure 10. After the spacecraft goes through about six revolutions, the radiator plate has reached an equilibrium temperature of approximately 210° R. The value of this temperature is dependent upon the radiating surface properties of the earth's shield, both top and bottom. The results shown herein assumed that the earth's shield has the aluminum side of an aluminum-coated mylar superinsulation for the bottom and an O.S.R. coating on the top. This particular set of surface properties may not be the optimum set, but was the first try for the described model. From this

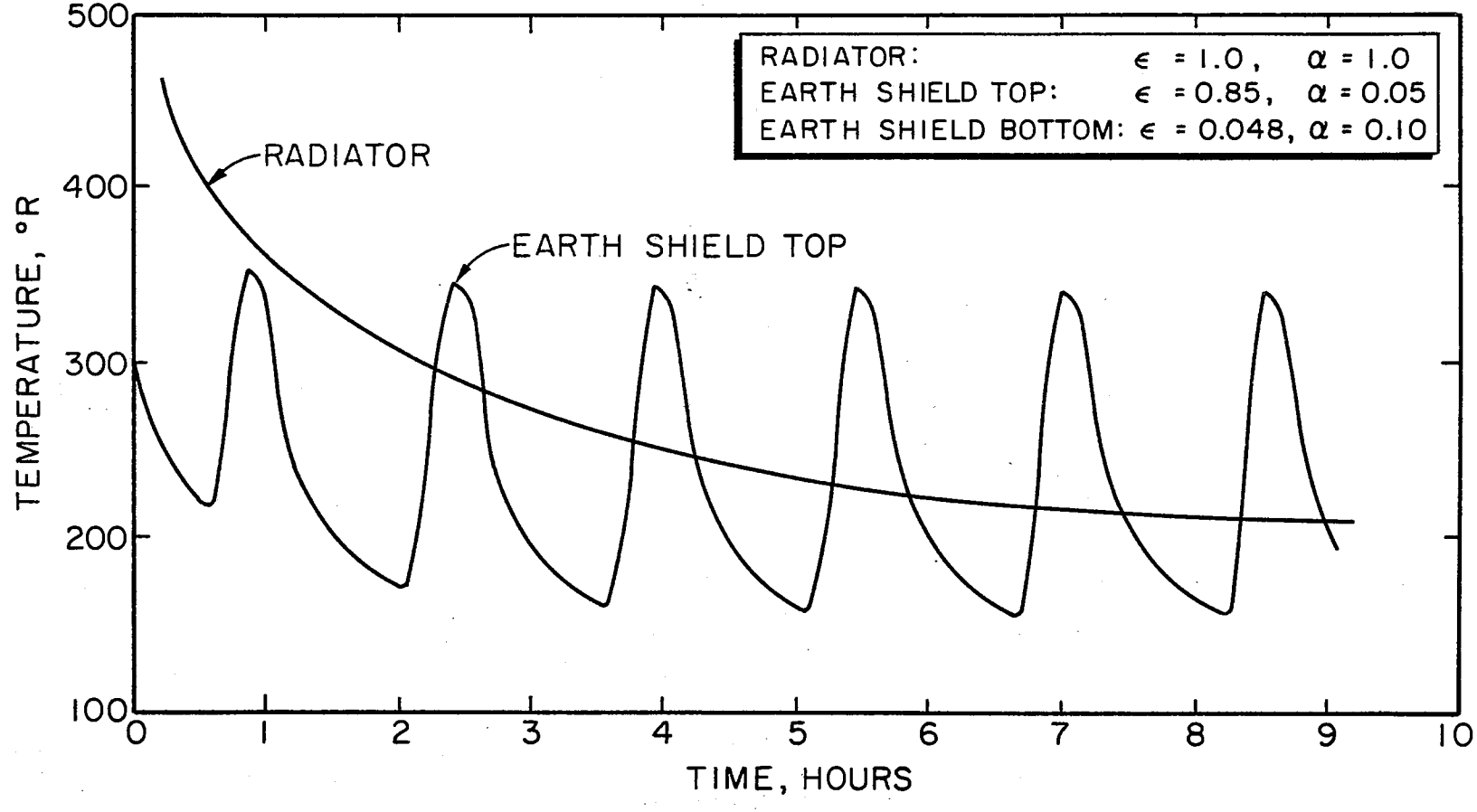

Figure 10. Radiator Performance

initial analysis, it can be seen that a temperature for the radiator of approximately 200° R is certainly a feasible value for the cryostat temperature. Although this is not an extremely low temperature for detector work, the value of 200° R would be useful with HgCdTe or other photoconductive type detectors. These detectors have a very good D* and are suitable for use in general earth resources surveying for the 10μ atmospheric window. They may also be tailored to meet wavelength requirements. In order to obtain lower temperatures, it will be necessary to eliminate the solar input to the top of the earth's shield.

Some perturbations in the design study were then conducted in order to find a means of reducing the radiator temperature of 210° R. These perturbations consisted in varying certain surface radiation properties and in reducing the satellite temperature from 520° R to 400° R. The results of these perturbations are shown in Figures 11 through 14.

None of the perturbations resulted in a serious decrease in the radiator temperature when considered for the ninth hour in orbit. This particular orbit time was arbitrarily chosen for a comparison point, rather than allow the solution to reach equilibrium in order to reduce the computer time for these preliminary analyses.

Figure 11 shows the results of introducing a satellite and an initial cryostat temperature distribution of 400° R through the system. The amplitude of the swing in the temperature of the earth shield top, as well as the radiator temperature is unchanged from that reported in Figure 10 at the nith hour of orbit.

Figure 12 indicates the results obtained from decreasing the emittance of the earth shield top from the value of 0.85 used in Figure 10 to a value of 0.425. This results in a slight increase in the

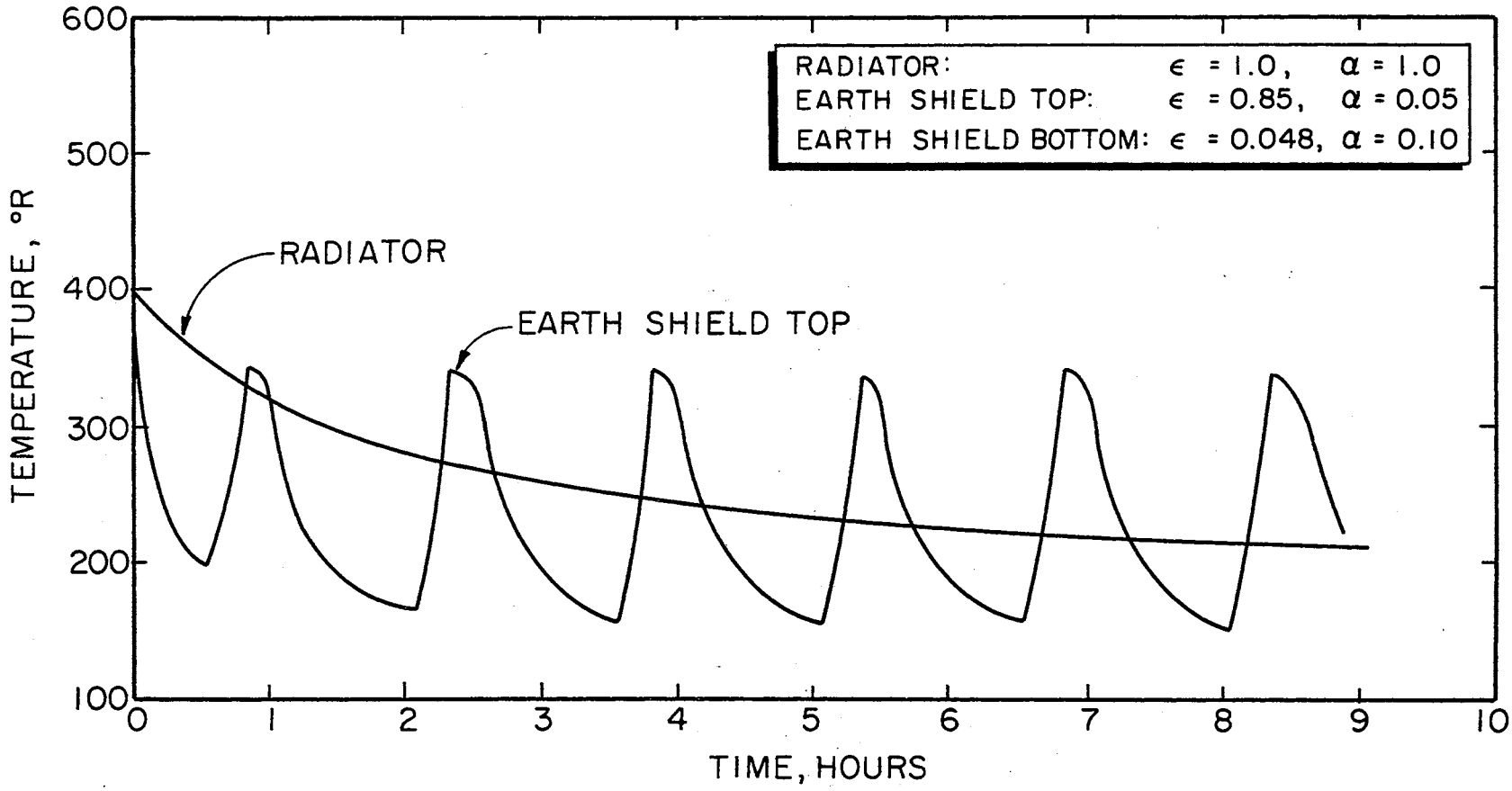

Figure 11. Radiator Performance

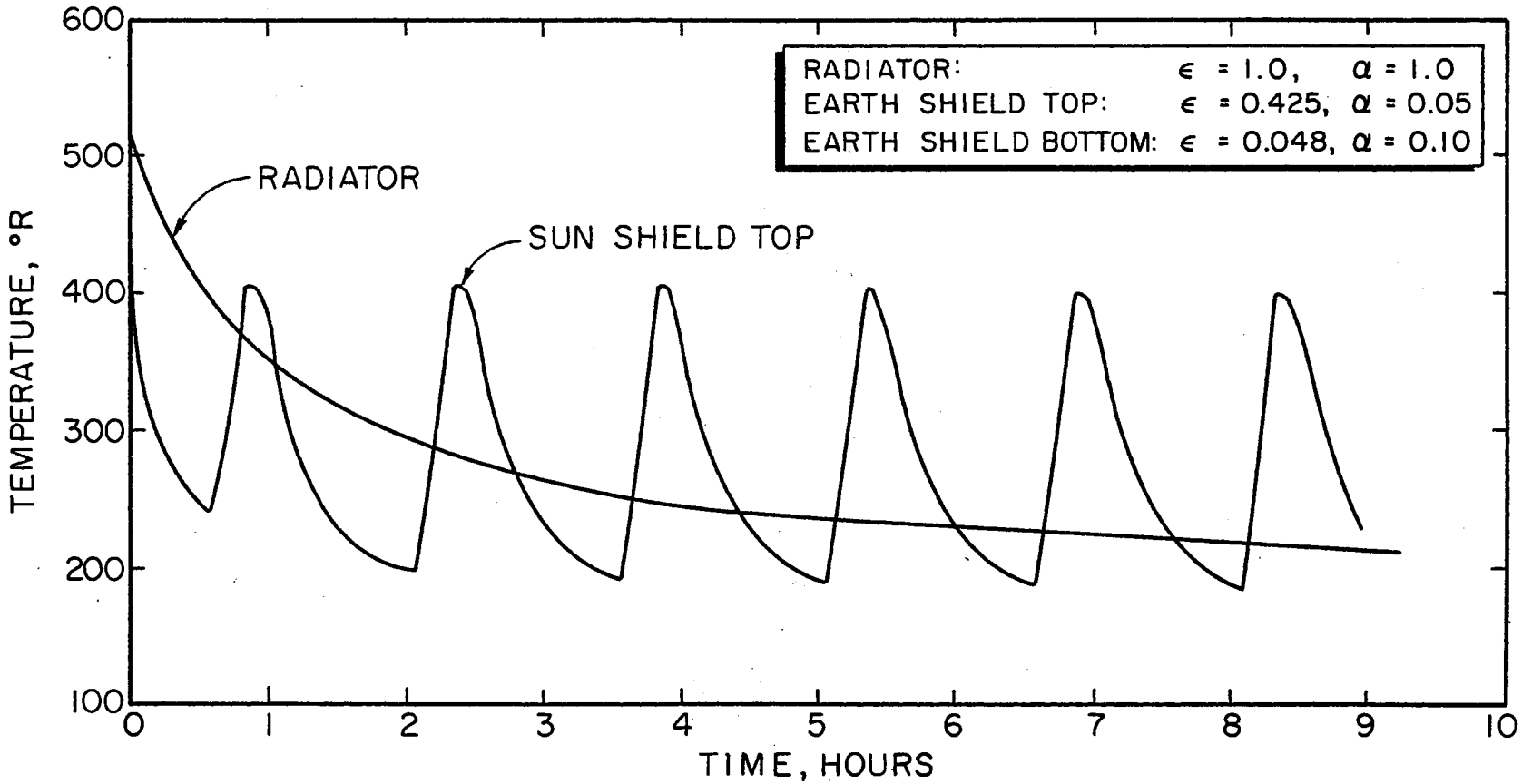

Figure 12. Radiator Performance

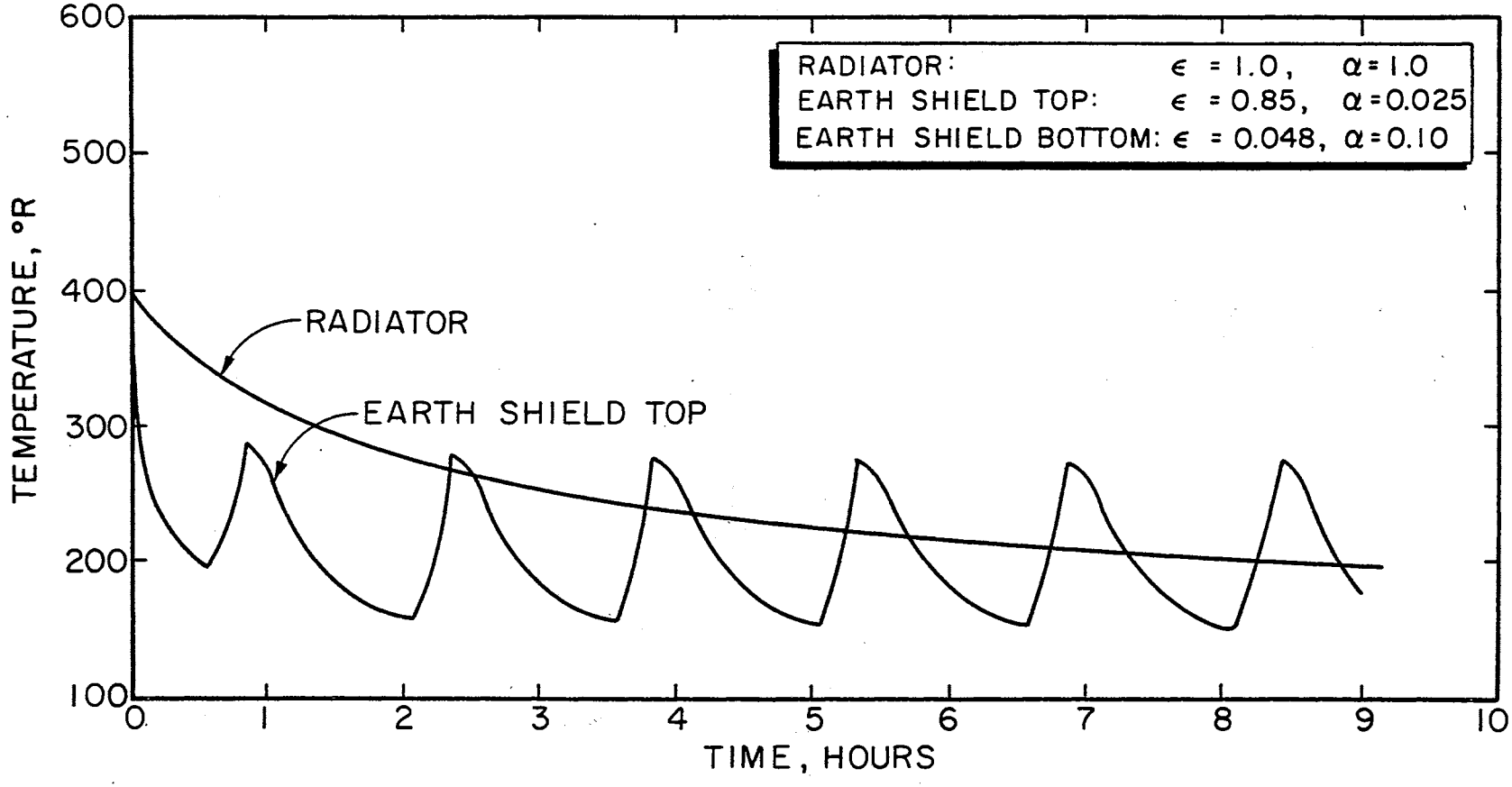

Figure 13. Radiator Performance

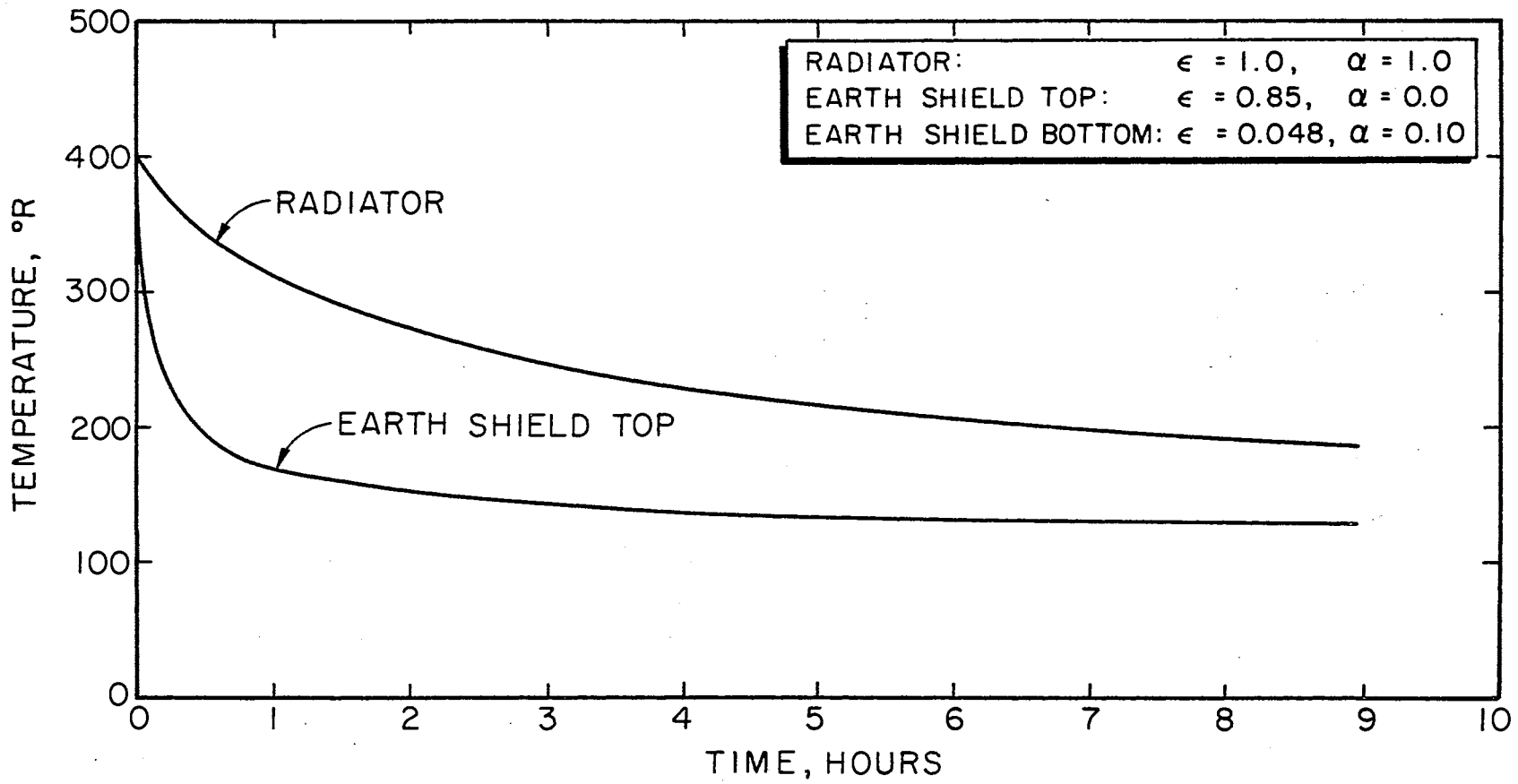

Figure 14. Radiator Performance

amplitude of the swing in the earth shield top temperature with essentially no change in the radiator temperature. The initial and satellite temperatures were 520° R.

Figure 13 resulted from a decrease in the solar absorptance of the earth shield top from 0.05, as used in Figure 10 to 0.025. The significant decrease (60° R) in the amplitude of the earth shield top temperature swing and a reduction in radiator temperature of about 10° R (to 200° R) resulted. Note that this problem uses initial and satellite temperatures of 400° R.

Figure 14 shows the results in using a solar absorptance for the earth shield top of 0.0. At nine hours, the radiator temperature is 25° R below that reported in Figure 10, and the earth shield top temperature is no longer a periodic function. The initial and satellite temperatures for this problem were 400° R.

Figure 14 is indicative of the type of temperature distribution which might be expected if sun shields were used to protect the top of the earth shield from direct solar irradiation. A direct comparison cannot be made, however, since this would require the sun shield to operate at absolute zero. Consequently, the higher temperature for both radiator and earth shield top would be expected with the introduction of the sun shield into the system.

A cryostat design utilizing a sun shield was then examined. This system consisted of the radiator earth shield sun shield arrangement, as shown in Figure 15.

The model chosen for analysis consisted of a black radiator surface, surface 1, which was insulated with two inches of superinsulation. On each side of the radiator, multilayer insulation with the

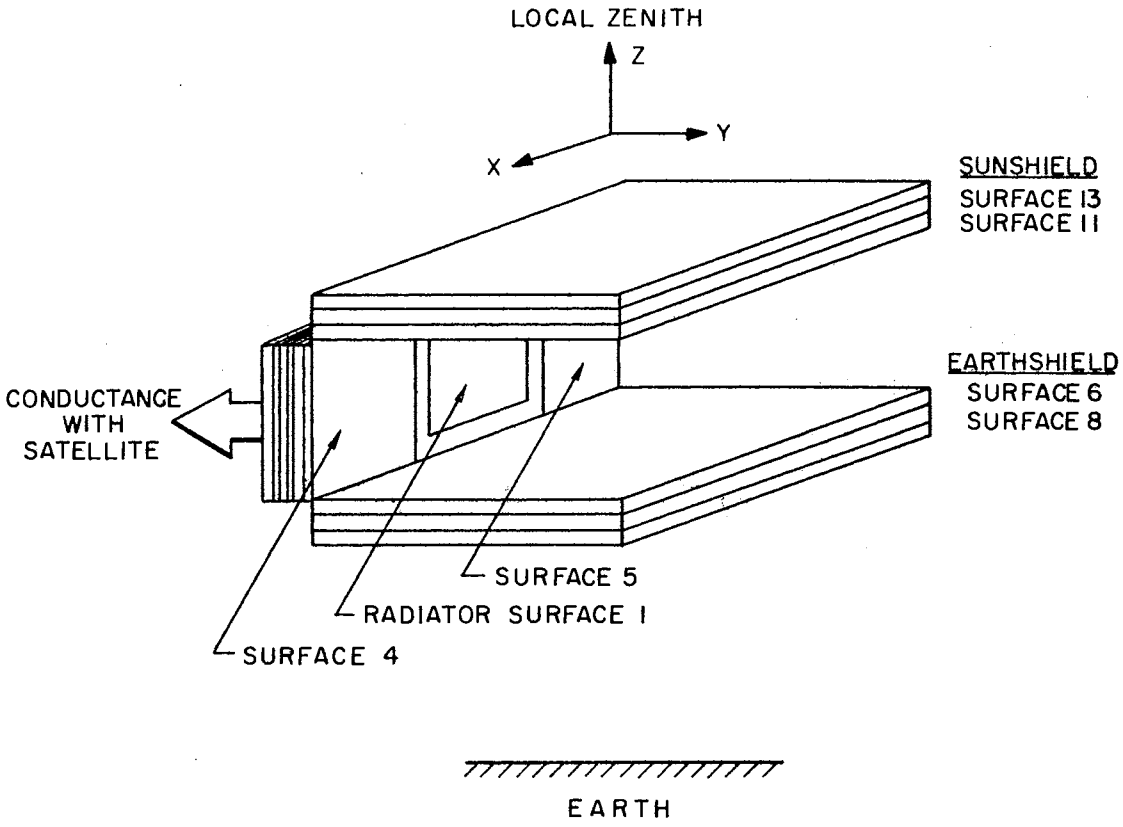

Figure 15. Radiator With Earth and Sun Shields

mylar side out was assumed. The properties used for the mylar side were $\alpha_s = 0.10$ and $\alpha_{IR} = 0.36$. Blankets of multilayer insulation were used for the earth shield and sun shield. These blankets were assumed to have a thickness of two inches. The surface properties used for the sun shield and earth shield surfaces were identical to the values used for the mylar side of the insulation; i.e., $\alpha_s = 0.10$, $\alpha_{IR} = 0.36$.

The various elements of the cryostat system were assumed to be coupled by radiative transfer only; i.e., conduction from the sun shield, earth shield, or other elements to the radiator or spacecraft was assumed to be zero. Conduction from the spacecraft was considered for the spacecraft radiator system, surface 1, but the conduction along any support system for the shields, surfaces 4 and 5, was assumed to be zero.

This cryostat system was assumed to be in a 300 statute-mile circular polar orbit, with the sun at local noon over the equator. This orbit would be the March 21 orbit for local noon at the spacecraft launch point or injection point. In such an orbit, a spacecraft makes one revolution in approximately 1.57 hours and spends slightly over one-half of this time in direct sunlight. Furthermore, at this altitude, the earth shine, consisting of both infrared and albedo energies, is quite large. For example, the average irradiation of a horizontal surface (in the X-Y plane of Figure 15) facing the earth due to earth emission is about 57 BTU/HR-FT^2. The energy from earth albedo is a variable which has a range from 0 to 127 BTU/HR-FT^2. The direct solar input during the time in the sun varies from zero to one solar constant for a horizontal surface facing upward.

Since these energy quantities are present in the low altitude orbit, the spacecraft was assumed to have planetary orientation such that the local zenith was always as shown in Figure 15, and the sun was always in the Y-Z plane in the negative Y direction. This implies that the spacecraft must be continually reoriented as it moves in the orbit. With these assumptions, the only surface which would ever receive direct sunlight is the top of the sun shield. Surfaces 4, 5, 8, and 11 receive solar energy after reflection from the earth. The radiator is shielded such that it never receives energy directly from the earth or the sun. The radiator only receives energy from the earth after reflection from surfaces 4, 5, 6, and 11. Surfaces 4, 5, and 11 receive earth-emitted energy and earth-reflected solar energy from essentially an infinite plane; i.e., the earth is so near that the entire horizon is essentially filled by the earth. For this reason, it is impractical to consider systems which completely eliminate a view of the earth.

The results of the analysis of this model are shown in Figures 16 through 21. The surface numbers as noted at the tops of these figures refer to the surfaces as shown in Figure 15. The average temperature of the radiator, Side 1, in Figure 16, is approximately 300° R. The other surfaces have much larger amplitudes of temperature variation because the thermal capacity of multilayer insulation is small. It is interesting to note that surface 6, the top of the earth's shield, has a lower average temperature than the radiator. This indicates that another geometry for the cryostat should be considered in which the relative positioning of the radiator was changed.

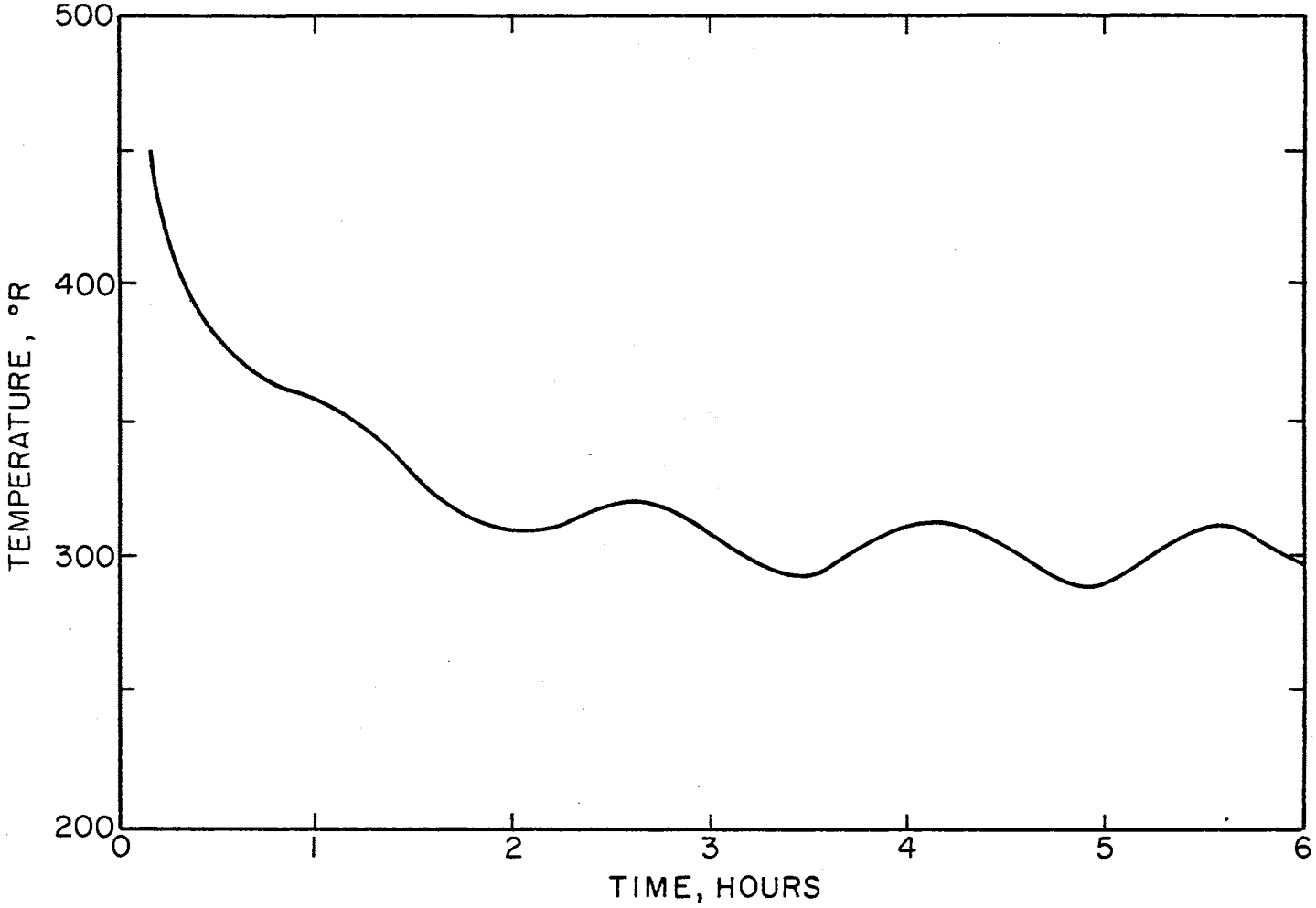

Figure 16. Temperature for Surface 1

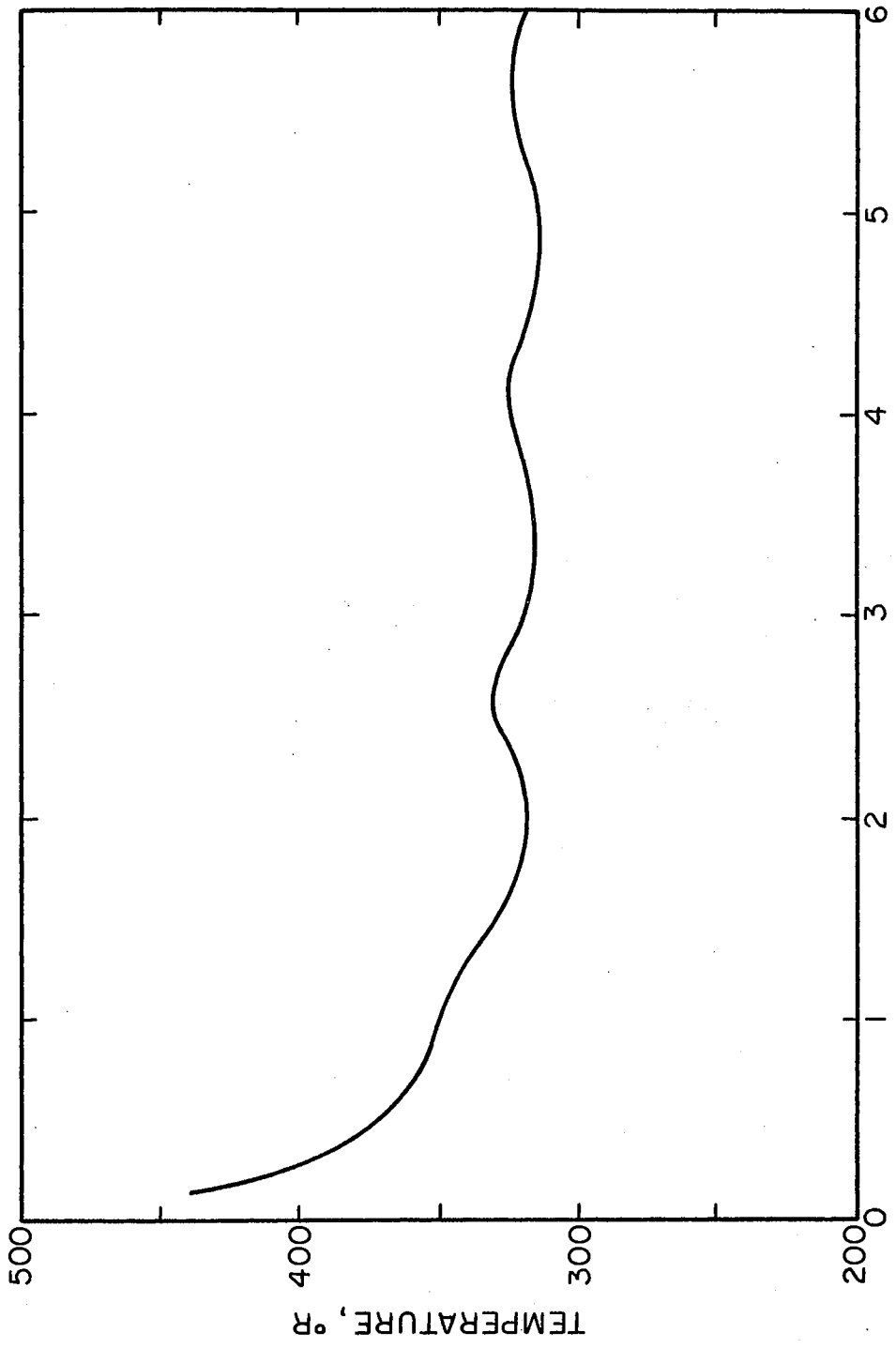

Figure 17. Temperature for Surface 4

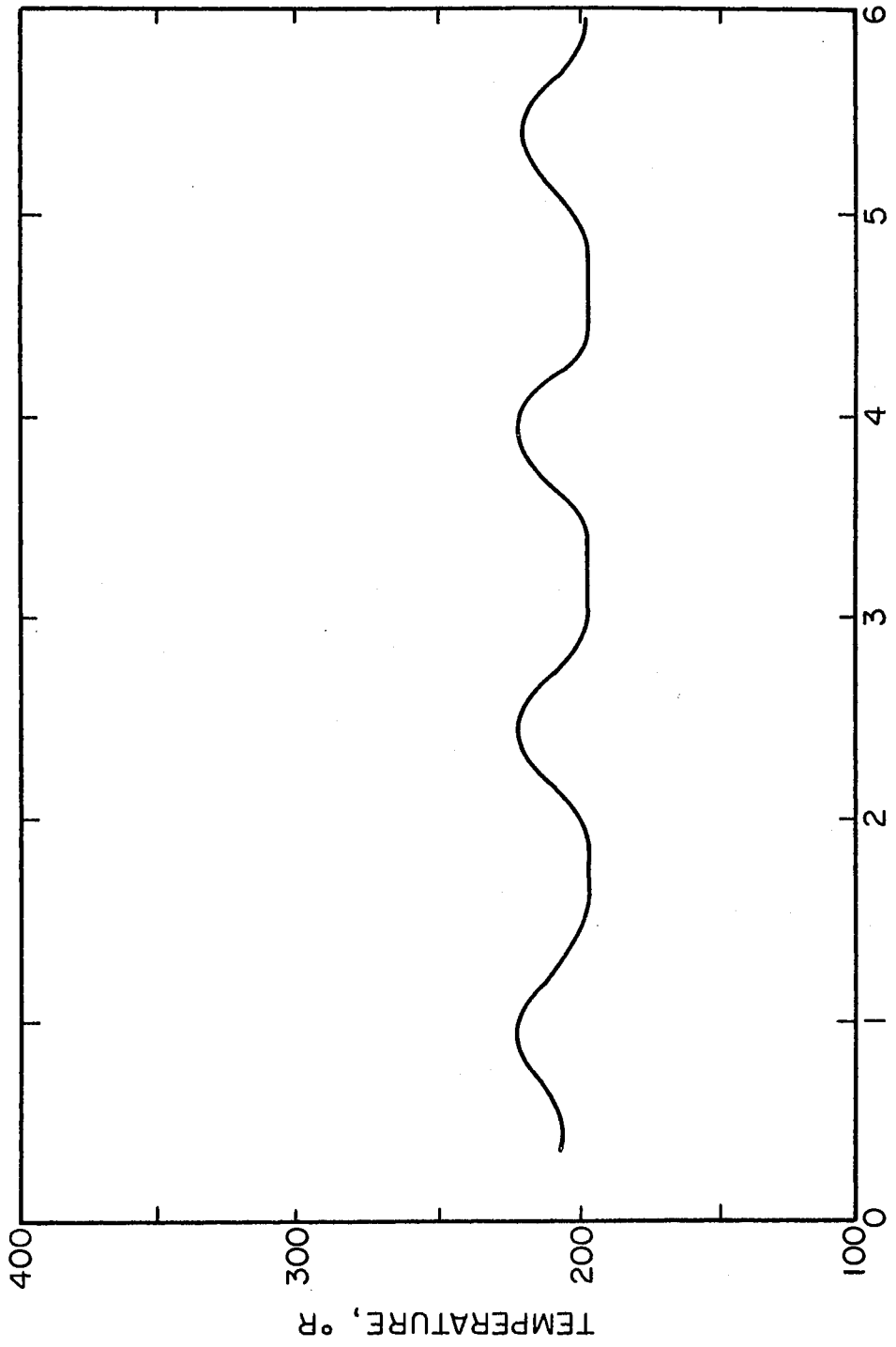

Figure 18. Temperature for Surface 6

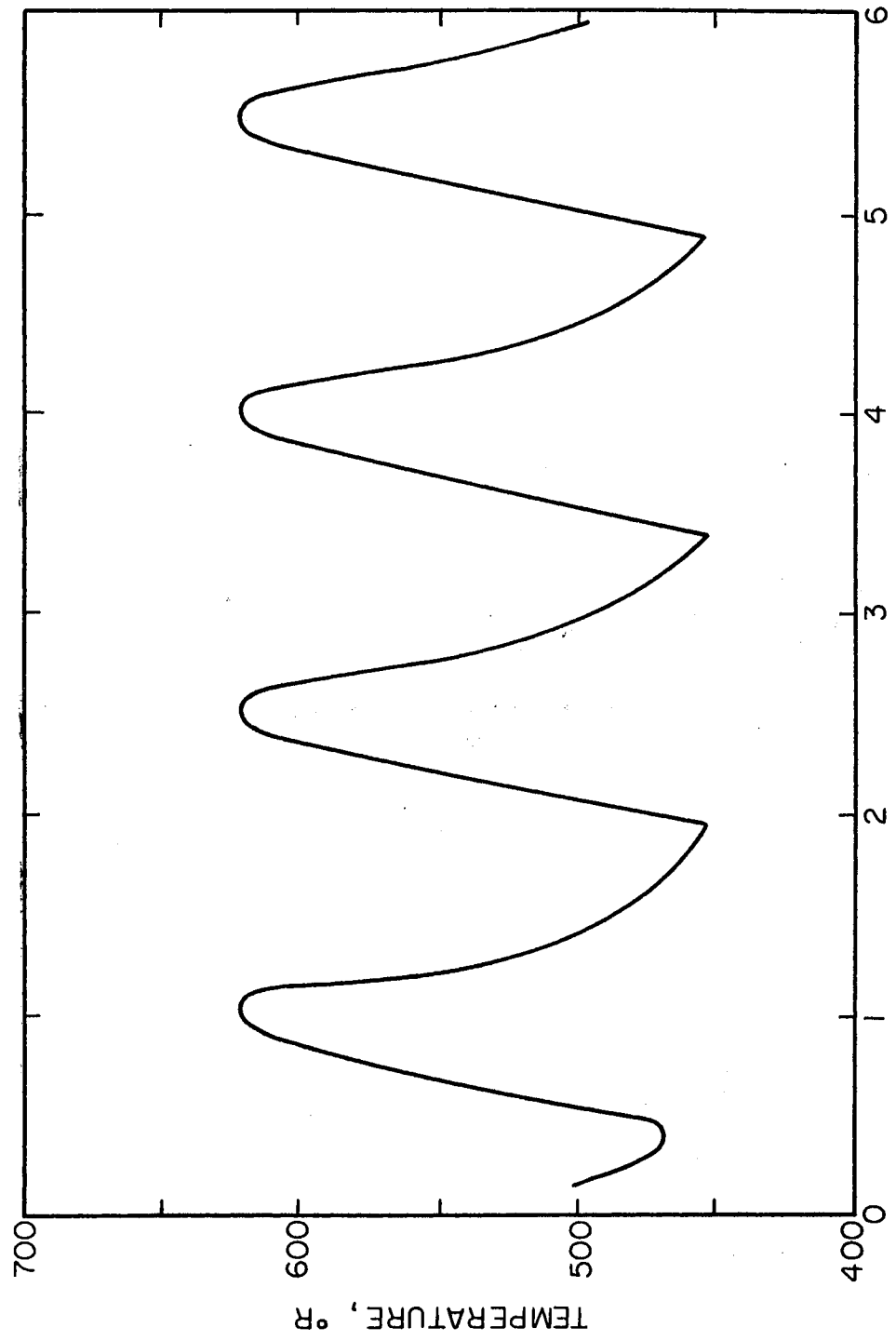

Figure 19. Temperature for Surface 8

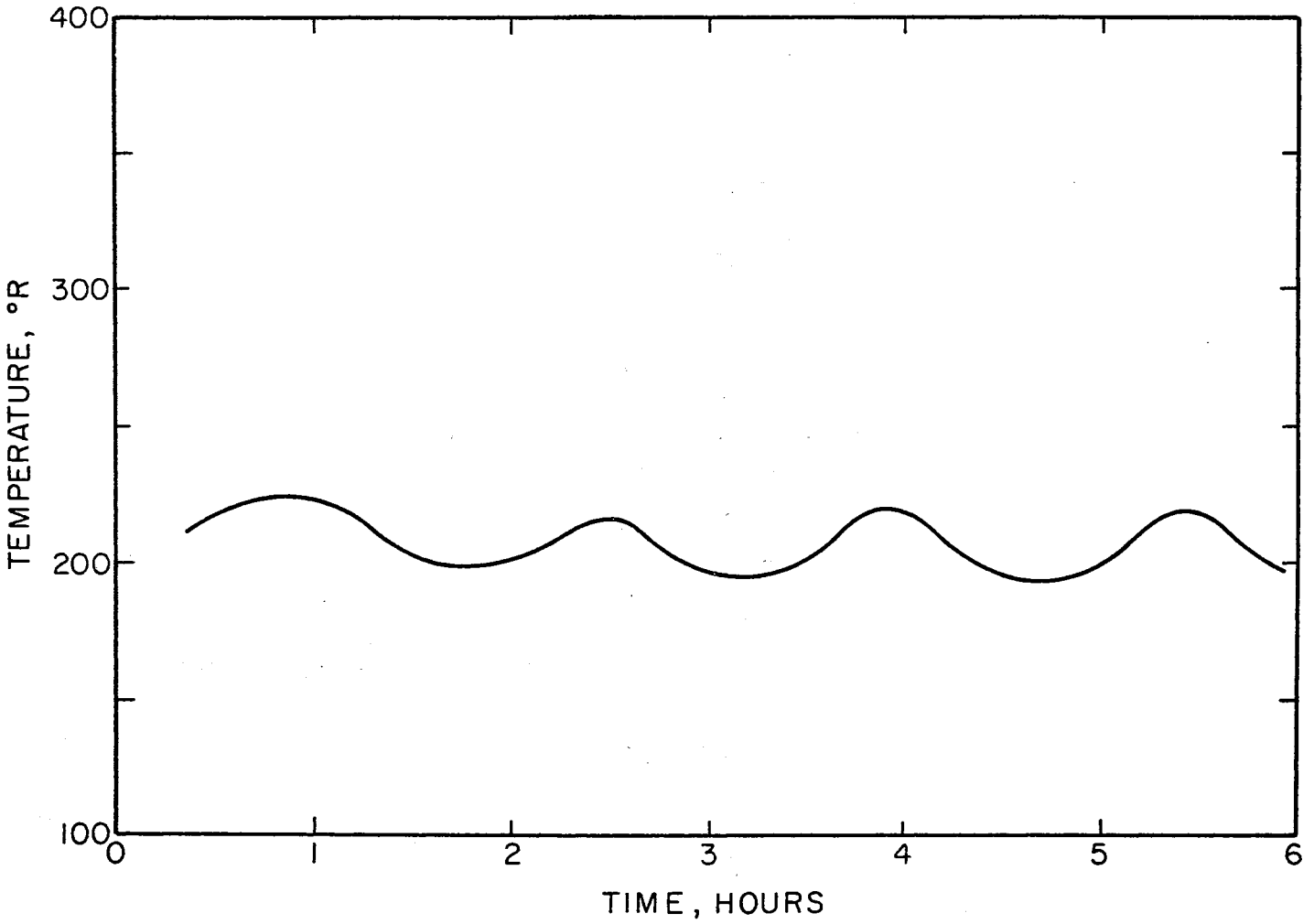

Figure 20. Temperature for Surface 11

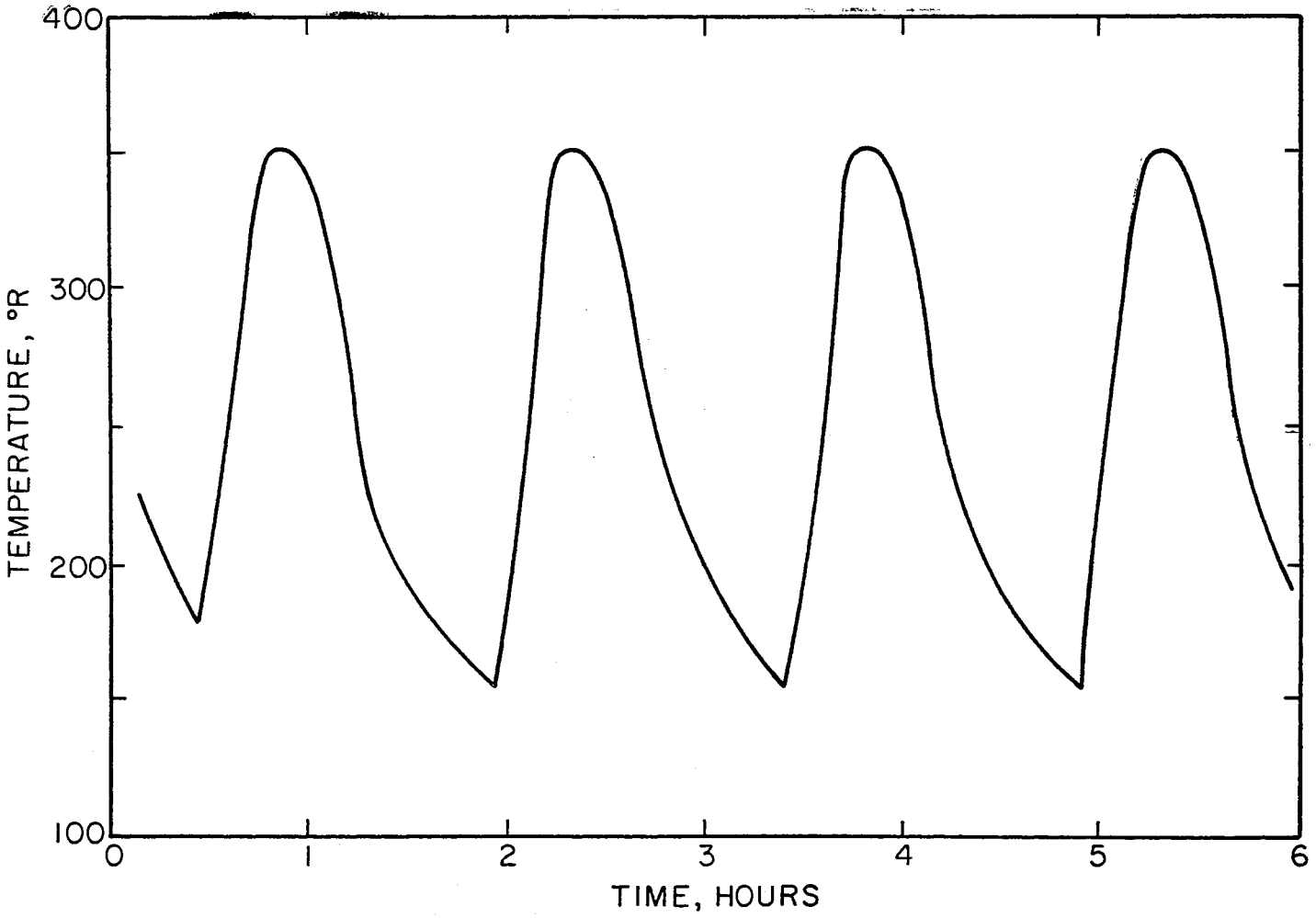

Figure 21. Temperature for Surface 13

CHAPTER V

DESIGN OF CRYOSTAT

Design Philosophy

In choosing a typical orbit for the final analysis, and therefore, the basis for a design philosophy, the two primary objectives were to obtain as low a circular orbit as possible and to allow the radiator to operate in a relatively severe heat flux environment. These objectives were bounded by the further stipulations that the design must be highly reliable, and must use no consumables. Therefore, the reorientation of the satellite while in orbit could not be considered.

The orbit finally chosen was one in which the satellite spends more than one-half of its time in sunlight, and which passes through the earth-sun line. Two examples of this type of orbit are shown in Figure 22.

With these goals, a design is suggested that is comprised of a blackbody radiator, protected on three sides by sun shields. The geometrical optimization of this design would then be the maximization of the view factor of the radiator to space, while minimizing the heat input to the radiator, due to its thermal environment.

To accomplish this task, the radiator, the sides and the top of the enclosure were insulated with multilayer superinsulation. The inner sides and top were defined to be specular reflecting surfaces exhibiting as high a specular reflectance as possible. To this enclosure were

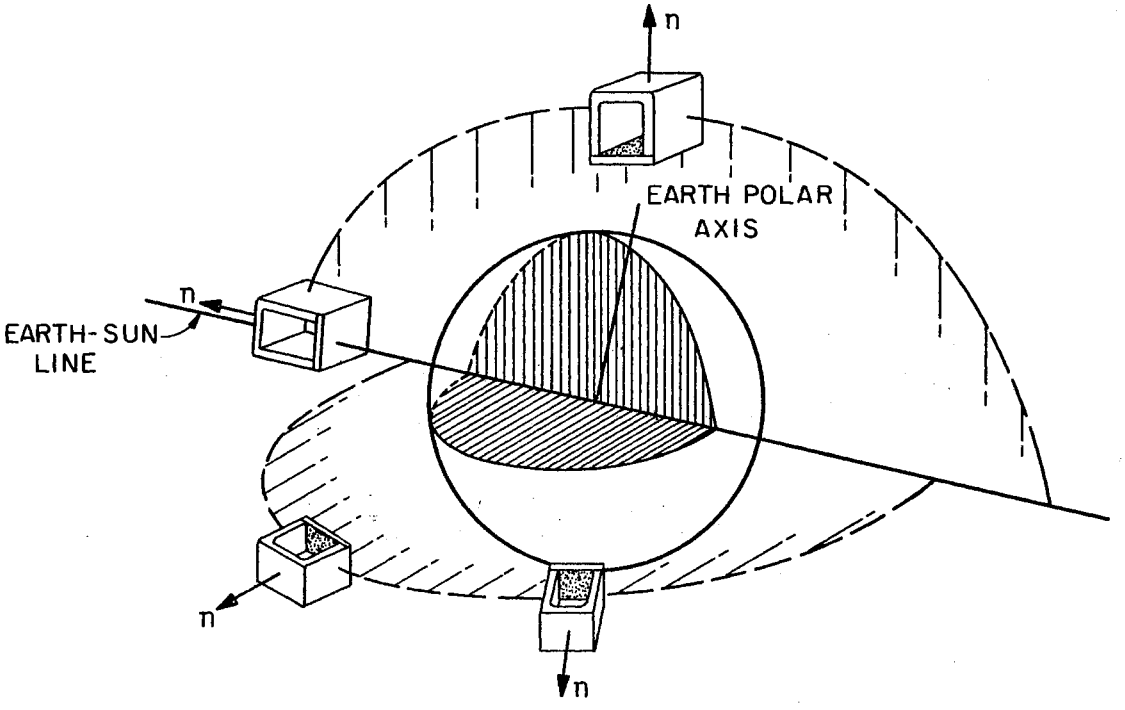

Figure 22. Typical Satellite Orbits

added plane specular reflectors which would effectively increase the view factor of the radiator to space while minimizing the heat input from environmental sources. This geometry is shown in Figure 23. The design and sizing of these reflectors are discussed in Appendix A and the configuration is shown in orbit in Figure 24.

Practical design considerations established in Chapter IV lead to a choice in a radiator size of 12 X 12 inches. Circular orbits of 300, 600 and 900 statute miles were considered for analysis. Reflector design procedures for these altitudes led to enclosure dimensions as shown in Table I.

TABLE I

ANALYTICAL MODEL ENCLOSURE DIMENSIONS

Orbit Altitude Statute Miles	Enclosure Height Inches	Reflector Angle Degrees
300	18.95	70
600	14.45	60
900	13.50	55

The three models which were considered were assigned a thermal nodal network, as shown in Figures 25 and 26. The insulation thickness, T, was chosen to be one inch. The enclosure height, H, and the reflector angle, β, are given in Table I for the various altitude configurations.

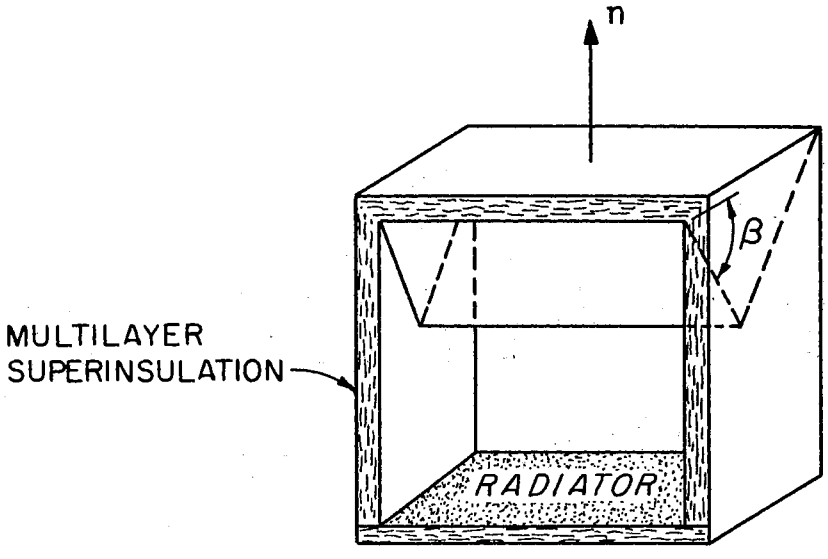

Figure 23. Basic Thermal Enclosure With β° Reflectors

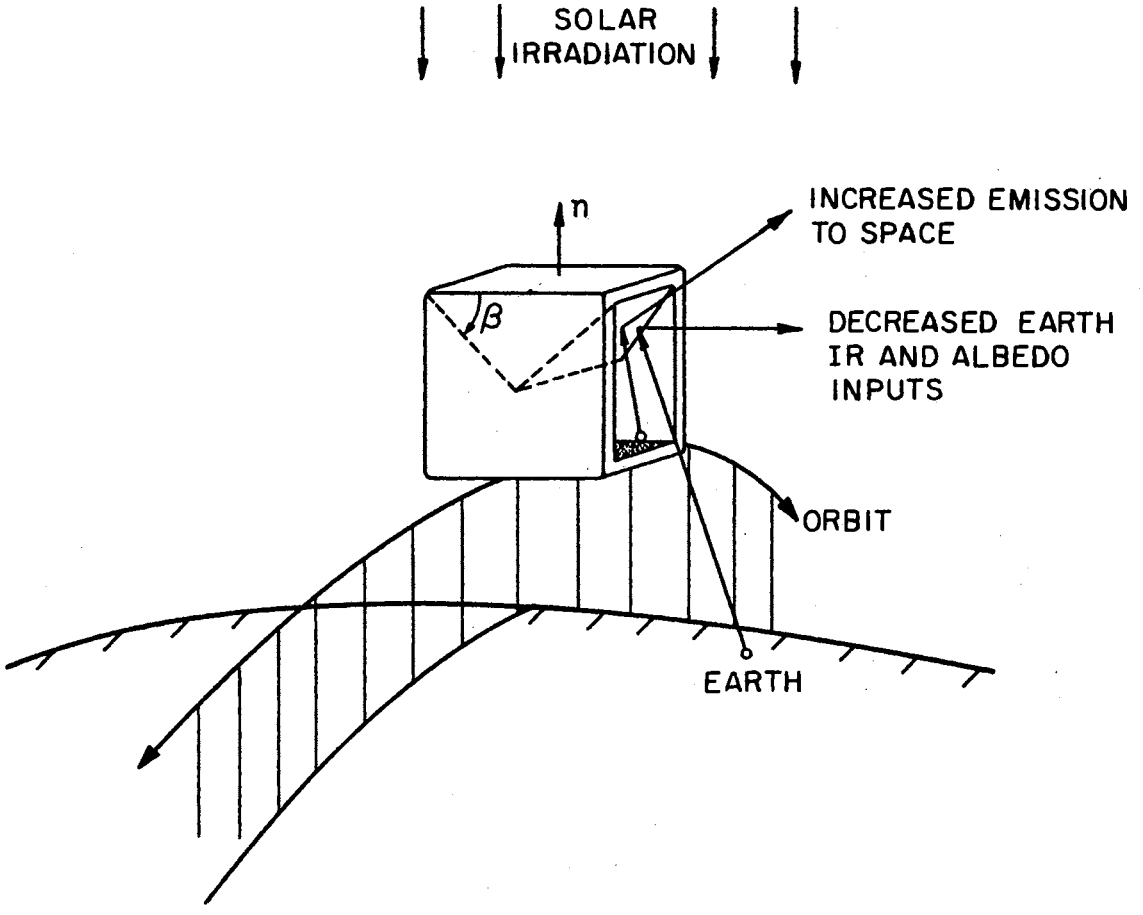

Figure 24. Enclosure With Specular Reflectors

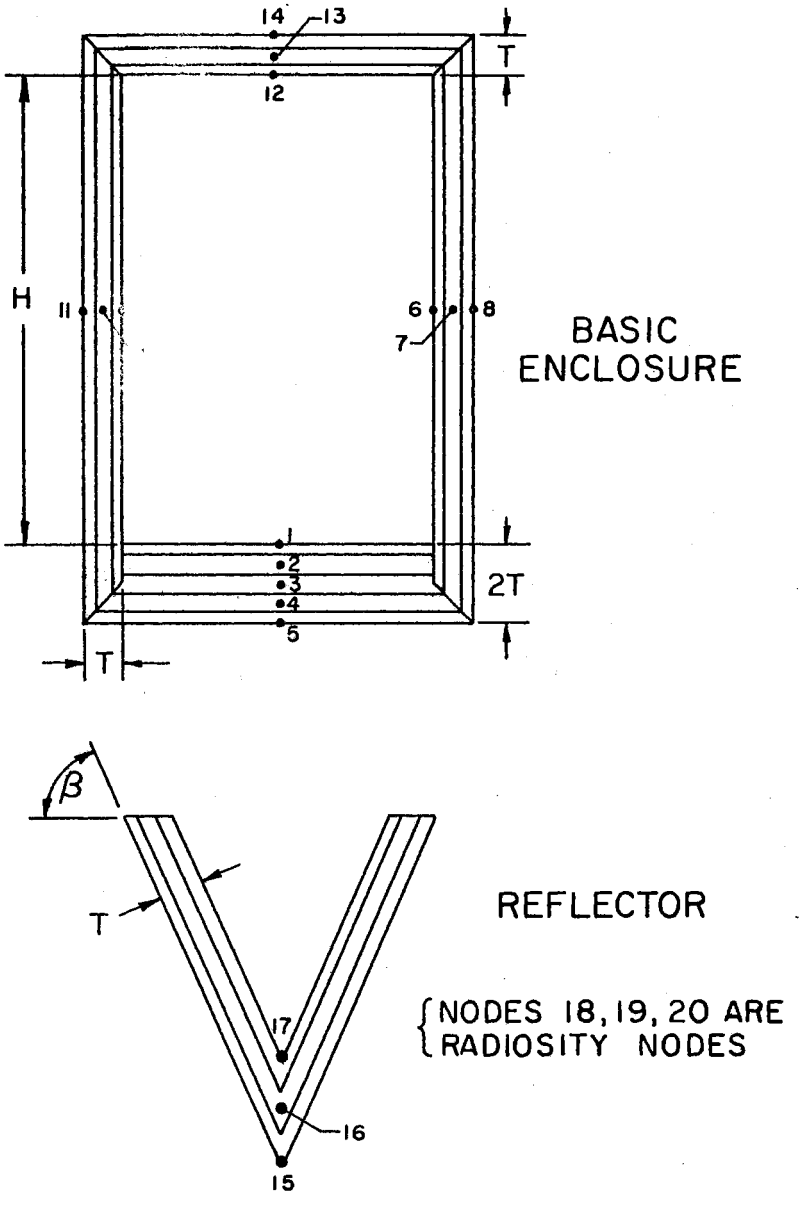

Figure 25. Nodal Model

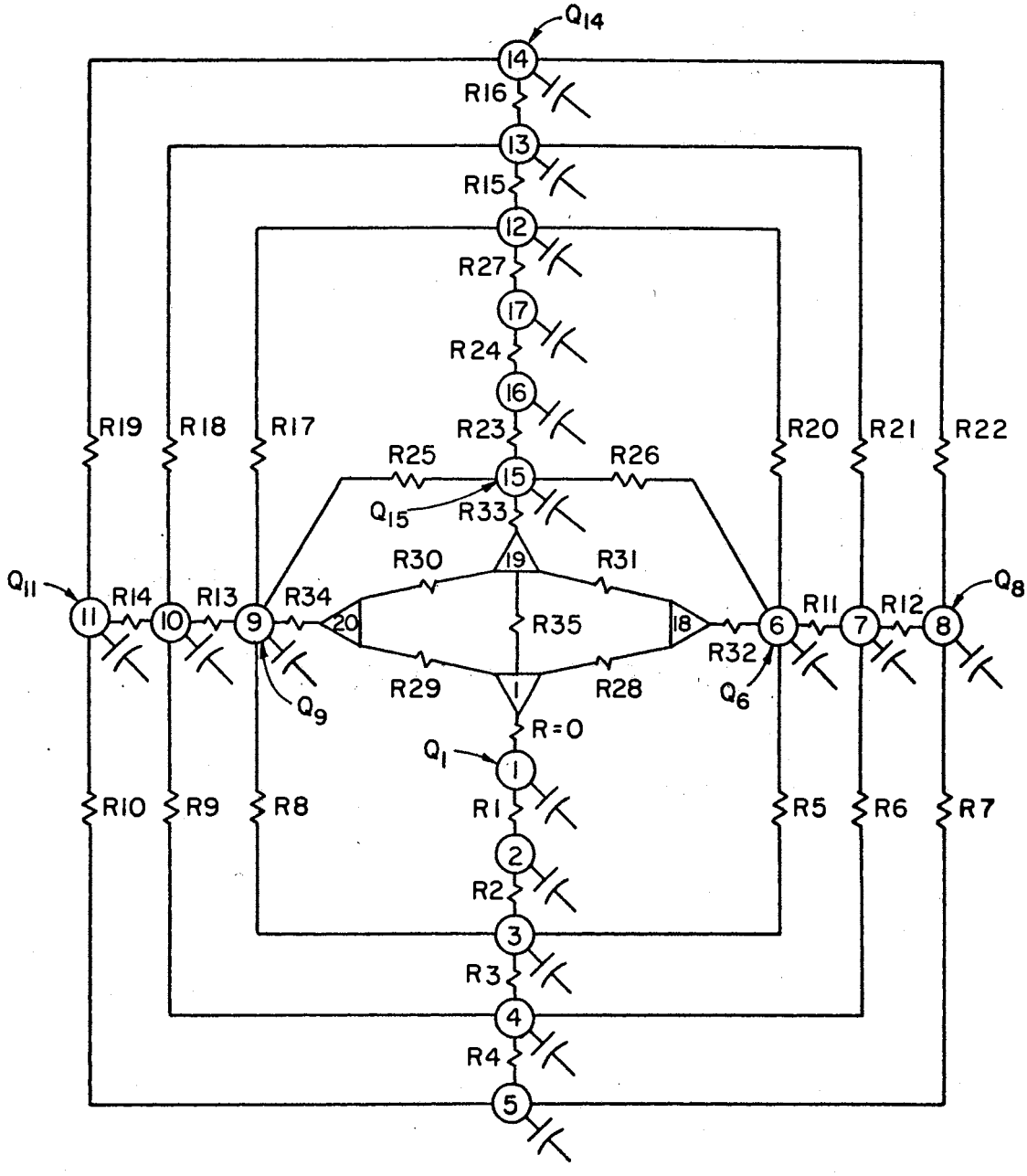

Figure 26. Analytical Network

The radiant interchange analysis was based on Oppenheim's radiosity analysis method as modified by J. Holman (9) to account for the possibility of allowing the surfaces to exhibit both specular and diffuse components of reflectances, as suggested by Seban (10) and discussed by Sparrow, Eckert and Jonsson (11).

The radiant interchange was considered for two spectra of energy; the solar spectrum and the infrared spectrum. The analysis assumed the following surface properties:

$$\rho\sigma_s = 0.90 \; ; \qquad \rho\delta_s = 0.05 \; ; \qquad \alpha_s = 0.05 \tag{5-1}$$

$$\rho\sigma_{IR} = 0.90 \; ; \qquad \rho\delta_{IR} = 0.05 \; ; \qquad \alpha_{IR} = 0.05 \tag{5-2}$$

The mass of the enclosure was assumed to exhibit the thermal properties of multilayer superinsulation, as given by reference (12) for 70 layers/inch. These properties are listed below.

density = 1.5 LBM/CU.FT.

specific heat = 0.135 BTU/LBM-$^{\circ}$R

thermal conductivity

a) normal to layers: 3.8×10^{-5} BTU/HR-FT-$^{\circ}$R

b) parallel to layers: 0.032 BTU/HR-FT-$^{\circ}$R

A computer program was written to calculate the thermal capacitances and resistances for the analytical model, as shown in Figure 26. This program used standard techniques for these calculations, and therefore, its listing is not included in this dissertation. These variables were used as input for the Lockheed Thermal Analyzer Program which was modified to operate on the O.S.U. IBM 360/50, and are given in Tables II, III and IV (13). The analytical techniques used for

TABLE II

ANALYTICAL THERMAL MODEL NETWORK PARAMETERS
(300 STATUTE MILE CIRCULAR ORBIT)

CAPACITORS (BTU/LBM-°R)

Node ID	Capacitance	Node ID	Capacitance
1	0.0042	11	0.0067
2	0.0084	12	0.0042
3	0.0084	13	0.0084
4	0.0084	14	0.0084
5	0.0042	15	0.0123
6	0.0067	16	0.0247
7	0.0133	17	0.0123
8	0.0067	18	0.0
9	0.0067	19	0.0
10	0.0133	20	0.0

RESISTORS (SEC-°R/BTU)

Resistor ID	Resistance	Resistor ID	Resistance
1	3.95×10^6	15	3.95×10^6
2	3.95×10^6	16	3.95×10^6
3	3.95×10^6	17	6.96×10^6
4	3.95×10^6	18	6.96×10^6
5	5.39×10^6	19	6.96×10^6
6	5.39×10^6	20	6.96×10^6
7	1.07×10^7	21	6.96×10^6
8	5.38×10^6	22	6.96×10^6
9	5.38×10^6	23	2.70×10^6
10	1.07×10^7	24	2.70×10^6
11	2.50×10^6	25	1.21×10^7
12	2.50×10^6	26	1.21×10^7
13	2.50×10^6	27	1.43×10^8
14	2.50×10^6		

RADIATION CONDUCTORS (FT^2)

Conductor ID	Conductance	Conductor ID	Conductance
28	9.87×10^{-6}	32	2.48×10^{-5}
29	9.87×10^{-6}	33	8.12×10^{-5}
30	8.22×10^{-7}	34	2.48×10^{-5}
31	8.22×10^{-7}	35	6.54×10^{-6}

TABLE III

ANALYTICAL THERMAL MODEL NETWORK PARAMETERS
(600 STATUTE MILE CIRCULAR ORBIT)

CAPACITORS (BTU/LBM-°R)

Node ID	Capacitance	Node ID	Capacitance
1	0.0042	11	0.0051
2	0.0084	12	0.0042
3	0.0084	13	0.0084
4	0.0084	14	0.0084
5	0.0042	15	0.0084
6	0.0051	16	0.0169
7	0.0101	17	0.0084
8	0.0051	18	0.0
9	0.0051	19	0.0
10	0.0101	20	0.0

RESISTORS (SEC-°R/BTU)

Resistor ID	Resistance	Resistor ID	Resistance
1	3.95×10^6	15	3.95×10^6
2	3.95×10^6	16	3.95×10^6
3	3.95×10^6	17	5.95×10^6
4	3.95×10^6	18	5.95×10^6
5	4.38×10^6	19	5.95×10^6
6	4.38×10^6	20	5.95×10^6
7	8.75×10^6	21	5.95×10^6
8	4.38×10^6	22	5.95×10^6
9	4.38×10^6	23	3.95×10^6
10	8.75×10^6	24	3.95×10^6
11	3.28×10^6	25	8.65×10^6
12	3.28×10^6	26	8.65×10^6
13	3.28×10^6	27	1.46×10^6
14	3.28×10^6		

RADIATION CONDUCTORS (FT^2)

Conductor ID	Conductance	Conductor ID	Conductance
28	5.57×10^{-6}	32	2.14×10^{-5}
29	5.57×10^{-6}	33	5.55×10^{-5}
30	5.98×10^{-7}	34	2.14×10^{-5}
31	5.98×10^{-7}	35	5.83×10^{-6}

TABLE IV

ANALYTICAL THERMAL MODEL NETWORK PARAMETERS
(900 STATUTE MILE CIRCULAR ORBIT)

CAPACITORS (BTU/LBM-°R)

Node ID	Capacitance	Node ID	Capacitance
1	0.0042	11	0.0047
2	0.0084	12	0.0042
3	0.0084	13	0.0084
4	0.0084	14	0.0084
5	0.0042	15	0.0073
6	0.0047	16	0.0147
7	0.0095	17	0.0073
8	0.0047	18	0.0
9	0.0047	19	0.0
10	0.0095	20	0.0

RESISTORS (SEC-°R/BTU)

Resistor ID	Resistance	Resistor ID	Resistance
1	3.95×10^6	15	3.95×10^6
2	3.95×10^6	16	3.95×10^6
3	3.95×10^6	17	5.73×10^6
4	3.95×10^6	18	5.73×10^6
5	4.16×10^6	19	5.73×10^6
6	4.16×10^6	20	5.73×10^6
7	8.32×10^6	21	5.73×10^6
8	4.16×10^6	22	5.73×10^6
9	4.16×10^6	23	4.53×10^6
10	8.32×10^6	24	4.53×10^6
11	3.51×10^6	25	7.44×10^6
12	3.51×10^6	26	7.44×10^6
13	3.51×10^6	27	1.48×10^6
14	3.51×10^6		

RADIATION CONDUCTORS (FT^2)

Conductor ID	Conductance	Conductor ID	Conductance
28	5.46×10^{-6}	32	2.13×10^{-5}
29	5.46×10^{-6}	33	4.84×10^{-5}
30	5.41×10^{-7}	34	2.13×10^{-5}
31	5.41×10^{-7}	35	5.48×10^{-6}

calculating the environmental heat inputs to the cryostat are described in Appendix B. The special techniques used to describe the radiation resistances of the specular-diffuse system are described in Appendix C.

The results of these transient analyses are presented in Figures 27, 28, and 29. The 600 statute mile orbit is shown to be the lowest orbit that meets the criteria of an average radiator temperature less than 200° R. This fact establishes the minimum orbit to be considered for the design and the optimization will be based on a similar circular orbit.

Some immediate comments may be made on Figures 27 through 29 concerning the improvement of the cryostat performance. It would be desirable to increase the thermal mass of the radiator in order to decrease its transient excursions. This is not expected to be a problem since the mass presently considered in the analysis is quite small. Also, the temperature of the outside surface of the sun shield, surfaces 4 and 5, could be lowered considerably if a low α/ε surface had been used. This in turn would lower the temperatures of the remaining interior surfaces of the enclosure.

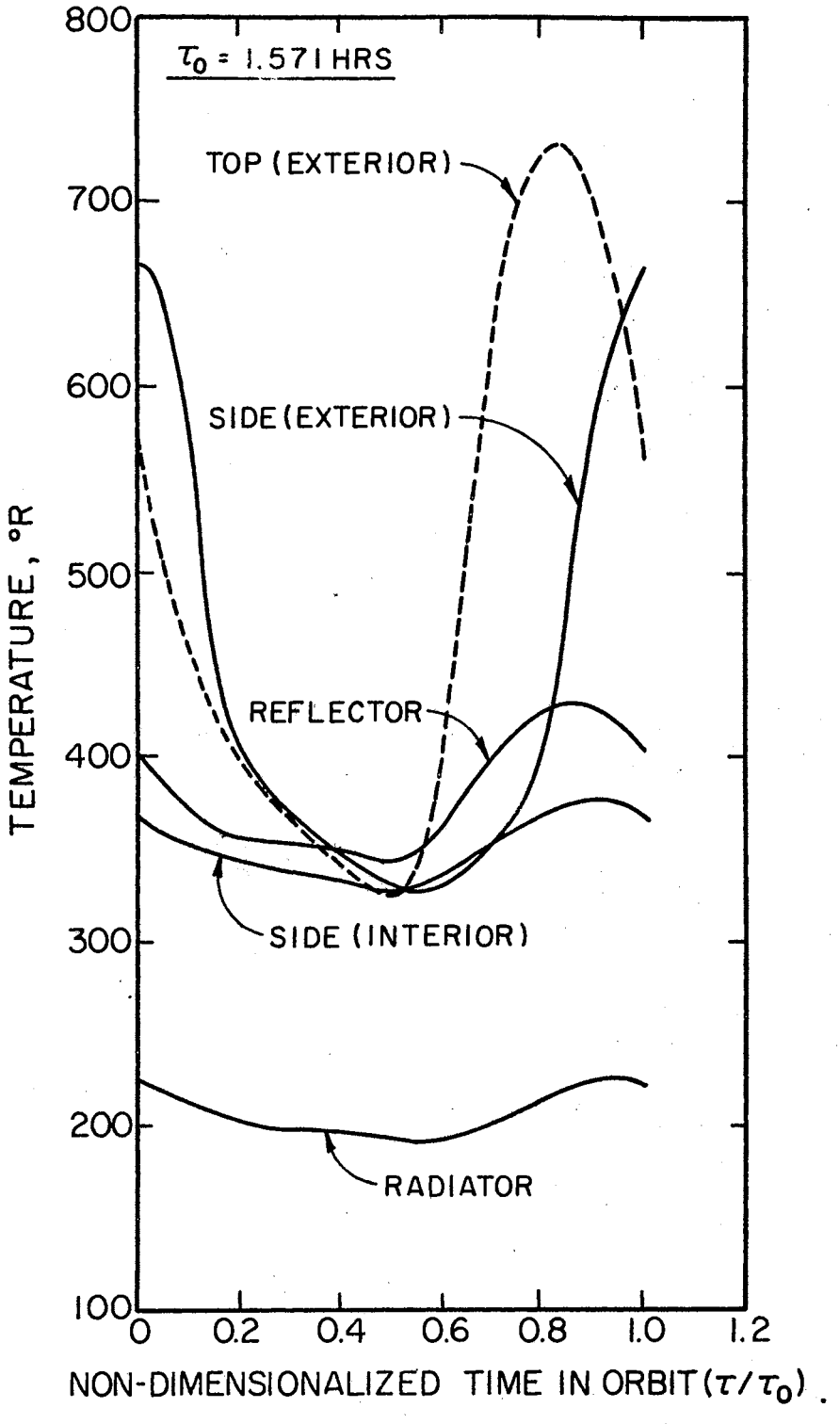

Figure 27. 300 Statute Mile Temperature Results

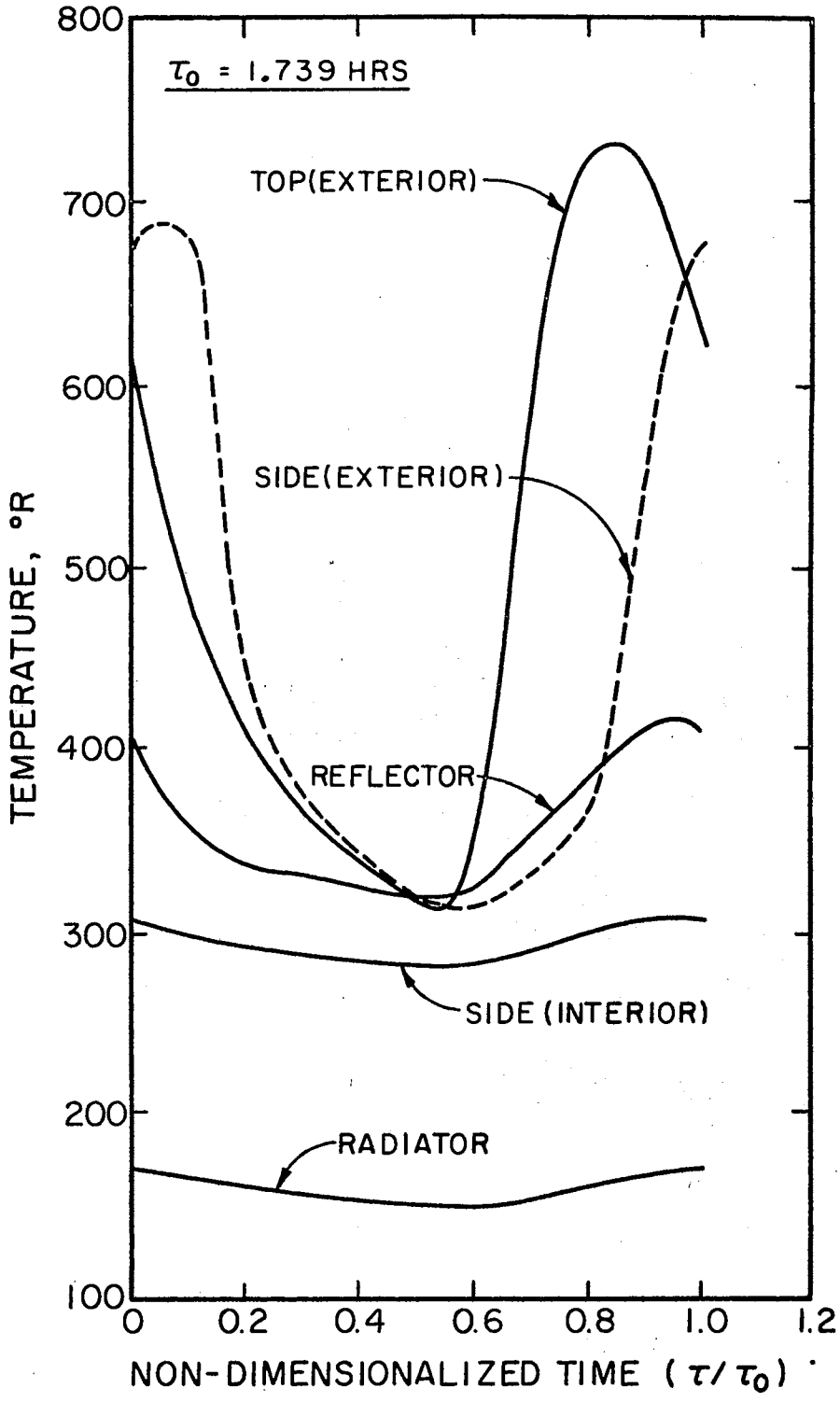

Figure 28. 600 Statue Mile Temperature Results

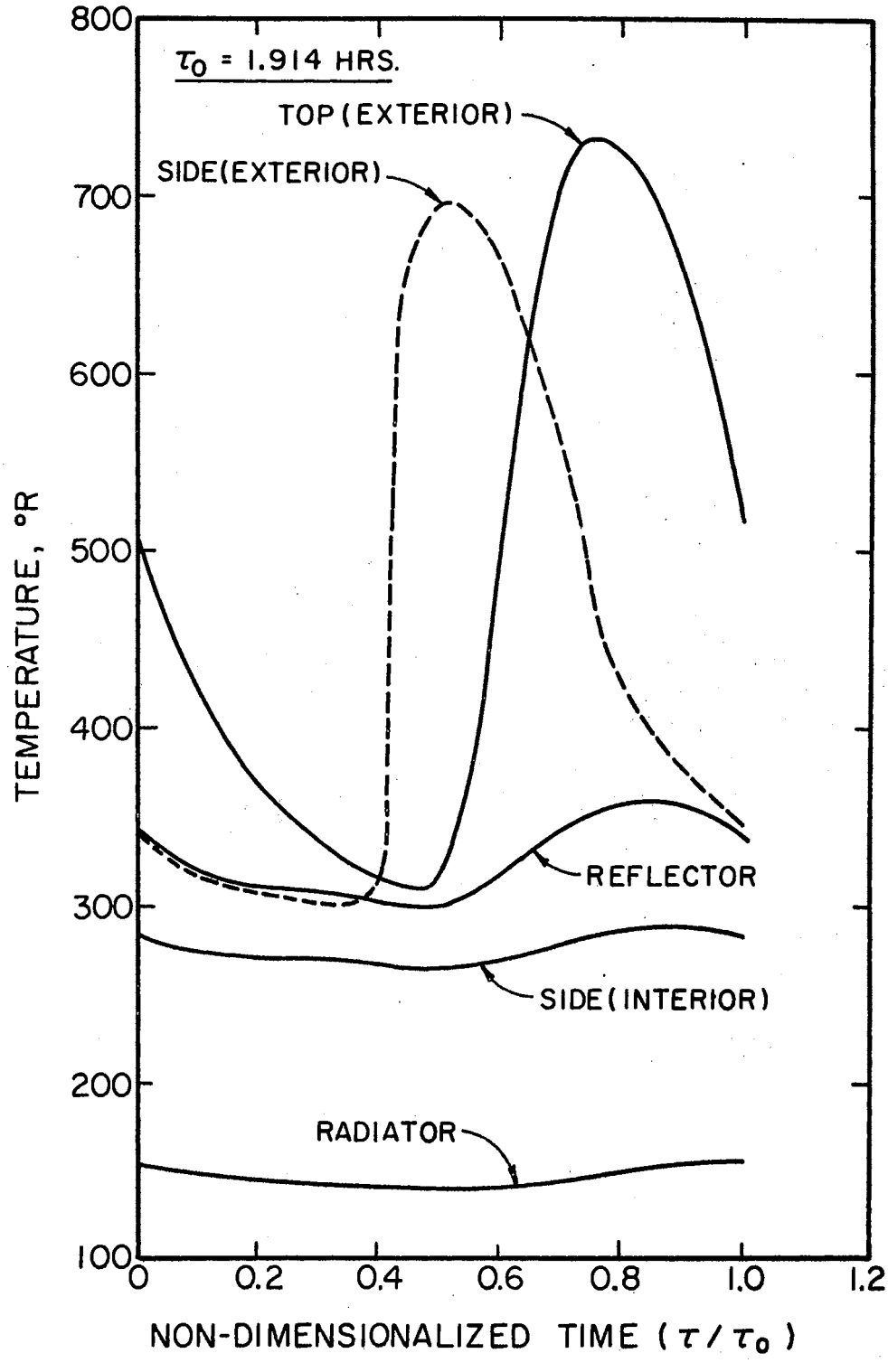

Figure 29. 900 Statute Mile Temperature Results

CHAPTER VI

EXPERIMENTAL PROGRAM

The prime objective of the experiment was to gain confidence in the techniques that were utilized in the analysis, especially those concerned with the radiative coupling in the system. Two energy spectra are of interest; the solar and the infrared. Since the techniques applied to each spectra are similar, a considerable simplification was made in only considering a test for the infrared spectrum. The objective was then obtained by a validation of the radiative coupling that would exist between the surfaces of the enclosure and an external infrared source. The tests were conducted for steady-state conditions.

The test model was a one-half scale model of the 600-statute mile orbit proposed design. The radiative boundary conditions of the model were symmetrical about a plane perpendicular to the radiator and passing through the vertex of the reflector. This condition is shown in Figure 30a. An infrared specular reflector was used in the position of this plane of symmetry, allowing radiative symmetry to exist. This plane, as well as the remaining surfaces of the model were insulated with one inch of multilayer insulation at 77 layers per inch. The insulation behind the symmetrical plane completed the requirements to approximate an adiabatic surface. The theoretical presence of this surface is easily accounted for in the analytical study.

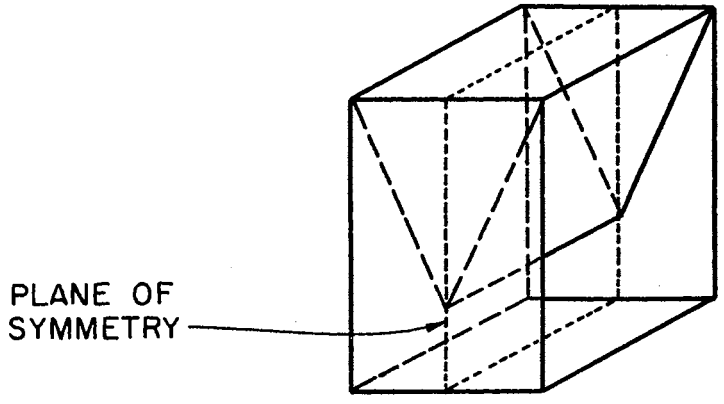

(a) PLANE OF THERMAL SYMMETRY

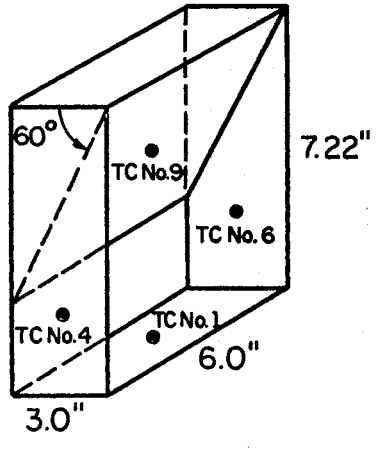

(b) TEST MODEL

Figure 30. Thermal Symmetry for Test Model

The fabrication of the model included a balsawood frame, to which the surfaces of the enclosure were attached. Balsawood insulators provided conductive isolation between the adjacent surfaces and between the surfaces and the frame. The sides, the back (the symmetrical plane) and the reflector were made from 1/32 inch brass shim stock, one side of which was highly polished. The radiator was made from 1/16 inch aluminum plate with the top face painted with four coats of 3M Black Velvet paint. Below the radiator, there was a total of two inches of multilayer insulation at 77 layers per inch. The thermocouples on the models were placed centered on the surfaces as shown in Figure 30b.

The infrared source, used to irradiate the model, was made from 1/16 inch sheet aluminum. The top of the plate was painted with four coats of 3M Black Velvet and an nikrome heating element was bonded to the bottom surface. The entire plate was insulated with one inch of multilayer insulation. The heater thermocouple positions and its general setup are described in Figure 31.

The test chamber was a vacuum chamber with a high emittance cold wall which could operate down to liquid nitrogen temperatures. Chamber pressure measurements were available from both thermocouple and ionization gauges. The temperatures of all the cold wall faces were monitored during the test.

The test setup is shown in Figure 32. The model and the infrared heater were held by a cradle suspended from the chamber with nylon cord. The model, heater and cold wall temperatures were continually monitored by a Daystrom multichannel recorder. Temperature data was taken from a millivolt meter. An ice junction was used for the thermocouple reference. Heater power was supplied by a constant voltage supply.

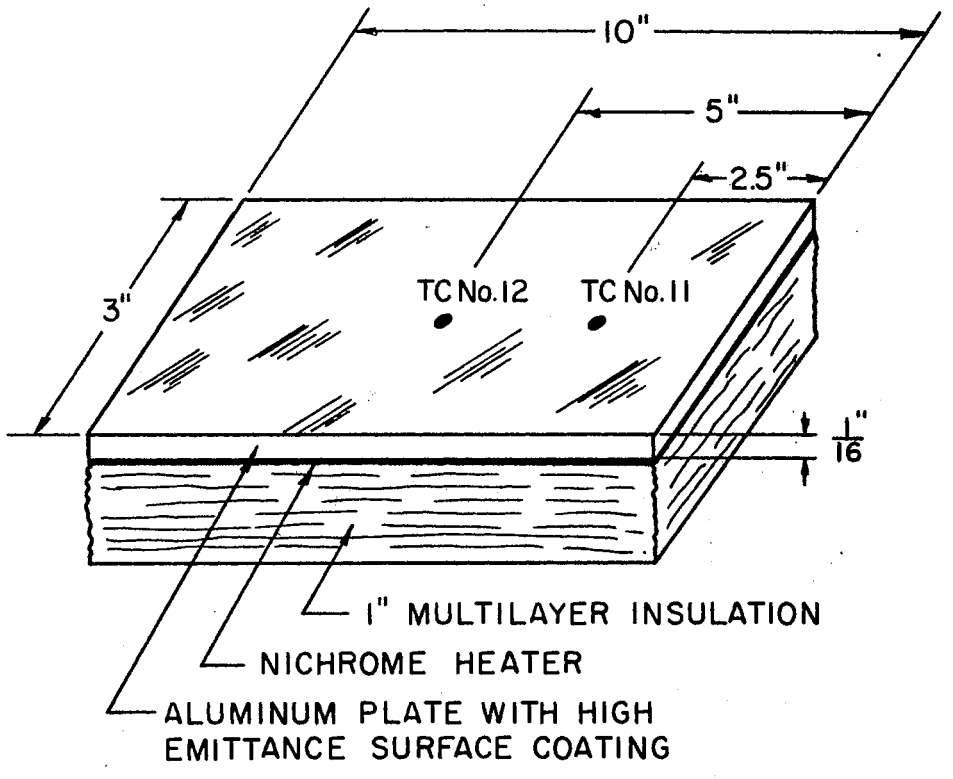

Figure 31. Infrared Source

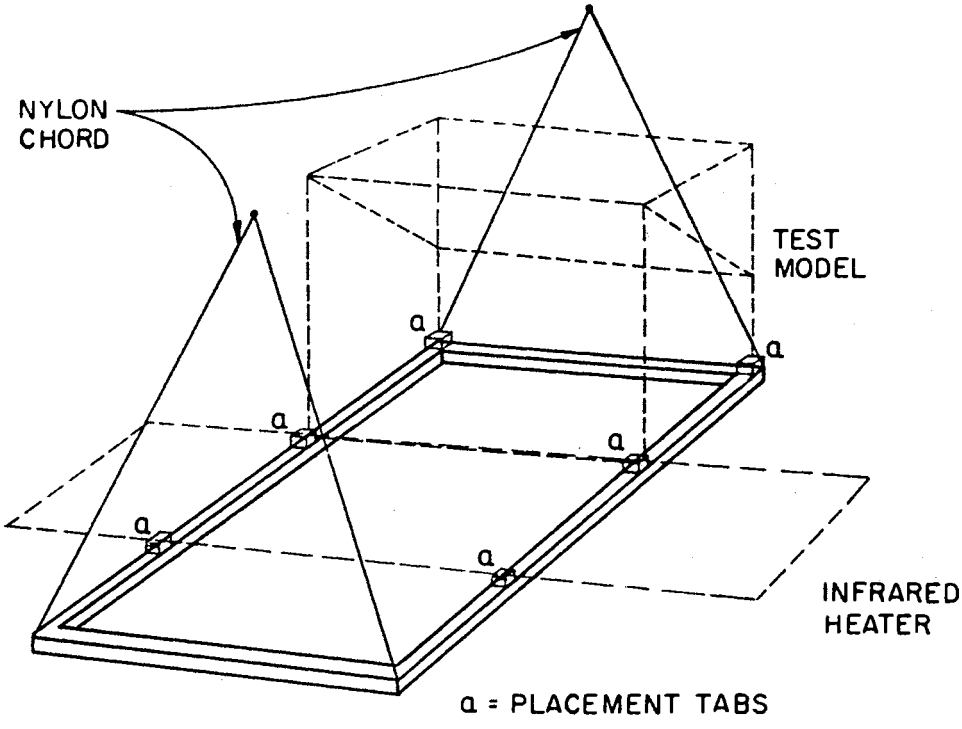

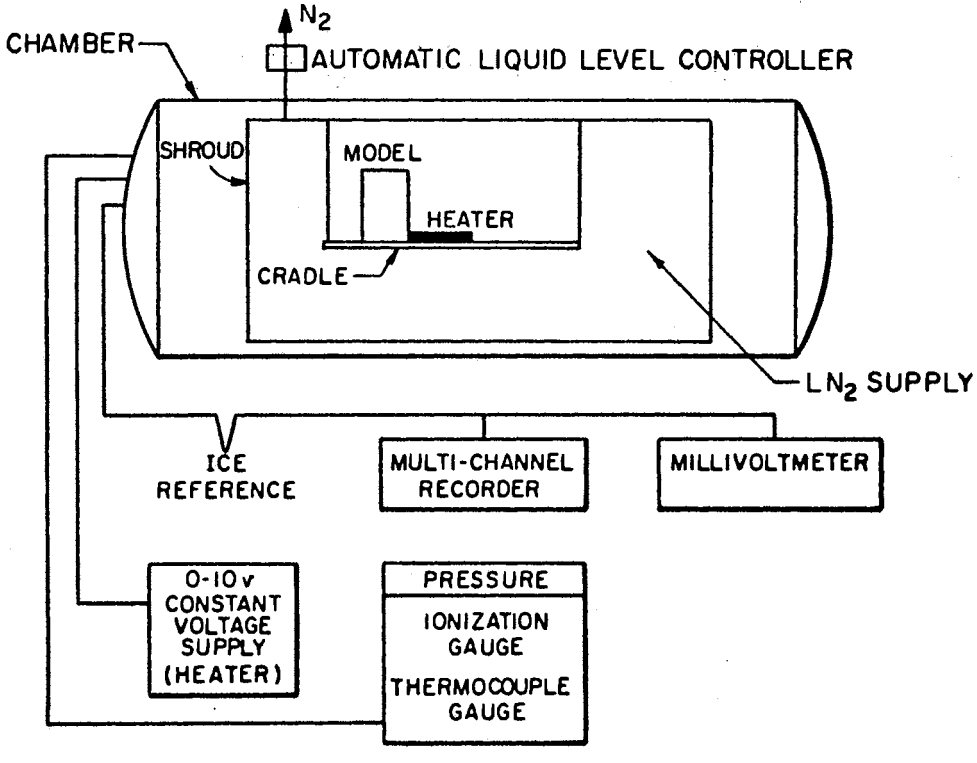

Figure 32. Test Set Up

The analysis of the test model was based on the same techniques as used for the previous analysis work as described in Chapter V. Sebans' assumption was invoked and the thermal surface properties which were used in the analysis are as follows:

a) Sides, Reflector and Back

$$\alpha_{IR} = \epsilon_{IR} = 0.05$$
$$\rho\sigma_{IR} = 0.90 \qquad (6\text{-}1)$$
$$\rho\delta_{IR} = 0.05$$

b) Radiator

$$\alpha_{IR} = \epsilon_{IR} = 1.0 \qquad (6\text{-}2)$$

Because of the scaling of the model dimensions, the network parameters, as given in Table III (for the 600-mile orbit model) were directly scaled to meet the model. The consideration of the infrared heater was a departure from the previous analysis and new geometric shaped factors had to be calculated between the enclosure and the heater. These shape factors are listed below:

$$F_{\text{side-heater}} = 0.060$$
$$F_{\text{reflector-heater}} = 0.125 \qquad (6\text{-}3)$$
$$F_{\text{side-space}} = 0.483$$
$$F_{\text{reflector-space}} = 0.598$$

A comparison of the test results with the predicted test temperatures is shown in Figures 33 and 34. The solid lines represent the results of a parametric analysis of the enclosure as a function of the cold wall effective temperature. The differences between these figures is the effective temperature of the infrared source and the effective cold wall temperature.

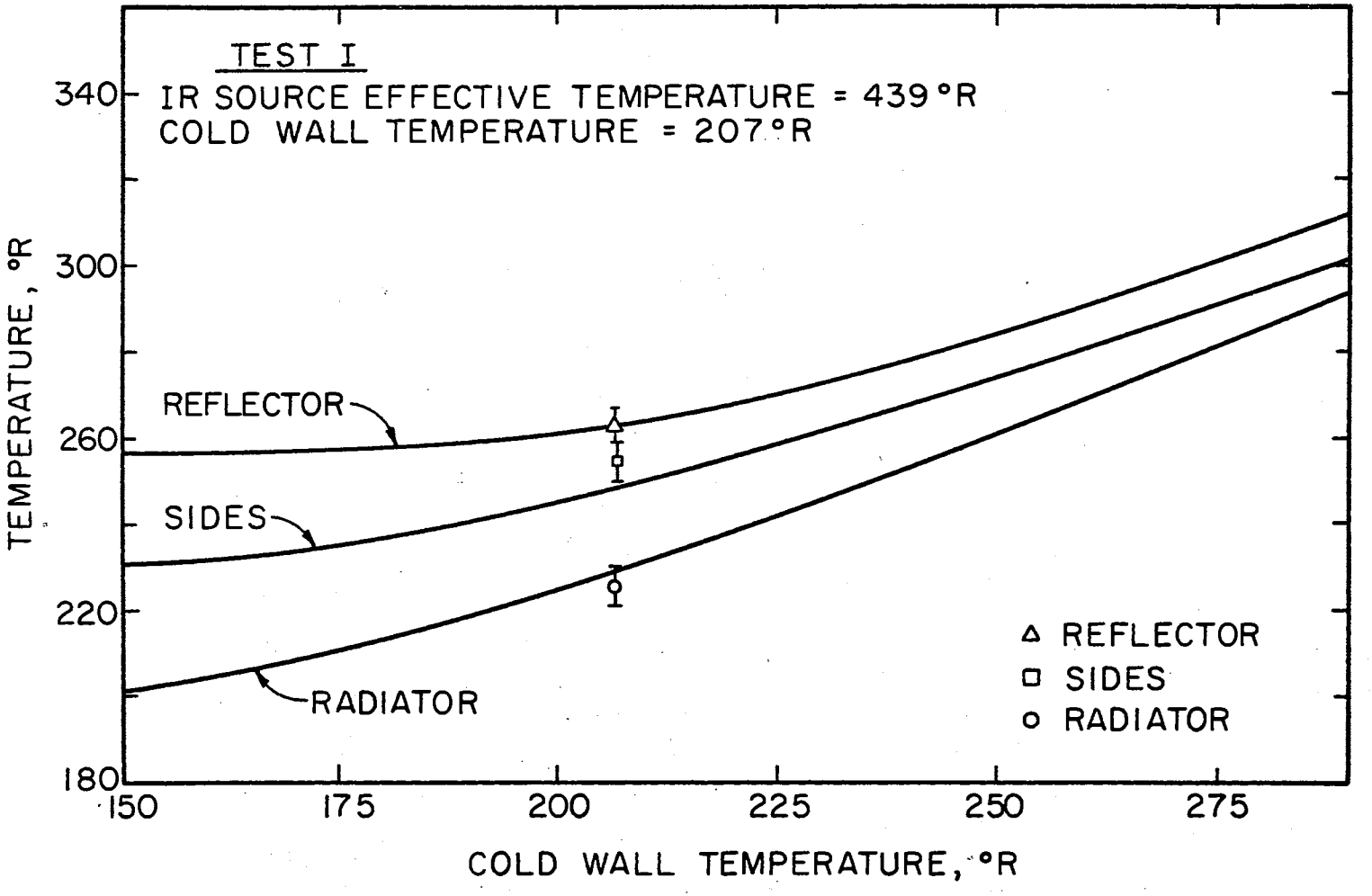

Figure 33. Test I Comparison: Test Data Versus Prediction

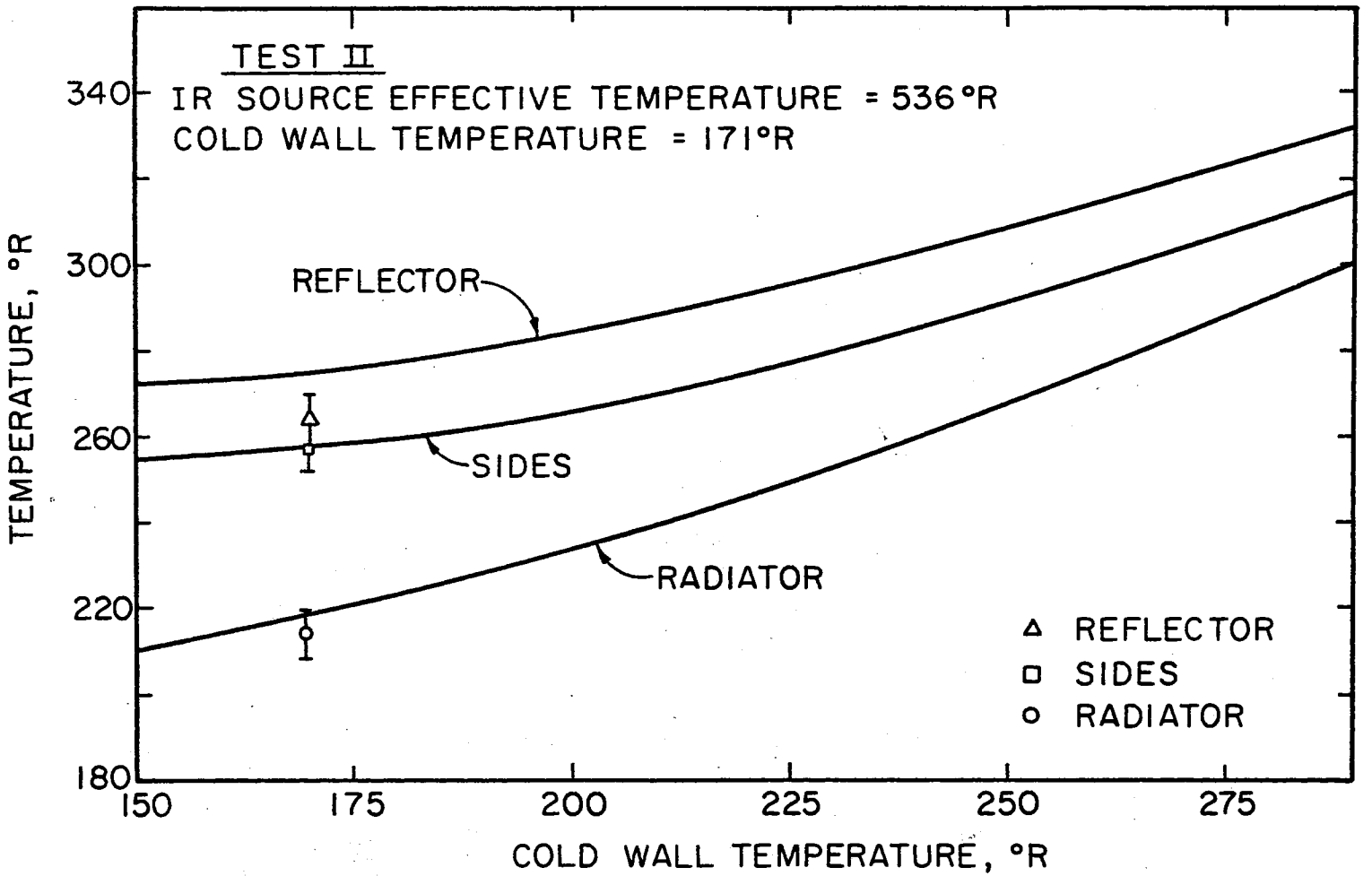

Figure 34. Test II Comparison: Test Data Versus Prediction

In Test 1, the infrared source effective temperature was 439° R and the cold wall temperature was 207° R. In Test 2, the infrared source effective temperature was 536° R and the cold wall was at 171° R.

The discrepancies between the theory and the test results are due to the uncertainties in the surface thermal properties, the thermocouple measurement error and the instrumentation error. The uncertainty in the surface thermal properties is expected to be approximately 5 per cent, thereby introducing a maximum error of ±3.75° R. The instrumentation error is assumed negligible and the thermocouple error was calculated as suggested by Newhouse (14) to yield the maximum error of less than one-half per cent of the absolute temperature, or ±1.5° R. The maximum variation between the test data and the analytical prediction should, therefore, be ±5.25° R. This band is shown as applied to the test data points in Figures 33 and 34 for tests 1 and 2.

The analytical predictions show that although lower radiator temperatures would be available from lower cold wall temperatures, the cold wall temperatures attained were sufficiently low to yield meaningful results.

The most important result desired from the analysis was to predict the radiator temperature as a function of its environment. The agreement between the analytical predictions and the test results has, thus, yielded the desired confidence in the analytical techniques which will be used in the thermal analysis for optimization of the surface radiative properties and the model geometry.

For both tests 1 and 2, the prediction of the radiator temperature was conservative. This conservative approach has been a part of the philosophy of the analytical techniques as used in this study.

CHAPTER VII

DERIVATION OF EQUATIONS

The analysis of the Cryostat System assumes that:

(1) Surfaces emit as diffuse gray surfaces.

(2) The irradiation is uniform over all surfaces.

(3) The surfaces are isothermal.

(4) Kirchoff's identity applies.

(5) Seban's assumption applies for both the solar as well as the infrared spectra.

Seban's assumption is written as

$$\rho_{total} = \rho\sigma + \rho\delta \tag{7-1}$$

where $\rho\sigma$ is the specular component of the reflectance and $\rho\delta$ is the diffuse component. The radiant interchange analysis is based on J. Holman's adaptation of Oppenheim's radiosity method (9) to account for Seban's assumption described in Equation (7-1).

The basic model to be analyzed is the enclosure of Figure 35. The radiator is shown as side 1; the closed sides are 2 and 4, and the reflector is side 3. The open sides are not labeled, but will be denoted by the subscript a.

An energy balance was derived for the internal surfaces of the enclosure with heat inputs from albedo and earth emission, conduction through the sides and a miscellaneous heat generation term added

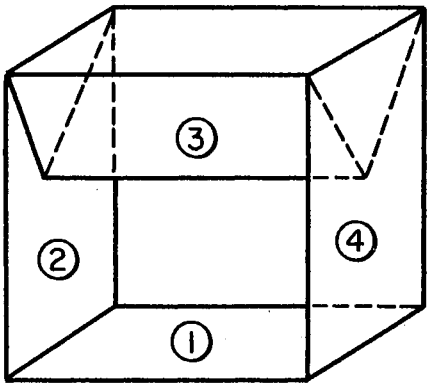

Figure 35. Analysis Model

separately to the surface. No direct solar input is present for any of the interior surfaces.

The radiant energy balance for each surface of the enclosure may be written as:

$$K_1 (J_1 - E_1) + K_5 (J_1 - J_2) + K_7 (J_1 - J_3) + K_9 (J_1 - J_4) + K_{10} (J_1 - E_5) = 0 \quad (7\text{-}2)$$

$$K_2 (J_2 - E_2) + K_5 (J_2 - J_1) + K_6 (J_2 - J_3) + K_{11} (J_2 - E_5) = 0 \quad (7\text{-}3)$$

$$K_3 (J_3 - E_3) + K_7 (J_3 - J_1) + K_6 (J_3 - J_2) + K_8 (J_3 - J_4) + K_{12} (J_3 - E_5) = 0 \quad (7\text{-}4)$$

$$K_4 (J_4 - E_4) + K_9 (J_4 - J_1) + K_8 (J_4 - J_3) + K_{13} (J_4 - E_5) = 0 \quad (7\text{-}5)$$

where E_i is the blackbody emission of surface i, J_i is the radiosity of surface i, and K_i is a thermal conductance. Surface 5 represents space. The preliminary study showed that one may assume space to be at absolute zero. Accounting for the temperature and geometric symmetry between surfaces 2 and 4 (which has already been implied in Equations (7-1) to (7-5), since no energy transfer between these surfaces has been included), the radiosity terms, J_i, may be written as:

$$J_1 = \left(\frac{K_1 E_1 + 2K_5 J_2 + K_7 J_3}{K_1 + 2K_5 + K_7 + K_{10}} \right) \quad (7\text{-}6)$$

$$J_2 = J_4 = \left(\frac{K_2 E_2 + K_5 J_1 + K_6 J_3}{K_2 + K_5 + K_6 + K_{11}} \right) \quad (7\text{-}7)$$

$$J_3 = \left(\frac{K_3 E_3 + K_7 J_1 + 2K_6 J_2}{K_3 + K_7 + 2K_6 + K_{12}} \right) . \quad (7\text{-}8)$$

The surface energy balance for each surface is written as:

$$J_1 = E_1 - Q_1 R_1 \quad (7\text{-}9)$$

$$J_2 = J_4 = E_2 - Q_2 R_2 \tag{7-10}$$

$$J_3 = E_3 - Q_3 R_3 \ . \tag{7-11}$$

Throughout the analysis, the identity $R_i = \frac{1}{K_i}$ applies. Incorporating Equations (7-9) to (7-11) into Equations (7-6) to (7-8) and rearranging, there results:

$$(2K_5 + K_7 + K_{10})E_1 - (2K_5)E_2 - (K_7)E_3$$

$$= R_1 (K_1 + 2K_5 + K_7 + K_{10})Q_1 - 2K_5 R_2 Q_2 - K_7 R_3 Q_3 \tag{7-12}$$

$$- (K_5)E_1 + (K_5 + K_6 + K_{11})E_2 - K_6 E_3$$

$$= -K_5 R_1 Q_1 + R_2 (K_2 + K_5 + K_6 + K_{11})Q_2 - K_6 R_3 Q_3 \tag{7-13}$$

$$- (K_7)E_1 - (2K_6)E_2 + (K_7 + 2K_6 + K_{12})E_3$$

$$= -K_7 R_1 Q_1 - 2K_6 R_2 Q_2 + R_3 (K_3 + K_7 + 2K_6 + K_{12})Q_3 . \tag{7-14}$$

Equations (7-12) to (7-14) are of the form:

$$a_{11}E_1 + a_{12}E_2 + a_{13}E_3 = a_{14} \tag{7-15}$$

$$a_{21}E_1 + a_{22}E_2 + a_{23}E_3 = a_{24} \tag{7-16}$$

$$a_{31}E_1 + a_{32}E_2 + a_{33}E_3 = a_{34} \ . \tag{7-17}$$

These equations appear to be linearized equations in temperature to the fourth power. However, there are non-linear (first power of temperature) terms that exist in a_{14}, a_{24}, and a_{34}. The solution accounted for these by iteration. Equations (7-15) to (7-17) are easily solved once the coefficients a_{ij} are known. As will be shown, these a_{ij} are functions of the vectors $\vec{Q}_i$ and $\vec{K}_i$. In turn, the $\vec{K}_i$ and $\vec{Q}_i$ are functions of the

thermal parameters of the analysis which are the absorptance and the specular and diffuse reflectance in both the solar and the infrared spectra for each surface. In total, this amounts to 12 independent surface thermal parameters to consider.

According to Holman's suggested procedure as described in Appendix C, the thermal conductance vector $\vec{K}$ is defined as follows:

$$K_1 = \epsilon_1 A_1 (1.0 - \rho 1,\sigma)/\rho 1,\delta \quad (7\text{-}18)$$

$$K_2 = \epsilon_2 A_2 (1.0 - \rho 2,\sigma)/\rho 2,\delta \quad (7\text{-}19)$$

$$K_3 = \epsilon_3 A_3 (1.0 - \rho 3,\sigma)/\rho 3,\delta \quad (7\text{-}20)$$

$$K_4 = K_2 ; \; K_8 = K_6 ; \; K_9 = K_5 \quad (7\text{-}21)$$

$$K_6 = A_1 [F_{1-2} + \rho 3,\sigma \; F_{1-2(3)} + \rho 4,\sigma \; F_{1-2(4)} + \rho 3,\sigma \; \rho 4,\sigma (F_{1-2(3,4)} + F_{1-2(4,3)})] \quad (7\text{-}22)$$

$$K_6 = A_3 [F_{3-2} + \rho 1,\sigma \; F_{3-2(1)} + \rho 4,\sigma \; F_{3-2(4)} + \rho 1,\sigma \; \rho 4,\sigma (F_{3-2(1,4)} + F_{3-2(4,1)})] \quad (7\text{-}23)$$

$$K_7 = A_1 [F_{1-3} + \rho 2,\sigma \; F_{1-3(2)} + \rho 4,\sigma \; F_{1-3(4)} + \rho 2,\sigma \; \rho 4,\sigma (F_{1-3(2,4)} + F_{1-3(4,2)})] \quad (7\text{-}24)$$

$$K_{10} = A_1 [F_{1-5} + \rho 2,\sigma \; F_{1-5(2)} + \rho 4,\sigma \; F_{1-5(4)} + \rho 3,\sigma \; F_{1-5(3)} + \rho 2,\sigma \; \rho 3,\sigma (F_{1-5(2,3)} + F_{1-5(3,2)}) + \rho 3,\sigma \; \rho 4,\sigma (F_{1-5(3,4)} + F_{1-5(4,3)}) + \rho 2,\sigma \; \rho 4,\sigma (F_{1-5(2,4)} + F_{1-5(4,2)})$$

$$+ \rho_{IR}^{2,\sigma}\ \rho_{IR}^{3,\sigma}\ \rho_{IR}^{4,\sigma}(F_{1-5(2,3,4)} + F_{1-5(3,4,2)} + F_{1-5(4,2,3)}$$

$$+ F_{1-5(4,3,2)} + F_{1-5(3,2,4)} + F_{1-5(2,4,3)})] \qquad (7\text{-}25)$$

$$K_{11} = A_2[F_{2-5} + \rho_{IR}^{3,\sigma}\ F_{2-5(3)} + \rho_{IR}^{4,\sigma}\ F_{2-5(4)} + \rho_{IR}^{1,\sigma}\ F_{2-5(1)}$$

$$+ \rho_{IR}^{1,\sigma}\ \rho_{IR}^{3,\sigma}(F_{2-5(1,3)} + F_{2-5(3,1)})$$

$$+ \rho_{IR}^{1,\sigma}\ \rho_{IR}^{4,\sigma}(F_{2-5(1,4)} + F_{2-5(4,1)})$$

$$+ \rho_{IR}^{4,\sigma}\ \rho_{IR}^{3,\sigma}(F_{2-5(4,3)} + F_{2-5(3,4)}) + \rho_{IR}^{2,\sigma}\ \rho_{IR}^{3,\sigma}\ \rho_{IR}^{4,\sigma}(F_{2-5(1,3,4)}$$

$$+ F_{2-5(3,4,1)} + F_{2-5(4,1,3)} + F_{2-5(4,3,1)} + F_{2-5(3,1,4)}$$

$$+ F_{2-5(1,4,3)})] \qquad (7\text{-}26)$$

$$K_{12} = A_3[F_{3-5} + \rho_{IR}^{1,\sigma}\ F_{3-5(1)} + \rho_{IR}^{2,\sigma}\ F_{3-5(2)} + \rho_{IR}^{4,\sigma}\ F_{3-5(4)}$$

$$+ \rho_{IR}^{2,\sigma}\ \rho_{IR}^{1,\sigma}(F_{3-5(2,1)} + F_{3-5(1,2)}) + \rho_{IR}^{4,\sigma}\ \rho_{IR}^{1,\sigma}(F_{3-5(4,1)} + F_{3-5(1,4)})$$

$$+ \rho_{IR}^{2,\sigma}\ \rho_{IR}^{4,\sigma}(F_{3-5(2,4)} + F_{3-5(4,2)}) + \rho_{IR}^{1,\sigma}\ \rho_{IR}^{2,\sigma}\ \rho_{IR}^{4,\sigma}(F_{3-5(1,2,4)}$$

$$+ F_{3-5(2,4,1)} + F_{3-5(4,1,2)} + F_{3-5(4,2,1)} + F_{3-5(2,1,4)}$$

$$+ F_{3-5(1,4,2)})] \qquad (7\text{-}27)$$

In Equations (7-18) to (7-27), many of the parameters for surface 4 were included to aid in their understanding. In all cases, however, all parameters for surfaces 2 and 4 were considered equivalent.

The vector $\vec{Q}$ is identified by considering the miscellaneous heat input, the conduction into the surface, the earth's emission input and the albedo input, and are defined as follows:

$$Q_1 = q1,\ \text{cond.} + q1,\ \text{misc.} + J_{IR}^{e}A_1\alpha_1[F_{1-e} + \sum_j \rho_{IR}^{j,\sigma}F_{1(j)-e}$$

$$+ \sum_j \rho_{j,\delta} F_{j-e} F_{j-1}] + J_{e_s} A_1 \alpha_{s1} [F_{1-e} + \sum_j \rho_{s_j,\sigma} F_{1(j)-e}$$

$$+ \sum_j \rho_{s_j,\delta} F_{j-e} F_{j-1}] \qquad (7\text{-}28)$$

$$Q_2 = q2,\text{cond.} + q2,\text{ misc.} + J_{e_{IR}} A_2 \alpha_{2_{IR}} [F_{2-e} + \sum_j \rho_{IR_j,\sigma} F_{2(j)-e}$$

$$+ \sum_j \rho_{IR_j,\delta} F_{j-e} F_{j-2}] + J_{e_s} A_2 \alpha_{s2} [F_{2-e} + \sum_j \rho_{s_j,\sigma} F_{2(j)-e}$$

$$+ \sum_j \rho_{s_j,\delta} F_{j-e} F_{j-2}] \qquad (7\text{-}29)$$

$$Q_3 = q3,\text{cond.} + q3,\text{ misc.} + J_{e_{IR}} A_3 \alpha_{s3} [F_{3-e} + \sum_j \rho_{IR_j,\sigma} + F_{3(j)-e}$$

$$+ \sum_j \rho_{IR_j,\delta} F_{j-e} F_{j-3}] + J_{e_s} A_3 \alpha_{s3} [F_{3-e} + \sum_j \rho_{s_j,\sigma} F_{3(j)-e}$$

$$+ \sum_j \rho_{s_j,\delta} F_{j-e} F_{j-3}] \qquad (7\text{-}30)$$

The term q_i, cond. is the conducted (non-linear term) heat input to the surface; qi, misc. is an arbitrary heat input, and $J_{e_{IR}}$ and J_{e_s} are the infrared and the solar spectra radiosity of the earth. The subscript e refers to the earth.

The conduction term q_i,cond. was obtained by considering the nodal conduction path as shown in Figure 36.

Energy arriving at surfaces 1, 2, and 3 from the exterior surfaces of the enclosure surfaces, 1b, 2b, and 3b, is given by the expression:

$$q_{i-i_b} = \frac{k_{i-i_b} A_{i-i_b}}{d_{i-i_b}} \left[T_{i_b} - \left(\frac{E_{i_b}}{\sigma} \right)^{1/4} \right] \qquad (7\text{-}31)$$

where k_{i-i_b} is the thermal conductivity normal to the layers of insulation taken as 3.8×10^{-5} BTU/HR-FT-$^\circ$R, and connecting the i node with the outside or i_b node. A_{i-i_b} is the conduction cross-section surface area and d_{i-i_b} is the thickness of insulation considered. T_{i_b} and E_{i_b} are

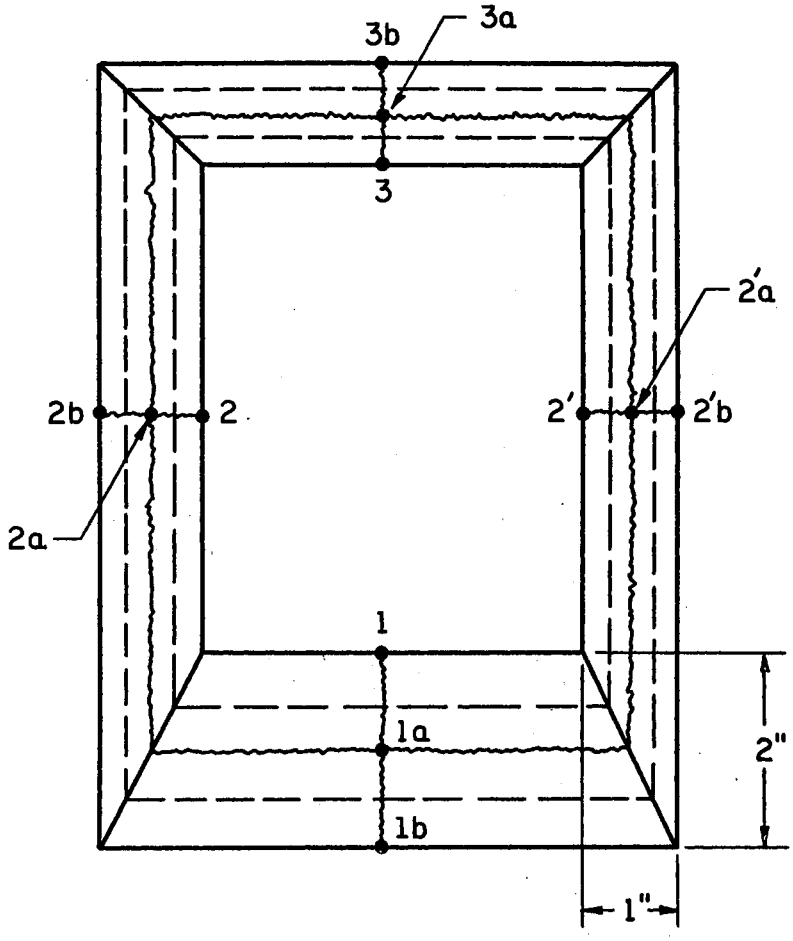

Figure 36. Nodal Conduction Path

the temperature and emissive power, respectively, of node i_b. The thermal conductivity parallel to the insulation layers was taken as .032 BTU/HR-FT-°F. A similar equation to (7-31) may be written for the energy conduction along the layers of insulation.

In the conduction input, the presence of the reflector was essentially ignored. This is conservative for the analysis and actual consideration is strongly dependent on the final design structure of the insulation and sides. In this case, the entire structure considered was comprised of insulation.

The arbitrary heat input, q_i, misc., was considered in order to study the effects of varying from the given calculated conducted energy input due to structural differences. This term was parametrically varied in the final analysis.

The earth radiosity terms of Equations (7-28) to (7-30) were calculated by the procedure described in Appendix B and are given as:

$$J_{IR_i} = G_{i,IR} / F_{O-i} \tag{7-32}$$

$$J_{s_i} = G_{i,s} / F_{O-i} \ . \tag{7-33}$$

Average values for F_{O-i} were obtained from ORAD and are listed in Appendix B in Tables VII to XVIII under the column "F" (18).

The shape factors required for many of the second and higher order multiple reflection terms in this part of the analysis could not be accurately determined with existing computer programs. The following procedure was used to estimate these shape factors. If $F_{i-j(k)}$ is a known first-order reflection term and $F_{i-j(k,l)}$ is an unknown second-order term, and if $r_{i-j(k)}$ is a mean path length between surface i and

surface j(k), and $r_{i-j(k,l)}$ is a mean path length between surface i and surface j(k,l), then the second order shape factor was formulated by

$$F_{i-j(k,l)} = F_{i-j(k)} \left(\frac{r_{i-j(k)}}{r_{i-j(k,l)}}\right)^2 . \tag{7-34}$$

Similarly, third order terms were found by

$$F_{i-j(k,l,m)} = F_{i-j(k)} \left(\frac{r_{i-j(k)}}{r_{i-j(k,l,m)}}\right)^2 . \tag{7-35}$$

The analysis is then summarized as a solution of an equation of the form (where i = 1, 2, 3),

$$\sum_{j=1}^{3} a_{ij} E_j = a_{i4} \tag{7-36}$$

where

$$a_{ij} = a_{ij}(\vec{K},\vec{Q}) \tag{7-37}$$

and

$$\vec{K} = K(P_i) \tag{7-38}$$

$$\vec{Q} = Q(P_i) \tag{7-39}$$

where P_i are the surface thermal parameters to be optimized. In general, if the reflectances are considered to be the independent parameters, all absorptances may be replaced by the term:

$$\alpha = 1 - \rho\sigma - \rho\delta . \tag{7-40}$$

The parameters to be considered are then defined in the following

way:

$$\rho\sigma_{IR},1 = P_1 \qquad \rho\sigma_{IR},2 = P_5 \qquad \rho\sigma_{IR},3 = P_9$$

$$\rho\delta_{IR},1 = P_2 \qquad \rho\delta_{IR},2 = P_6 \qquad \rho\delta_{IR},3 = P_{10}$$

$$\rho\sigma_{s},1 = P_3 \qquad \rho\sigma_{s},2 = P_7 \qquad \rho\sigma_{s},3 = P_{11}$$

$$\rho\delta_{s},1 = P_4 \qquad \rho\delta_{s},2 = P_8 \qquad \rho\delta_{s},3 = P_{12} \tag{7-41}$$

where

$$\alpha 1_{IR} = 1.0 - P_1 - P_2 = \epsilon_1$$

$$\alpha 2_{IR} = 1.0 - P_5 - P_6 = \epsilon_2$$

$$\alpha 3_{IR} = 1.0 - P_9 - P_{10} = \epsilon_3$$

$$\alpha 1_{s} = 1.0 - P_3 - P_4$$

$$\alpha 2_{s} = 1.0 - P_7 - P_8$$

$$\alpha 3_{s} = 1.0 - P_{11} - P_{12} . \tag{7-42}$$

In order to optimize these parameters, a grid search routine obtained from Mischke (15) was used. The particular subroutine which was used is called GRID 4 and is explained in detail in reference (15). It is not duplicated in this report. GRID 4 does not assure the user of avoiding false optimum solutions and the results must be considered quite thoroughly in a sensitivity check. The GRID 4 procedure forms the local optimum by allowing the search pattern to alternate between a hypercube and a hyperstar in considering the evaluation of the merit ordinant at nodes on the cube, or the star, and the midpoint. The optimum merit function then determines the new direction, as well as the center for the continuing formation of the hypervolumes. This process

continues until such time as a solution is within predetermined constraints.

In order to obtain a reasonable optimization of the proposed system, certain parameters had to be considered independently. These parameters were functions describing the thermal environment of the system. They include the orbital flux definition, which is a transient function, and the consideration of a parametric power input to the radiator, the sides and the reflector.

The orbit altitude and type have already been chosen as a result of the detailed analyses of Chapter V. The orbit is a circular polar orbit of 600 statute miles that is sun synchronous at the local noon. Having defined the orbit, Costello's (16) suggestions are followed in that if the thermally critical elements of the satellite are buried within the vehicle (the critical element in this case being the detector), and if the temperature fluctuations of thermally critical elements outside the satellite (the radiator) may be minimized by increasing the effective mass of that element, then discrete environmental conditions may be considered to replace the transient functions in order to consider the optimization of the system. Consequently, three discrete orbital thermal environmental conditions were chosen by considering the sum of the earth emission and the albedo which enters the enclosure. These conditions are given as:

1. The maximum flux condition:

   Infrared flux = 28.536 BTU/HR-FT^2

   Solar flux = 15.310 BTU/HR-FT^2

2. The average flux condition:

   Infrared flux = 13.485 BTU/HR-FT^2

Solar flux = 9.344 BTU/HR-FT^2

3. The minimum flux condition:

Infrared flux = 11.145 BTU/HR-FT^2

Solar flux = 0.0 BTU/HR-FT^2

Because of numerical requirements in the computer program, the solar flux of condition #3 could not be used. The actual value that was assigned to the solar flux was 0.001 BTU/HR-FT^2.

The final consideration for the thermal environmental conditions included the possibility of departing from the physical structure, as already considered in the derivation of the equations which will be used in the optimization program. Since it would present too limited an approach in accomplishing this task by considering other structural arrangements, it was decided to consider the inclusion of miscellaneous inputs to the radiator, the sides, and the reflector. In order to determine what these powers might be, it is noted that if radiator temperatures in the order of 200°R are to be considered, then for one square foot of area, the maximum power rejection would be 2.74 BTU per hour. For the sides and the reflector, higher temperatures and correspondingly higher powers would result. Based on this rationale, the following powers were chosen for consideration:

1. 0.0 BTU/HR.
2. 0.341 BTU/HR.
3. 3.41 BTU/HR.

The optimization of the entire system then considers the possible parametric conditions as described in Table V.

TABLE V

PARAMETRIC CONDITIONS FOR OPTIMIZATION ANALYSIS

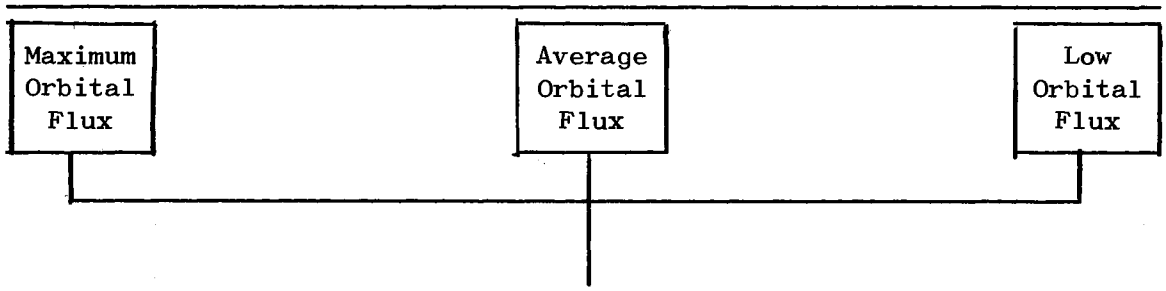

Radiator Power (BTU/HR)	Side Power (BTU/HR)	Reflector Power (BTU/HR)
0.0	0.0	0.0
0.341	0.0	0.0
3.41	0.0	0.0
0.0	0.341	0.0
0.0	3.41	0.0
0.0	0.0	0.341
0.0	0.0	3.41
0.341	0.341	0.341
3.41	3.41	3.41

CHAPTER VIII

OPTIMIZATION ANALYSIS

The optimization for the proposed design can be stated as the minimization of the radiator emissive power, E_1, where E_1 is a function of the 16 independent parameters:

$$E_1 = E_1(a, b, c, \beta, p_1, p_2, \ldots, p_{12}) \qquad (8\text{-}1)$$

The parameters a, b and c are the geometrical dimensions of the enclosure and the angle β is the angle defining the positioning of the reflector. The parameters p_1 through p_{12} are the thermal surface parameters, as described by Equation (7-41).

Initial consideration was to produce this optimization problem through the solution of the equation

$$dE_1 = 0 \, . \qquad (8\text{-}2)$$

Preliminary considerations, however, indicated that this solution may not exist for real surface properties, and therefore, a decision was made to consider a numerical solution on the digital computer which would solve the equation

$$E_1 = E_{1\,\text{minimum}} \qquad (8\text{-}3)$$

The problem was solved by treating the geometrical and the thermal parameters separately. This allowed the optimization of the geometrical

parameters to be treated as an individual problem, based on the results of the previous thermal analysis which considered the 300, 600, and 900 statute mile circular polar orbits.

The geometric parameters associated with the design include three linear dimensions and the reflector angle. Three of these parameters were initially defined by the reflector design criterion, as described in Appendix A. These include the height, the width of the closed side and the reflector angle. The remaining parameter is the width of the open side.

In consideration of the model configuration, it was evident that the optimization of the open side width would occur as the shape factor of the radiator to space increases, while no further increase in power input to the radiator is allowed. This would occur as the open side of the enclosure becomes very large. Since this is not practical, a criterion was developed that would allow an optimum, yet reasonably sized radiator. The dimensions of interest are those that describe the open side area. As described in Figure 37, the non-dimensional ratio c/a can be considered for this purpose. Since one dimension of the enclosure must be chosen to establish a base design, the value of b = 12 inches was assumed. This assumption is implicitly constrained by the requirement, established in the preliminary analyses, that the radiator area should not be less than one square foot. Through the analysis of Appendix A, the value of a is thereby defined as 14.45 inches and β as 60°. The remaining dimension, c, is left to be defined.

If the radiant inputs to the radiator are considered, neglecting the lower order reflection terms, an indication of the effect of the

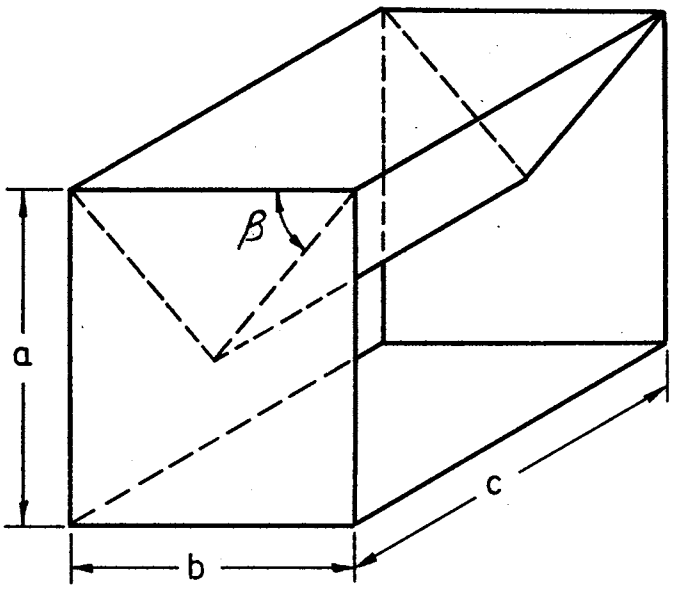

Figure 37. Enclosure Geometry

open side, Side c, can be determined as follows. From an energy balance on the radiator, the blackbody emissive power of the radiator can be written as:

$$E_1 = \left(\frac{2\ A_2F_{2-1}}{A_1F_{1-o}}\right)E_2 + \tfrac{1}{2}\left(\frac{A_4F_{4-1}}{A_1F_{1-o}}\right)E_4 \tag{8-4}$$

From the results of the previous analysis as shown in Figure 28, the following approximation between the side and the reflector temperature is made.

$$\begin{aligned} T_2 &= k_a T_4 \\ E_2 &= k_a^4 E_4 \end{aligned} \tag{8-5}$$

Using $T_2 = 290^\circ$ R and $T_4 = 340^\circ$ R, a value of k_a^4 is obtained as

$$k_a^4 = 0.853 \tag{8-6}$$

so that

$$E_2 = 0.853\ E_4 \tag{8-7}$$

Substituting Equation (8-7) into Equation (8-4) there results

$$E_1 = \left(\frac{1.706\ A_2F_{2-1} + .50\ A_4F_{4-1}}{A_1F_{1-o}}\right)E_4 \tag{8-8}$$

which is of the form:

$$E_1 = K^*E_4 \tag{8-9}$$

where

$$K^* = \left(\frac{1.706\ A_2F_{2-1} + .50\ A_4F_{4-1}}{A_1F_{1-o}}\right) \tag{8-10}$$

As K^* becomes smaller, the value of E_1 also becomes smaller. Figure 38 shows the variation of K^* with the non-dimensionalized

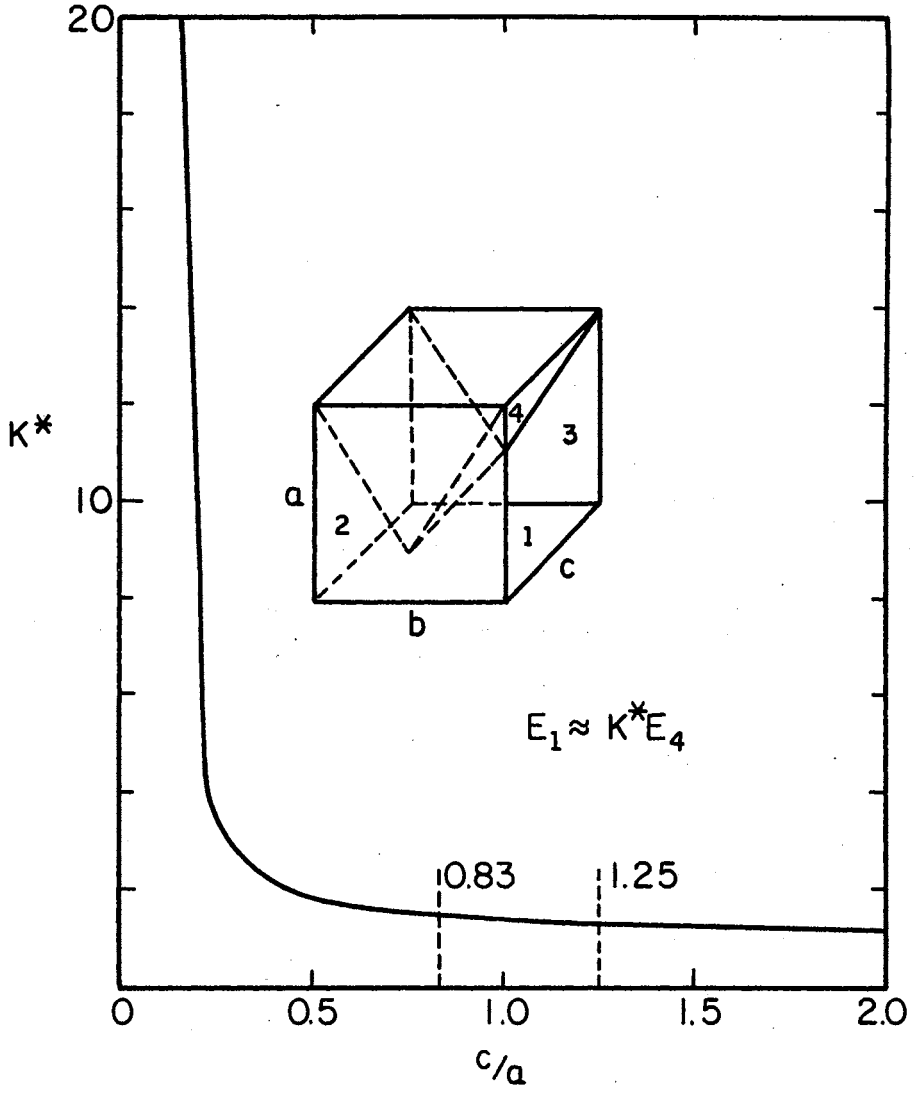

Figure 38. Variation of K* With Enclosure Size

parameter c/a, the ratio of the enclosure height to the open side width. The curve indicates that as the open side dimension, c, increases, K* causes the radiator temperature to decrease. K* is nearly constant for values of $c/a \geq 1.25$. The value of $c/a = 0.83$ is the value used for the previous analysis. The dimensional values as used in the previous work for the 600 statute-mile circular orbit may, therefore, be slightly improved to yield a more optimum design. This change increases the radiator area to 1.51 square feet. The new dimensional parameter values are:

$$a = 14.5 \text{ inches}$$

$$b = 12 \text{ inches}$$

$$c = 18.1 \text{ inches}$$

In light of this result, one can see that a similar situation does not exist for the optimization of b/a. If a is held constant and b is increased, then surface (1) could see itself in the reflector, and this contradicts the design constraint as outlined in Appendix A. If b is decreased by a constant, then β must also change. This would increase the view factor of surface (1) to space but the area of surface (1) would decrease below the desired value of 1.51 square feet as just established.

The change in the c dimension causes a slight increase in the view factor to space, but more importantly, increases the radiating area of the radiator by almost 50 per cent. There will be a proportional increase in the environmental input to the enclosure; however, this will be much less than 50 per cent. The shape factors, as used in the previous study would still be valid for the optimized enclosure dimensions, due to the absolute accuracy of their prediction methods.

CHAPTER IX

RESULTS

Two modes of analysis of the thermal parameters were considered for this problem. The first was an exploratory mode in which the general response of the parameters were investigated with direct applicability to a set of engineering surfaces, while restraining the parameters to what was considered realistic bounds. The second mode was an actual surface definition for the optimum design. The series of analyses for this final design are noted as Series M and all other work was preliminary to this series. The discussion of these modes will be considered separately. The optimized results and the sensitivity analyses are presented in tabular form in Appendix D.

Preliminary investigations show two main points. First, for the low heat loads being considered, the radiator should not be a black surface as originally assumed, but should have a relatively lower absorptance in the infrared in the order of 0.7. The diffuse infrared component of reflectance optimizes at a value of 0.0; however, for this analysis, a minimum value of 0.0458 or 0.05 was set as a constraint depending on the computer run considered. The solar absorptance of the radiator optimizes at a value of 0.0 and, therefore, a constraint of a solar absorptance of 0.05 was established. The sides and the reflector optimized in a method similar to each other. The true optimum defined a specular reflectance of 1.0 in both the infrared and solar spectra.

An initial constraint of an absorptance of 0.10 for both spectra yielded the optimum reflectance being a specular reflectance of 0.90 with a diffuse component of 0.0. Consequently, an additional constraint for a diffuse reflectance minimum of 0.05 was added. False optimum points due to the predetermined sensitivity considered for the merit function showed up in some of the results in the solar spectrum reflectances. This consistently yielded specular reflectances of 0.44 and diffuse reflectances of 0.43. A sensitivity check on these parameters showed that the analysis was quite insensitive to a variation in these parameters. However, the true optimum values were consistent with the previous pattern of a high specular value and a low diffuse value. This is true for both the solar and the infrared spectra.

Since the actual design of the cryostat must be of parametric interest at this stage, the optimization of the parameters was considered for typical environmental fluxes, as previously used in the transient analysis. Three environmental positions were considered:

1. A minimum flux which corresponds to the satellite being in the earth's shadow.
2. A maximum flux which corresponds to the maximum albedo flux position in orbit.
3. An average flux which corresponds to the position of average solar albedo input.

The values obtained for these fluxes are listed in Chapter VII.

These fluxes correspond to the powers entering the enclosure and were originally obtained from the data of Appendix B.

Further parametric information of interest are the energy inputs to each of the sides of the enclosure, in addition to that conducted

through the insulation. This would produce a useful set of optimized design data relating to the enclosure.

The tables of Appendix D present the design results and a sensitivity analysis of the models considered. Temperatures are given to one degree Rankine. Although this shadows some of the small temperature effects, particularly as concerns P_3 and P_4 of Series M, they are not felt to be important in light of the accuracy of the design effort. Blanks in the tables are read as the last value to the far left of the particular row. The first column of data presents the optimized parameters as obtained in the analysis. The adjacent columns present variations in these parameters. These variations indicate the shape of the temperature merit surface in the neighborhood of the optimum parameter. In many cases, the variation of the parameter cause the constraint to be exceeded. These cases verified the preliminary indications that were used in the introduction of these constraints. An example of this is seen in Table XXVI where the value of T_1 is reduced to 209° R due to the decrease in the diffuse reflectance below the constrained value of 0.05.

The final optimization study is made for various orbital heating conditions and various suitable internal heating levels, and is noted as Series M. The optimum parameters are given in Tables LXII to LXXXII.

The solar reflectances of the radiator are very insensitive to changes in energy inputs. Any value that was considered for these parameters within the constraints made less than 1.0° R difference in radiator temperature. The resulting design definition is then given as follows:

ITEM	MATERIAL
Radiator	Second Surface Mirrors
Sides	Highly Polished, Gold-Plated Aluminum
Reflector	Highly Polished, Gold-Plated Aluminum

Without explicit consideration, the exterior surfaces of the enclosure can be seen to require a low α/ϵ stable coating. The temperatures assumed for these surfaces in the analyses are typical for this type of coating.

The resulting temperature predictions for the interior surfaces of the enclosure are presented in Figures 39 to 41. The temperatures are plotted versus heat load which does not include the conductive input through the insulation that is always present from a 520° R exterior surface. This heat load to the surface could be due to detector Joulean heating, preamplifier heat dissipation, extra support conduction, radiation chopper and associated drivers, detector irradiation, or other miscellaneous items. Typically, the total miscellaneous energy should be no more than about 3.41 BTU/HR for all surfaces. The variations in Q_1, Q_2, and Q_3 show that the best way to remove this energy, if possible, would be via the reflector (Q_3). This would imply that all internal dissipation items should be thermally tied directly to the reflector. This is not quite true, since the reflector is still a fair radiant source of energy for the radiator. Therefore, it becomes obvious that the exterior surfaces of the enclosure, painted with a low α/ϵ coating, could be used to dissipate a considerable portion of the energy and, thereby, reduce the direct radiative load on the radiator. This could be accomplished by a system similar to that shown in Figure 8 in which

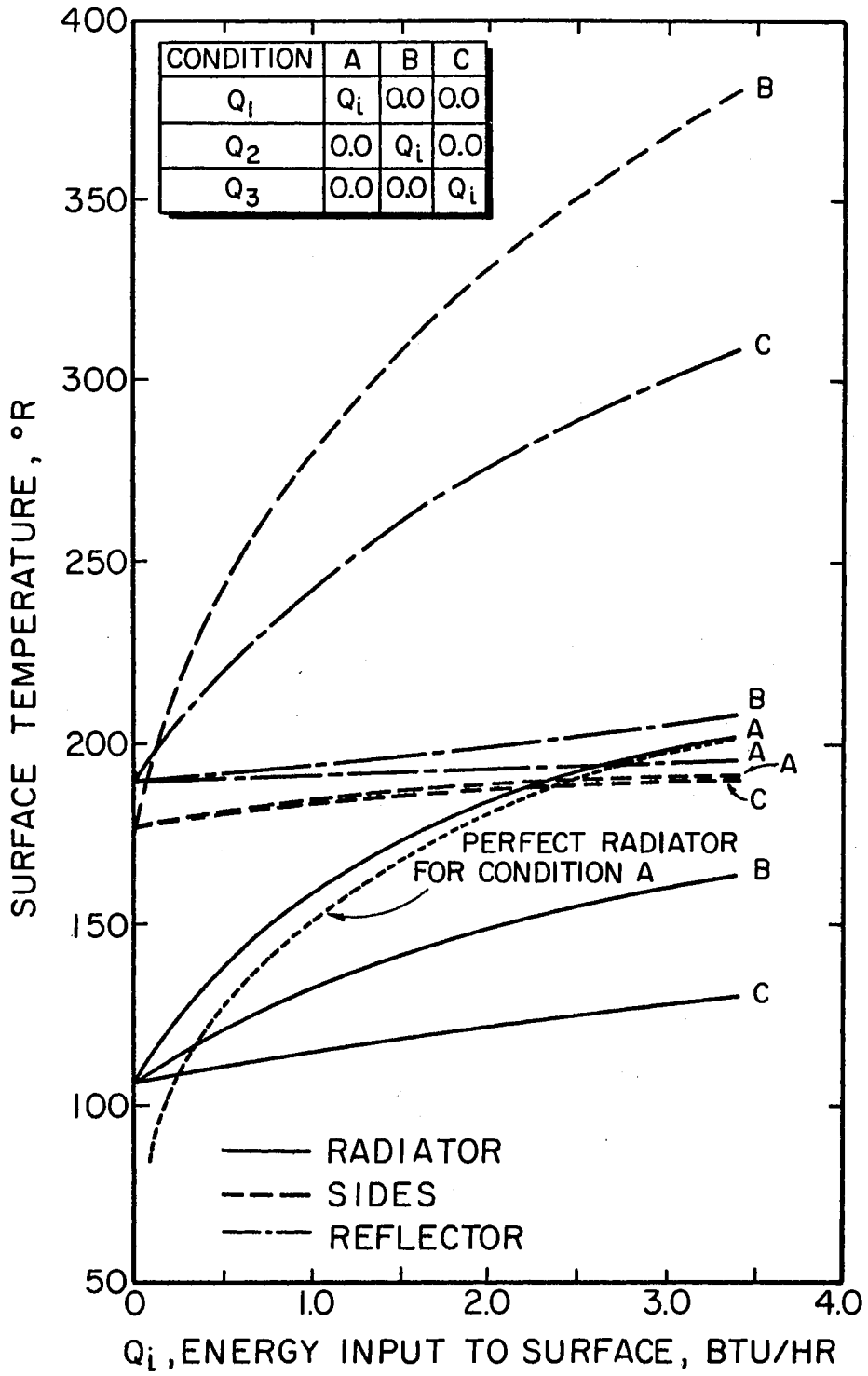

Figure 39. Parametric Surface Temperatures for Optimum Design: Minimum Environmental Heating

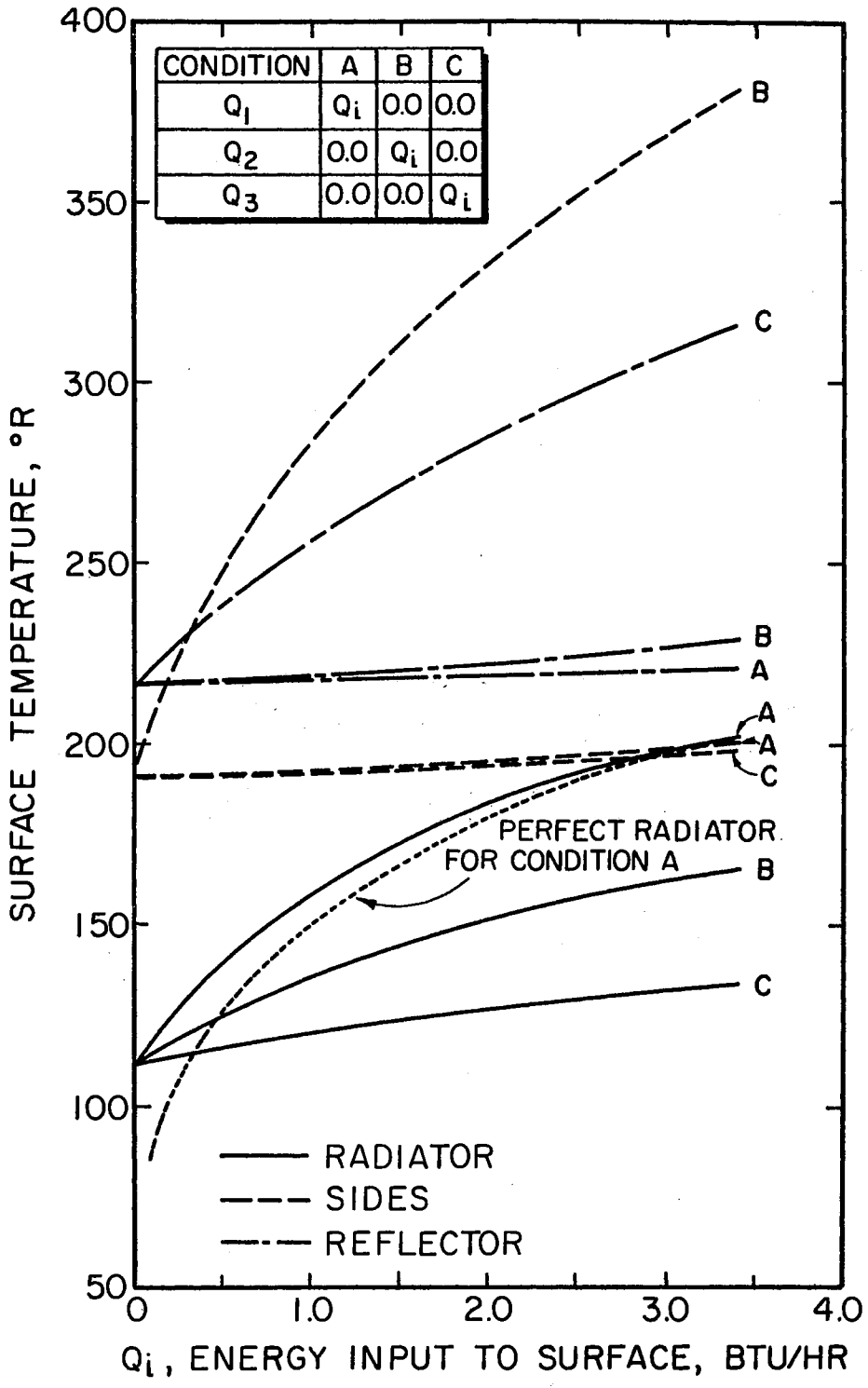

Figure 40. Parametric Surface Temperatures for Optimum Design: Average Environmental Heating

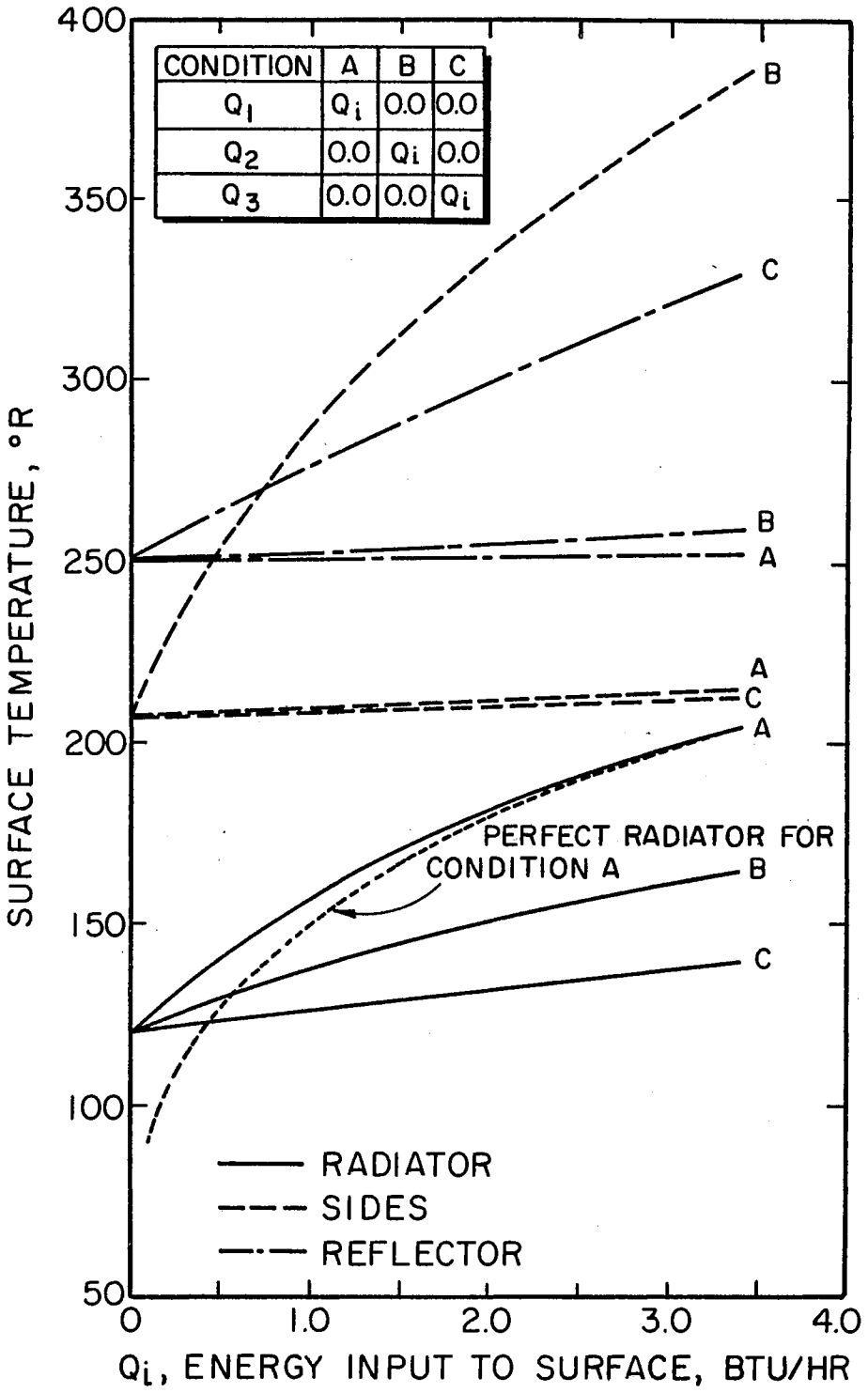

Figure 41. Parametric Surface Temperatures for Optimum Design: Maximum Environmental Heating

the majority of the heat leak from the satellite could be detoured around the radiator to the exterior surfaces of the enclosure. This approach has been implicitly incorporated into the analysis by allowing the exterior surfaces to be at a fixed temperature of 520° R.

In Figures 39-41, the surface temperatures of the sides, the reflector and the radiator are presented for heating conditions, as listed for the table on each figure. For these curves, there is heating to only one surface at a time. Figure 42 presents the results for heating of all surfaces simultaneously.

At times, the temperature of the sides is greater than that of the reflector. This is due to heat input not being on a per-unit area basis. The radiating area of the reflector is greater than that of the sides and this radiating area effectively overcompensates to yield a lower temperature.

Figures 39-42 present what is labeled as the perfect radiator curve. This was calculated for a surface of equal area and emittance, but having a view factor to space of unity. As the power input to the radiator is increased, other powers being zero, the optimum design temperature approaches the perfect radiator condition. This is shown as radiator Condition "A". Conditions "B" and "C" for the radiator do not show the results for direct heating to the radiator, but that which is conducted through the insulation from the reflector or the sides. The reflector is being heated for Condition "C" and the sides are heated for Condition "B".

At an energy input to the surface of $Q_i = 0.0$, the resulting temperature is the radiation equilibrium wall temperature, due to the

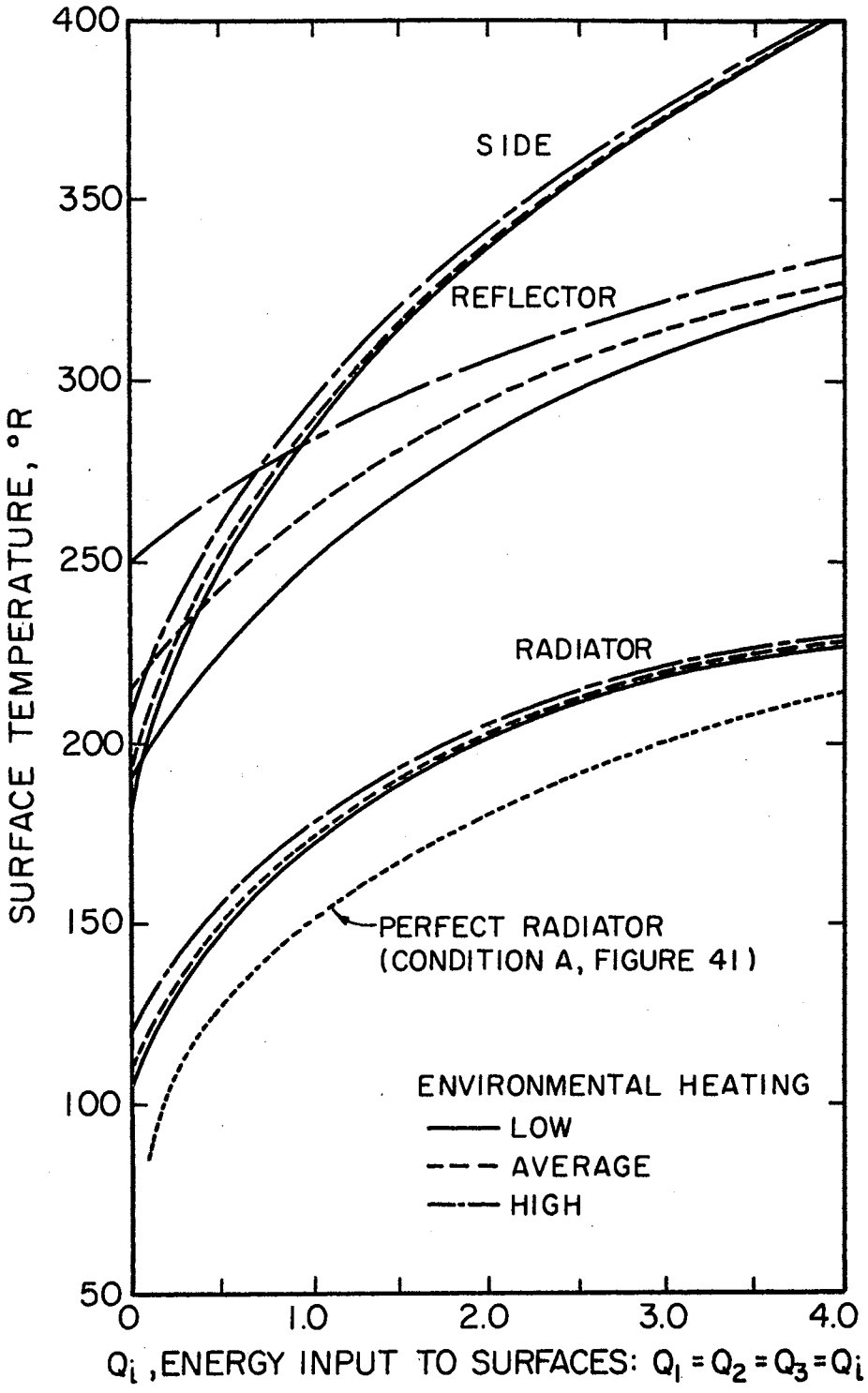

Figure 42. Parametric Surface Temperatures for Optimum Design: Equal Power for All Surfaces

conducted input through the insulation from 520° R surfaces and environmental heating through the enclosure opening.

From Figures 39 through 41 it may be noted that as the energy input to the surfaces increases to about 2.0 BTU/HR there is little difference in the resulting radiator temperatures for the various environmental heating conditions. This is a very important advantage in that a realistic cooling system for detectors would have a temperature stability criterion depending on the desired accuracy of the detector. The radiator is, therefore, sufficiently detached from the environmental energy inputs, which are highly transient, to provide this potentially stable sink for the detector. Although the analysis does not include the effects of transients on the external surfaces of the enclosure or due to the operation of internal mechanisms, it is felt that these problem areas are relatively minor and would be sensitive to the design of a particular instrument.

CHAPTER X

SUMMARY, CONCLUSIONS AND RECOMMENDATIONS

The primary objective of this study has been to design an optimized, passive, cooling system which could provide a heat sink for infrared detectors in a thermally severe earth orbit. The design goal was to provide a minimum, circular polar orbit which would result in a maximum radiator temperature of 200° R, while absorbing typical heat loads expected in such an environment, and of such a system.

Preliminary design considerations showed that for a maximum reliability (minimum solar degradation) of the thermal control surfaces, a radiator which is protected from direct solar irradiation must be used. The proposed enclosure initially utilized a black radiator with highly specularly reflecting sides and a reflector to prevent the irradiation of the radiator by earth infrared or albedo. Considering specular-diffuse reflections within the enclosure of the proposed design, analytical models were developed for circular polar orbits that were sun synchronous at the local noon and for altitudes of 300, 600 and 900 statute miles. The enclosure attitude was earth-oriented, thus allowing a consistent view to the earth by any detector foreoptics. The 200° R maximum radiator temperature established the 600-mile circular orbit as the minimum feasible orbit altitude and, therefore, the altitude adopted for the remainder of the analyses.

Thermal vacuum tests were conducted for a one-half scale radiative model, irradiated by a "hot plate" infrared source. Through comparison with the analytical predictions for the tests, the results confirmed the required confidence in the analytical techniques adopted for the study.

The optimization in the geometry for the 600-mile orbit model resulted in the consideration of a feasibility constraint rather than the choice of a true optimum due to the unacceptable system size resulting from the optimization process.

The analytical model was then refined to include higher order specular reflection terms and a set of non-linear algebraic equations were derived from an energy balance on the system. The solution of these equations was accomplished by an iterative procedure while simultaneously optimizing the thermal radiative surface properties of the system. The optimization was accomplished by a grid search computer routine.

The optimization procedure was based on the solution for the minimum radiator temperature for three sets of environmental conditions representing the maximum, the minimum, and the average infrared and solar heating, as well as suitable internal heating of the various internal components of the enclosure.

The final optimization model, Series M of Appendix D, indicated that the surface thermal properties were the same for all boundary conditions considered. A major change in the proposed model resulted from the fact that the optimum radiator emittance was not unity as had been previously assumed, but was closer to a value of 0.7. Such would be

the case for second surface mirrors. Also, the radiator area was increased by 50 per cent.

The major advantages of the system include high reliability, low weight, long life, simplicity, and the ability to operate in a low thermally severe orbit. As the orbit altitude increases, the need for such a system decreases since the high input due to earth infrared decreases. A more simple arrangement, such as a flat plate-second surface mirror radiator system, held normal to the earth's surface and directed away from the sun, would then be suitable for the same temperature level. The primary feature of the present design is that it provides a way to eliminate a direct earth emission or albedo input to the radiator. As compared to the flat plate arrangement just discussed, this reduces the direct environmental heating by 95 per cent, assuming the diffuse reflectance of the internal surfaces is about five per cent. As the altitude of the orbit increases, the absolute magnitude of this term approaches that of the internal heating and, consequently, little gain would result from such a design over the flat plate.

The use of this passive cooling method may be adapted to provide low-power input sinks for many other applications. A notable example would be the cooling for an inflight calibration source as used by microwave detectors.

BIBLIOGRAPHY

(1) Fuschillo, N., C. Schultz, and R. Gibson. "Radiation Cooled Cryostat for Infrared Detectors." Supplement to IEEE Transactions on Aerospace (June, 1955).

(2) Annable, R. V. "Radiant Cooling." Applied Optics, Vol. 9, No. 1 (January, 1970), pp. 185-193.

(3) Goldberg, I. L., L. Foshee, W. Nordberg, and C. E. Catoe. Proceedings of the Third Symposium on Remote Sensing of the Environment. Ann Arbor: University of Michigan Press, 1964, pp. 141-151.

(4) Nordberg, W. Science, 150, 559 (1965).

(5) Houis, W. A. Jr., W. A. Kley, and M. G. Strange. Applied Optics, 6, 1057 (1967).

(6) Houis, W. A. Jr., and M. Tobin. Applied Optics, 6, 1399 (1967).

(7) Christensen, E., W. C. Snoddy, R. P. Lipkis, R. E. Kidwell, Jr. "Spacecraft Thermal Design: Practical Experience." AIAA Progress in Astronautics and Aeronautics, edited by G. B. Heller. New York: Academic Press, Vol. 18, Chap. 6, 1966, p. 797.

(8) Greenberg, S. A., D. A. Vance, and E. R. Streed. "Low Solar Absorptance Surfaces With Controlled Emittance: A Second Generation of Thermal Control Coatings." AIAA Progress in Astronautics and Aeronautics, edited by G. B. Heller. New York: Academic Press, Vol. 20, Chap. 2, 1967, p. 297.

(9) Holman, J. P. "Radiation Networks for Specular-Diffuse Reflecting and Transmitting Surfaces." ASME Paper 66-WA/HT-9 (1967).

(10) Seban, R. A. Discussion on Reference (11).

(11) Sparrow, E. M., E. R. G. Eckert, and V. K. Jonsson. "An Enclosure Theory for Radiative Exchange Between Specularly and Diffusely Reflecting Surfaces." Trans. ASME, J. Heat Transfer, 84c, 294 (1962).

(12) "Handbook of Thermal Design Data for Multilayer Insulation Systems," Lockheed Missiles and Space Company, NASA-CR-67352 (1965).

(13) "Thermal Analyzer Computer Program." Lockheed California Co., LR-18-902 (1965).

(14) Newhouse, K. N. "Thermocouple Conduction Errors in a Vacuum Cold-Wall Environment." ASME Paper #67-HT-57 given at the ASME-AIChE Heat Transfer Conference, Seattle, Washington, August 6-19, 1967.

(15) Mische, C. R. An Introduction to Computer Aided Design. Englewood Cliffs, New Jersey: Prentice-Hall, Inc., 1968.

(16) Costello, F. A., T. P. Harper, R. Kidwell, and G. L. Schrenk. Selection of Spacecraft Optical Coatings for Temperature Control." AIAA Journal of Spacecraft and Rockets (December, 1969).

(17) Wiebelt, J. A. Engineering Radiation Heat Transfer. New York: Holt, Rinehart and Winston, 1966.

(18) "Computer Program for the Calculation of Incident Orbital Heat Flux." Lockheed California Company, LR-18-904 (1965).

(19) "A General Computer Program for the Determination of Radiant Interchange Configuration and Form Factors - CONFAC II." North American Aviation Inc., Space and Information Systems Division Report SID-65-10432 (1965).

APPENDIX A

REFLECTOR DESIGN METHOD

In order to optimally position the reflectors, two variables must be simultaneously considered. These are the radiator size and the orbit altitude.

A satellite in a circular orbit of altitude A_0 sees the earth through a conical angle of β_{A_0} as shown in Figure 43a. Insofar as the geometric shape factor to earth is concerned, the effective earth disc, as defined by the conical angle between the satellite and the spherical earth may be considered to take the place of the earth.

If the open side of the enclosure is now considered, all energy arriving at the enclosure from either earth emission or albedo, neglecting the input from the atmosphere, must come from a conical angle of less than β_{A_0}, where β_{A_0} is defined as

$$\beta_{A_0} = \sin^{-1}\left(\frac{r_e}{r_e + A_0}\right) \qquad \text{(A-1)}$$

where r_e = earth radius (3970 statute miles).

A radiator dimension X is chosen to be the same as that of the top of the reflector. In order to allow for some small error in the positioning of the enclosure, a small increment of ΔX is added to each side of the radiator, making the entire dimension of interest equal to $X + \Delta X$.

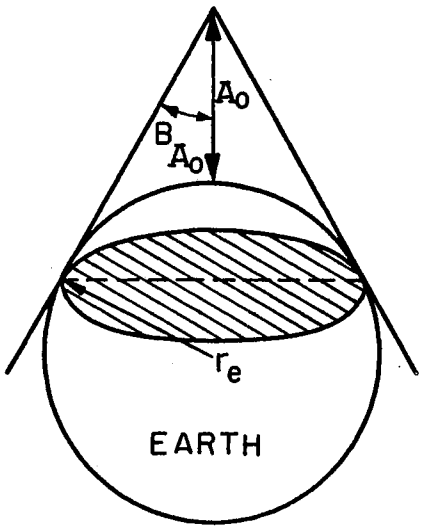

(a) EARTH DISC

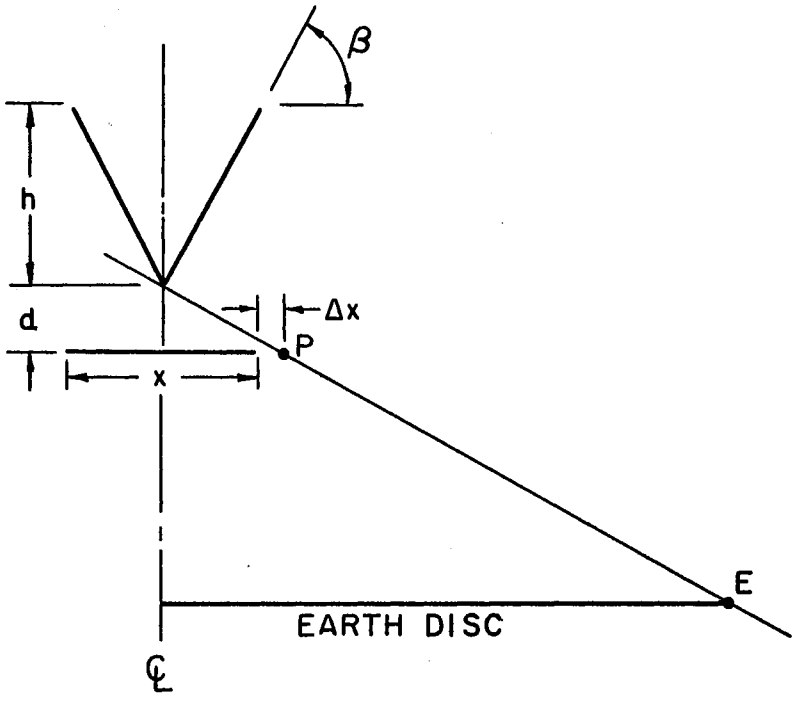

(b) REFLECTOR DESIGN

Figure 43. Reflector Design Geometry

A ray is constructed through points P and the edge of the earth disc, E. At the intersection of this ray and the centerline, a line is constructed normal to the ray and extending to the right a distance of X/2, ending at a point directly over the edge of the radiator, and thus forming the triangle shown in Figure 43b.

If the maximum value of β is thus defined, then any beam of energy originating at an angle less than β will specularly reflect in the enclosure due to the reflectors, and will eventually leave the enclosure. Consequently, a minimum value of β is determined.

If the dimensions X and ΔX, and the satellite altitude A_0 are chosen, then the dimensions of the optimum enclosure are given by the following equations:

$$H = h + d \tag{A-2}$$

$$h = \left(\frac{X}{2}\right) \tan[\beta_{A_0}] \tag{A-3}$$

$$d = \frac{\left(\frac{X}{2} + \Delta X\right)}{\tan[\beta_{A_0}]} . \tag{A-4}$$

Since β has been chosen considering the earth disc, and since the earth disc is at the larger β than any point on the radiator, then any energy that leaves the radiator and specularly reflects from the reflectors will also leave the enclosure. Further, it may be seen that any energy leaving the radiator will leave the enclosure, due to specular reflections where combinations of specular reflections occur from either the sides and/or the reflector.

Since it is impossible to obtain perfect specular reflectors, consideration will be made of the possibility of both specular and diffuse

reflectances in the analysis.

Equations (A-1) and (A-2) were solved for various orbit altitudes, and the results are shown in Figure 44 which presents the enclosure height, H, and the reflector angle, β, as a function of the orbit altitude.

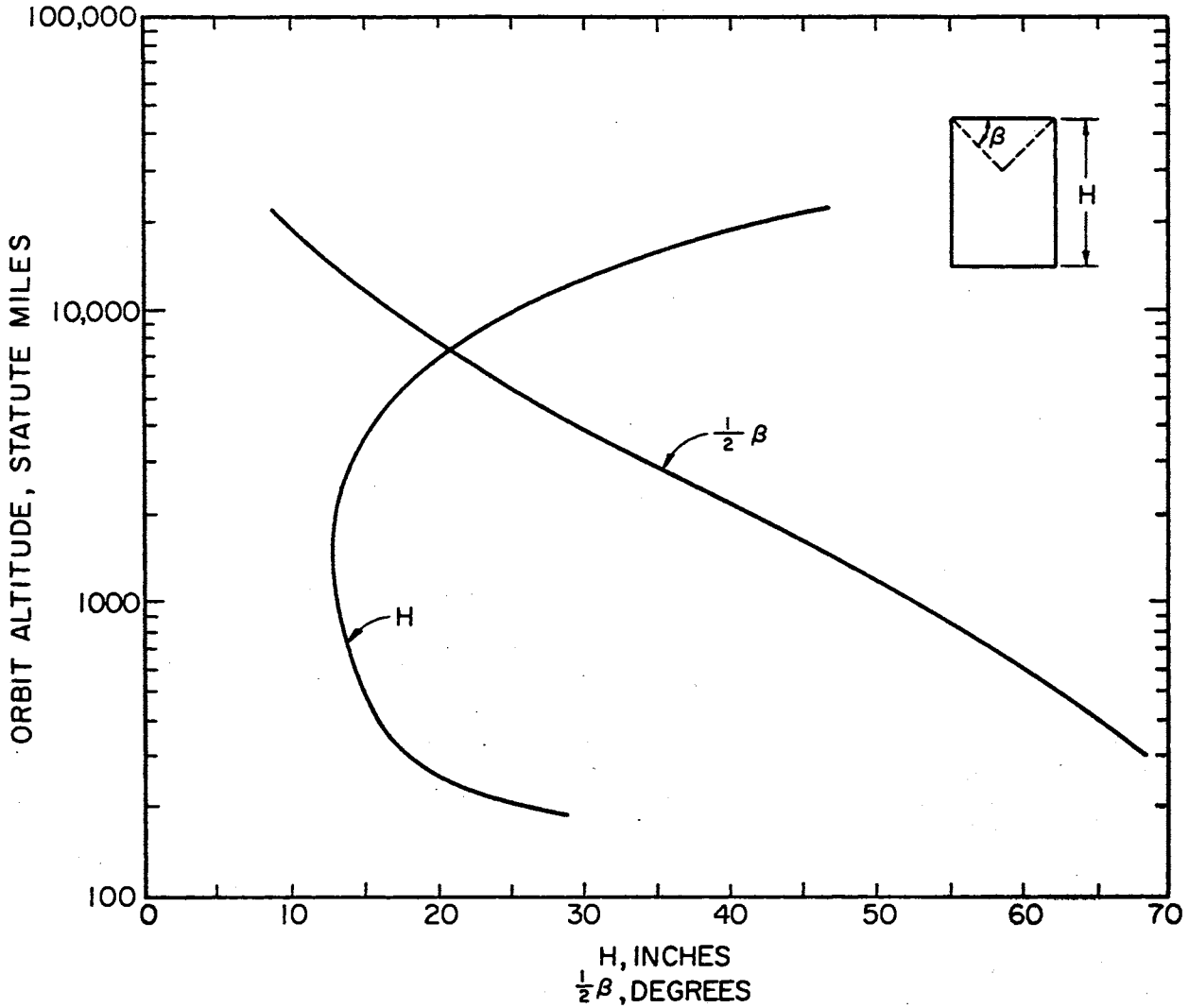

Figure 44. Enclosure Height and Reflector Angle Versus Altitude

APPENDIX B

ENVIRONMENTAL HEAT INPUTS TO THE CRYOSTAT ENCLOSURE

The major assumptions made in considering the dynamics of the environmental heat flux are as follows:

1. Diffuse reflections were ignored.
2. Specularly reflected energy was ignored after the second reflection.

A further assumption was that the radiation conductance between the two sides of the enclosure was not included in the analysis, since the sides are expected to have equal radiosities.

Based on these assumptions, the heat flux to the interior nodes of the cryostat enclosure were treated as individual heat inputs to each surface, and consideration was given to the energy entering the enclosure until after its second specular reflection. In order to determine the absorbed flux for each interior surface of the enclosure, first consider the energy which enters the open face. The earth's radiosity is considered as separable into the infrared and solar spectra, and the total irradiation of the open face of the enclosure is given as

$$A_0 G_{0_{total}} = (G_{0,IR} + G_{0,s})A_0 \tag{B-1}$$

$$A_0 (G_{0,IR} + G_{0,s}) = (J_{e,IR} + J_{e,s})A_e F_{e-0} \tag{B-2}$$

where G is the irradiation, J is the radiosity, A is the area and F is the shape factor. The subscript e refers to the earth and 0 refers to

the open face.

Using reciprocity and separating the energy spectra, Equation (B-2) may be rewritten as

$$G_{0,s} = J_{e,s} F_{0-e} \tag{B-3}$$

$$G_{0,IR} = J_{e,IR} F_{0-e} \cdot \tag{B-4}$$

Values for $G_{0,s}$, $G_{0,IR}$, and F_{0-e} were obtained from the computer program ORAD as functions of position in orbit and, therefore, time. These values are presented in Tables VI to XVII. The surfaces for these tables are described in Figure 45 where

$$G_{0,s} \equiv Q_{solar} \tag{B-5}$$

$$G_{0,IR} \equiv Q_{IR} \tag{B-6}$$

$$F_{0-e} \equiv F \tag{B-7}$$

and the terms on the right side of these equations are those appearing in the tables of this Appendix. The effective radiosity of the earth is then given as

$$J_{e,s} = G_{0,s}/F_{0-e} \tag{B-8}$$

$$J_{e,IR} = G_{0,IR}/F_{0-e} \cdot \tag{B-9}$$

The radiator receives no direct or specularly reflected energy from the earth and its environmental inputs are thereby given as

$$Q_{IR,1} = 0.0 \tag{B-10}$$

$$Q_{s,1} = 0.0 \tag{B-11}$$

TABLE VI

SURFACE 1 AND 3 HEAT FLUX; 300 MILE CIRCULAR POLAR ORBIT

	θ	T	Q_P	Q_{PR}	Q_S	Q_{solar}	Q_{IR}	F
	0.	0.0	16.891	2.109	0.0	2.109	16.891	0.31302
	15.	0.065	15.366	0.005	0.0	0.005	15.366	0.27138
	21.	0.092	15.898	0.000	0.0	0.000	15.898	0.27182
SH	22.	0.096	16.054	0.0	0.0	0.0	16.054	0.27242
SH	30.	0.131	16.194	0.0	0.0	0.0	16.194	0.26253
SH	45.	0.196	18.682	0.0	0.0	0.0	18.682	0.27513
SH	60.	0.262	20.782	0.0	0.0	0.0	20.782	0.27856
SH	75.	0.327	21.648	0.0	0.0	0.0	21.648	0.28106
SH	90.	0.393	21.514	0.0	0.0	0.0	21.514	0.28179
SH	105.	0.458	21.936	0.0	0.0	0.0	21.936	0.28086
SH	120.	0.524	21.321	0.0	0.0	0.0	21.321	0.27856
SH	135.	0.589	19.696	0.0	0.0	0.0	19.696	0.27513
SH	150.	0.654	17.536	0.0	0.0	0.0	17.536	0.26230
SH	158.	0.689	17.127	0.0	0.0	0.0	17.127	0.27217
	159.	0.694	16.960	0.000	0.0	0.000	16.960	0.27182
	165.	0.720	16.345	0.006	0.0	0.006	16.345	0.27123
	180.	0.785	15.906	2.294	0.0	2.294	15.906	0.27195
	195.	0.851	16.345	18.259	0.0	18.259	16.345	0.27123
	210.	0.916	17.085	27.605	0.0	27.605	17.085	0.25551
	225.	0.982	19.573	30.524	0.0	30.524	19.573	0.27341
	240.	1.047	21.321	29.195	0.0	29.195	21.321	0.27856
	255.	1.113	21.936	36.218	0.0	36.216	21.936	0.28086
	270.	1.178	21.514	41.515	0.0	41.515	21.514	0.28179
	285.	1.243	21.616	33.902	0.0	33.902	21.616	0.28065
	300.	1.309	20.782	28.475	0.0	28.475	20.782	0.27856
	315.	1.374	18.567	28.743	0.0	28.743	18.567	0.27341
	330.	1.440	15.764	21.831	0.0	21.831	15.764	0.25552
	345.	1.505	16.366	16.734	0.0	16.734	15.366	0.27138
	360.	1.571	16.891	2.109	0.0	2.109	16.891	0.31302

TABLE VII

SURFACE 2 HEAT FLUX; 300 MILE CIRCULAR POLAR ORBIT

	θ	T	Q_P	Q_{PR}	Q_S	Q_{solar}	Q_{IR}	F
	0.	0.0	17.275	6.844	447.340	454.184	17.275	0.32010
	15.	0.065	15.806	0.046	432.097	432.144	15.806	0.28464
	21.	0.092	15.758	0.000	417.628	417.628	15.758	0.28062
SH	22.	0.096	14.804	0.0	0.0	0.0	14.804	0.26319
SH	30.	0.131	15.965	0.0	0.0	0.0	15.965	0.26836
SH	45.	0.196	18.566	0.0	0.0	0.0	18.566	0.28056
SH	60.	0.262	20.353	0.0	0.0	0.0	20.353	0.28176
SH	75.	0.327	21.674	0.0	0.0	0.0	21.674	0.28183
SH	90.	0.393	21.294	0.0	0.0	0.0	21.294	0.28183
SH	105.	0.458	21.937	0.0	0.0	0.0	21.937	0.28183
SH	120.	0.524	22.066	0.0	0.0	0.0	22.066	0.28177
SH	135.	0.589	20.456	0.0	0.0	0.0	20.456	0.28152
SH	150.	0.654	19.458	0.0	0.0	0.0	19.458	0.27998
SH	158.	0.689	17.193	0.0	0.0	0.0	17.193	0.26390
	159.	0.694	18.176	0.0	0.0	0.0	18.176	0.28048
	165.	0.720	17.196	0.0	0.0	0.0	17.195	0.27981
	180.	0.785	15.907	0.0	0.0	0.0	15.907	0.27195
	195.	0.851	16.621	12.863	0.0	12.863	16.621	0.28001
	210.	0.916	17.023	27.053	0.0	27.053	17.023	0.26836
	225.	0.982	19.817	31.059	0.0	31.059	19.817	0.28056
	240.	1.047	20.944	28.821	0.0	28.821	20.944	0.28176
	255.	1.113	22.031	34.206	0.0	34.206	22.031	0.28183
	270.	1.178	21.812	41.750	0.0	41.750	21.812	0.28183
	285.	1.243	21.598	36.703	115.776	152.479	21.598	0.28183
	300.	1.309	21.550	29.002	223.666	252.668	21.550	0.28178
	315.	1.374	19.596	30.550	316.314	346.864	19.596	0.28152
	330.	1.440	17.814	26.174	387.406	413.579	17.814	0.27998
	345.	1.505	16.142	21.225	432.096	453.321	16.142	0.27981
	360.	1.571	17.275	6.844	447.340	454.184	17.275	0.32011

TABLE VIII

SURFACE 4 HEAT FLUX; 300 MILE CIRCULAR POLAR ORBIT

	θ	T	Q_P	Q_{PR}	Q_S	Q_{solar}	Q_{IR}	F
	0.	0.0	16.946	0.0	0.0	0.0	16.946	0.31406
	15.	0.065	16.142	0.0	0.0	0.0	16.142	0.27982
	21.	0.092	16.949	0.0	0.0	0.0	16.949	0.28048
SH	22.	0.095	16.002	0.0	0.0	0.0	16.002	0.26391
SH	30.	0.131	17.815	0.0	0.0	0.0	17.815	0.27998
SH	45.	0.196	19.596	0.0	0.0	0.0	19.596	0.28152
SH	60.	0.262	21.550	0.0	0.0	0.0	21.550	0.28177
SH	75.	0.327	21.598	0.0	0.0	0.0	21.598	0.28183
SH	90.	0.393	21.812	0.0	0.0	0.0	21.812	0.28183
SH	105.	0.458	22.031	0.0	0.0	0.0	22.031	0.28183
SH	120.	0.524	20.944	0.0	0.0	0.0	20.944	0.28176
SH	135.	0.589	19.817	0.0	0.0	0.0	19.817	0.28056
SH	150.	0.654	17.023	0.0	0.0	0.0	17.023	0.26836
SH	158.	0.689	15.739	0.0	0.0	0.0	15.739	0.26309
	159.	0.694	16.745	0.000	417.626	417.626	16.745	0.28033
	165.	0.720	16.621	0.052	432.097	432.148	16.621	0.28000
	180.	0.785	16.322	7.444	447.340	454.784	16.322	0.27906
	195.	0.851	17.195	24.366	432.098	456.464	17.195	0.27981
	210.	0.916	19.458	31.687	387.409	419.096	19.458	0.27998
	225.	0.982	20.456	31.490	316.319	347.809	20.456	0.28152
	240.	1.047	22.066	31.278	223.673	254.951	22.066	0.28177
	255.	1.113	21.936	38.710	115.783	154.494	21.936	0.28183
	270.	1.178	21.294	40.321	0.004	40.325	21.294	0.28183
	285.	1.243	21.674	31.909	0.0	31.909	21.674	0.28183
	300.	1.309	20.353	29.460	0.0	29.460	20.353	0.28176
	315.	1.374	18.566	27.871	0.0	27.871	18.566	0.28056
	330.	1.440	15.965	20.901	0.0	20.901	15.965	0.26836
	345.	1.505	15.806	12.128	0.0	12.128	15.806	0.28463
	360.	1.571	16.946	0.0	0.0	0.0	16.946	0.31405

TABLE IX

SURFACE 5 HEAT FLUX; 300 MILE CIRCULAR POLAR ORBIT

	θ	T	Q_P	Q_{PR}	Q_S	Q_{solar}	Q_{IR}	F
	0.	0.0	0.0	0.0	0.000	0.000	0.0	0.0
	15.	0.065	0.0	0.0	0.0	0.0	0.0	0.0
	21.	0.092	0.0	0.0	0.0	0.0	0.0	0.0
SH	22.	0.096	0.0	0.0	0.0	0.0	0.0	0.0
SH	30.	0.131	0.0	0.0	0.0	0.0	0.0	0.0
SH	45.	0.196	0.0	0.0	0.0	0.0	0.0	0.0
SH	60.	0.262	0.0	0.0	0.0	0.0	0.0	0.0
SH	75.	0.327	0.0	0.0	0.0	0.0	0.0	0.0
SH	90.	0.393	0.0	0.0	0.0	0.0	0.0	0.0
SH	105.	0.458	0.0	0.0	0.0	0.0	0.0	0.0
SH	120.	0.524	0.0	0.0	0.0	0.0	0.0	0.0
SH	135.	0.589	0.0	0.0	0.0	0.0	0.0	0.0
SH	150.	0.654	0.0	0.0	0.0	0.0	0.0	0.0
SH	158.	0.689	0.0	0.0	0.0	0.0	0.0	0.0
	159.	0.694	0.0	0.0	0.0	0.0	0.0	0.0
	165.	0.720	0.0	0.0	0.0	0.0	0.0	0.0
	180.	0.785.	0.0	0.0	0.0	0.0	0.0	0.0
	195.	0.851	0.0	0.0	115.778	115.778	0.0	0.0
	210.	0.916	0.0	0.0	223.668	223.668	0.0	0.0
	225.	0.982	0.0	0.0	316.315	316.315	0.0	0.0
	240.	1.047	0.0	0.0	387.406	387.406	0.0	0.0
	255.	1.113	0.0	0.0	432.097	432.097	0.0	0.0
	270.	1.178	0.0	0.0	447.340	447.340	0.0	0.0
	285.	1.243	0.0	0.0	432.098	432.098	0.0	0.0
	300.	1.309	0.0	0.0	387.410	387.410	0.0	0.0
	315.	1.374	0.0	0.0	316.320	316.320	0.0	0.0
	330.	1.440	0.0	0.0	223.674	223.674	0.0	0.0
	345.	1.505	0.0	0.0	115.785	115.785	0.0	0.0
	360.	1.571	0.0	0.0	0.005	0.005	0.0	0.0

TABLE X

SURFACE 1 AND 3 HEAT FLUX; 600 MILE CIRCULAR POLAR ORBIT

	θ	T	Q_P	Q_{PR}	Q_S	Q_{solar}	Q_{IR}	F
	0.	0.0	11.262	2.336	0.0	2.336	11.262	0.20400
	15.	0.072	11.363	0.070	0.0	0.070	11.363	0.19818
	29.	0.140	12.256	0.000	0.0	0.000	12.256	0.19856
SH	30.	0.145	11.146	0.0	0.0	0.0	11.146	0.17915
SH	45.	0.217	13.374	0.0	0.0	0.0	13.374	0.19604
SH	60.	0.290	14.837	0.0	0.0	0.0	14.837	0.19942
SH	75.	0.362	15.346	0.0	0.0	0.0	15.346	0.20006
SH	90.	0.435	15.310	0.0	0.0	0.0	15.310	0.20003
SH	105.	0.507	15.574	0.0	0.0	0.0	15.574	0.19988
SH	120.	0.580	15.229	0.0	0.0	0.0	15.229	0.19942
SH	135.	0.652	14.086	0.0	0.0	0.0	14.086	0.19604
SH	150.	0.725	12.027	0.0	0.0	0.0	12.027	0.17894
	151.	0.730	11.844	0.0	0.0	0.0	11.844	0.17650
	165.	0.797	12.111	0.075	0.0	0.075	12.111	0.19793
	180.	0.870	11.735	2.560	0.0	2.560	11.735	0.19787
	195.	0.942	12.111	12.676	0.0	12.676	12.111	0.19793
	210.	1.015	11.560	18.103	0.0	18.103	11.560	0.17193
	225.	1.087	13.882	20.979	0.0	20.979	13.882	0.19317
	240.	1.160	15.183	21.084	0.0	21.084	15.183	0.19881
	255.	1.232	15.574	25.540	0.0	25.540	15.574	0.19988
	270.	1.305	15.310	28.536	0.0	28.536	15.310	0.20003
	285.	1.377	15.319	24.080	0.0	24.080	15.319	0.19970
	300.	1.450	14.792	20.419	0.0	20.419	14.792	0.19881
	315.	1.522	13.182	19.671	0.0	19.671	13.182	0.19317
	330.	1.594	10.701	14.694	0.0	14.694	10.701	0.17193
	345.	1.667	11.364	11.096	0.0	11.096	11.364	0.19818
	360.	1.739	11.262	2.336	0.0	2.336	11.262	0.20400

TABLE XI

SURFACE 2 HEAT FLUX; 600 MILE CIRCULAR POLAR ORBIT

	θ	T	Q_P	Q_{PR}	Q_S	Q_{solar}	Q_{IR}	F
	0.	0.0	11.548	7.581	447.340	454.920	11.548	0.20917
	15.	0.072	11.438	0.454	432.097	432.551	11.438	0.20762
	29.	0.140	11.580	0.000	391.253	391.253	11.580	0.19817
SH	30.	0.145	10.207	0.0	0.0	0.0	10.207	0.17362
SH	45.	0.217	12.636	0.0	0.0	0.0	12.636	0.19579
SH	60.	0.290	14.148	0.0	0.0	0.0	14.148	0.19959
SH	75.	0.362	15.247	0.0	0.0	0.0	15.247	0.19998
SH	90.	0.435	15.210	0.0	0.0	0.0	15.210	0.20005
SH	105.	0.507	15.468	0.0	0.0	0.0	15.468	0.19996
SH	120.	0.580	15.634	0.0	0.0	0.0	15.634	0.19980
SH	135.	0.652	14.788	0.0	0.0	0.0	14.788	0.19946
SH	150.	0.725	13.896	0.0	0.0	0.0	13.896	0.19781
	151.	0.730	13.800	0.0	0.0	0.0	13.800	0.19756
	165.	0.797	12.642	0.0	0.0	0.0	12.642	0.19883
	180.	0.870	11.735	0.0	0.0	0.0	11.735	0.19787
	195.	0.942	11.812	6.415	0.0	6.415	11.812	0.19973
	210.	1.015	10.880	15.853	0.0	15.853	10.880	0.17363
	225.	1.087	13.608	21.597	0.0	21.597	13.608	0.19579
	240.	1.160	14.666	20.868	0.0	20.868	14.666	0.19959
	255.	1.232	15.563	22.878	0.0	22.878	15.563	0.19998
	270.	1.305	15.530	28.299	0.0	28.299	15.530	0.20005
	285.	1.377	15.250	27.475	115.776	143.251	15.250	0.19997
	300.	1.450	15.317	21.736	223.666	245.403	15.317	0.19980
	315.	1.522	14.292	20.940	316.314	337.254	14.292	0.19947
	330.	1.594	12.889	19.285	387.405	406.690	12.889	0.19781
	345.	1.667	11.804	15.260	432.096	447.355	11.804	0.19888
	360.	1.739	11.549	7.581	447.340	464.921	11.549	0.20917

TABLE XII

SURFACE 4 HEAT FLUX; 600 MILE CIRCULAR POLAR ORBIT

	θ	T	Q_P	Q_{PR}	Q_S	Q_{solar}	Q_{IR}	F
	0.	0.0	11.271	0.0	0.0	0.0	11.271	0.20415
	15.	0.072	11.804	0.0	0.0	0.0	11.804	0.19883
	29.	0.140	12.886	0.0	0.0	0.0	12.836	0.19802
SH	30.	0.145	12.890	0.0	0.0	0.0	12.890	0.19782
SH	45.	0.217	14.292	0.0	0.0	0.0	14.292	0.19947
SH	60.	0.290	15.317	0.0	0.0	0.0	15.317	0.19980
SH	75.	0.362	15.250	0.0	0.0	0.0	15.250	0.19997
SH	90.	0.435	15.530	0.0	0.0	0.0	15.530	0.20005
SH	105.	0.507	15.563	0.0	0.0	0.0	15.563	0.19998
SH	120.	0.580	14.666	0.0	0.0	0.0	14.666	0.19959
SH	135.	0.652	13.608	0.0	0.0	0.0	13.608	0.19579
SH	150.	0.725	10.880	0.0	0.0	0.0	10.880	0.17363
	151.	0.730	10.695	0.0	391.249	391.249	10.695	0.17067
	165.	0.797	11.812	0.492	432.097	432.588	11.812	0.19973
	180.	0.870	12.042	8.305	447.340	455.645	12.042	0.20304
	195.	0.942	12.642	18.644	432.098	450.741	12.642	0.19882
	210.	1.015	13.896	22.279	387.409	409.688	13.896	0.19781
	225.	1.087	14.788	21.253	316.319	337.572	14.788	0.19946
	240.	1.160	15.634	23.355	223.673	247.028	15.634	0.19980
	255.	1.232	15.468	28.433	115.733	144.216	15.468	0.19996
	270.	1.305	15.210	27.084	0.004	27.088	15.210	0.20005
	285.	1.377	15.247	21.511	0.0	21.511	15.247	0.19998
	300.	1.450	14.148	20.758	0.0	20.758	14.148	0.19959
	315.	1.522	12.636	18.484	0.0	18.484	12.636	0.19579
	330.	1.594	10.207	12.731	0.0	12.781	10.207	0.17363
	345.	1.667	11.438	6.000	0.0	6.000	11.438	0.20762
	360.	1.739	11.270	0.0	0.0	0.0	11.270	0.20415

TABLE XIII

SURFACE 5 HEAT FLUX; 600 MILE CIRCULAR POLAR ORBIT

	θ	T	Q_P	Q_{PR}	Q_S	Q_{solar}	Q_{IR}	F
	0.	0.0	0.0	0.0	0.000	0.000	0.0	0.0
	15.	0.072	0.0	0.0	0.0	0.0	0.0	0.0
	29.	0.140	0.0	0.0	0.0	0.0	0.0	0.0
SH	30.	0.145	0.0	0.0	0.0	0.0	0.0	0.0
SH	45.	0.217	0.0	0.0	0.0	0.0	0.0	0.0
SH	60.	0.290	0.0	0.0	0.0	0.0	0.0	0.0
SH	75.	0.362	0.0	0.0	0.0	0.0	0.0	0.0
SH	90.	0.435	0.0	0.0	0.0	0.0	0.0	0.0
SH	105.	0.507	0.0	0.0	0.0	0.0	0.0	0.0
SH	120.	0.580	0.0	0.0	0.0	0.0	0.0	0.0
SH	135.	0.652	0.0	0.0	0.0	0.0	0.0	0.0
SH	150.	0.725	0.0	0.0	0.0	0.0	0.0	0.0
	151.	0.730	0.0	0.0	0.0	0.0	0.0	0.0
	165.	0.797	0.0	0.0	0.0	0.0	0.0	0.0
	180.	0.870	0.0	0.0	0.0	0.0	0.0	0.0
	195.	0.942	0.0	0.0	115.778	115.778	0.0	0.0
	210.	1.015	0.0	0.0	223.668	223.668	0.0	0.0
	225.	1.087	0.0	0.0	316.315	316.315	0.0	0.0
	240.	1.160	0.0	0.0	387.406	387.406	0.0	0.0
	255.	1.232	0.0	0.0	432.097	432.097	0.0	0.0
	270.	1.305	0.0	0.0	447.340	447.340	0.0	0.0
	285.	1.377	0.0	0.0	432.098	432.098	0.0	0.0
	300.	1.450	0.0	0.0	387.410	387.410	0.0	0.0
	315.	1.522	0.0	0.0	316.320	316.320	0.0	0.0
	330.	1.594	0.0	0.0	223.674	223.674	0.0	0.0
	345.	1.667	0.0	0.0	115.785	115.785	0.0	0.0
	360.	1.739	0.0	0.0	0.005	0.005	0.0	0.0

TABLE XIV

SURFACE 1 AND 3 HEAT FLUX; 900 MILE CIRCULAR POLAR ORBIT

	θ	T	Q_P	Q_{PR}	Q_S	Q_{solar}	Q_{IR}	F
	0.	0.0	8.694	2.174	0.0	2.174	8.694	0.15470
	15.	0.080	8.886	0.160	0.0	0.160	8.886	0.15306
	30.	0.159	9.583	0.001	0.0	0.001	9.583	0.15319
	35.	0.186	9.863	0.000	0.0	0.000	9.863	0.15307
SH	36.	0.191	9.276	0.0	0.0	0.0	9.276	0.14272
SH	45.	0.239	10.273	0.0	0.0	0.0	10.273	0.14992
SH	60.	0.319	11.377	0.0	0.0	0.0	11.377	0.15336
SH	75.	0.399	11.763	0.0	0.0	0.0	11.763	0.15379
SH	90.	0.478	11.785	0.0	0.0	0.0	11.785	0.15368
SH	105.	0.558	11.938	0.0	0.0	0.0	11.938	0.15363
SH	120.	0.638	11.686	0.0	0.0	0.0	11.686	0.15336
SH	135.	0.718	10.805	0.0	0.0	0.0	10.805	0.14992
SH	144.	0.766	9.933	0.0	0.0	0.0	9.933	0.14273
	145.	0.771	9.810	0.0	0.0	0.0	9.810	0.14151
	150.	0.797	10.300	0.001	0.0	0.001	10.300	0.15300
	165.	0.877	9.488	0.174	0.0	0.174	9.488	0.15284
	180.	0.957	9.195	2.442	0.0	2.442	9.195	0.15281
	195.	1.037	9.488	9.354	0.0	9.354	9.488	0.15284
	210.	1.116	10.299	14.845	0.0	14.845	10.299	0.15300
	225.	1.196	10.636	15.638	0.0	15.638	10.636	0.14753
	240.	1.276	11.644	16.339	0.0	16.339	11.644	0.15279
	255.	1.356	11.938	19.395	0.0	19.395	11.938	0.15363
	270.	1.435	11.785	21.243	0.0	21.243	11.785	0.15368
	285.	1.515	11.739	18.411	0.0	18.411	11.739	0.15347
	300.	1.595	11.336	15.736	0.0	15.736	11.336	0.15279
	315.	1.675	10.113	14.613	0.0	14.613	10.113	0.14753
	330.	1.754	9.573	12.334	0.0	12.334	9.573	0.15301
	345.	1.834	8.886	7.983	0.0	7.983	8.886	0.15307
	360.	1.914	8.694	2.174	0.0	2.174	8.694	0.15470

TABLE XV

SURFACE 2 HEAT FLUX; 900 MILE CIRCULAR POLAR ORBIT

	θ	T	Q_P	Q_{PR}	Q_S	Q_{solar}	Q_{IR}	F
	0.	0.0	8.919	7.055	447.340	454.395	8.919	0.15869
	15.	0.080	8.895	0.935	432.097	433.032	8.895	0.16135
	30.	0.159	8.950	0.007	387.408	387.415	8.950	0.15386
	35.	0.186	9.144	0.000	366.440	366.440	9.144	0.15298
SH	36.	0.191	8.281	0.0	0.0	0.0	8.281	0.13761
SH	45.	0.239	9.430	0.0	0.0	0.0	9.430	0.14843
SH	60.	0.319	10.691	0.0	0.0	0.0	10.691	0.15319
SH	75.	0.399	11.604	0.0	0.0	0.0	11.604	0.15361
SH	90.	0.478	11.726	0.0	0.0	0.0	11.726	0.15370
SH	105.	0.558	11.835	0.0	0.0	0.0	11.835	0.15361
SH	120.	0.638	11.993	0.0	0.0	0.0	11.993	0.15347
SH	135.	0.718	11.512	0.0	0.0	0.0	11.512	0.15328
SH	144.	0.766	11.085	0.0	0.0	0.0	11.085	0.15290
	145.	0.771	11.028	0.0	0.0	0.0	11.028	0.15283
	150.	0.797	10.871	0.0	0.0	0.0	10.871	0.15321
	165.	0.877	9.964	0.0	0.0	0.0	9.964	0.15304
	180.	0.957	9.195	0.0	0.0	0.0	9.195	0.15281
	195.	1.037	9.127	3.657	0.0	3.657	9.127	0.15409
	210.	1.116	9.514	11.910	0.0	11.910	9.514	0.15327
	225.	1.196	10.179	15.976	0.0	15.976	10.179	0.14843
	240.	1.276	11.153	16.205	0.0	16.205	11.153	0.15319
	255.	1.356	11.875	16.991	0.0	16.991	11.875	0.15361
	270.	1.435	11.954	20.868	0.0	20.868	11.954	0.15370
	285.	1.515	11.718	21.491	115.776	137.267	11.718	0.15361
	300.	1.595	11.772	17.423	223.666	241.039	11.772	0.15347
	315.	1.675	11.173	15.878	316.314	332.192	11.173	0.15328
	330.	1.754	10.187	15.150	387.406	402.556	10.187	0.15321
	345.	1.834	9.275	12.040	432.096	444.136	9.275	0.15305
	360.	1.914	8.919	7.055	447.340	454.395	8.919	0.15870

TABLE XVI

SURFACE 4 HEAT FLUX; 900 MILE CIRCULAR POLAR ORBIT

	θ	T	Q_P	Q_{PR}	Q_S	Q_{solar}	Q_{IR}	F
	0.	0.0	8.696	0.0	0.0	0.0	8.696	0.15474
	15.	0.080	9.275	0.0	0.0	0.0	9.275	0.15305
	30.	0.159	10.187	0.0	0.0	0.0	10.187	0.15321
	35.	0.186	10.519	0.0	0.0	0.0	10.519	0.15292
SH	36.	0.191	10.584	0.0	0.0	0.0	10.584	0.15291
SH	45.	0.239	11.173	0.0	0.0	0.0	11.173	0.15328
SH	60.	0.319	11.772	0.0	0.0	0.0	11.772	0.15347
SH	75.	0.399	11.718	0.0	0.0	0.0	11.718	0.15361
SH	90.	0.478	11.954	0.0	0.0	0.0	11.954	0.15370
SH	105.	0.558	11.875	0.0	0.0	0.0	11.875	0.15361
SH	120.	0.638	11.153	0.0	0.0	0.0	11.153	0.15319
SH	135.	0.718	10.179	0.0	0.0	0.0	10.179	0.14843
SH	144.	0.766	8.922	0.0	0.0	0.0	8.922	0.13761
	145.	0.771	8.802	0.0	366.437	366.437	8.802	0.13571
	150.	0.797	9.514	0.008	387.407	387.415	9.514	0.15327
	165.	0.877	9.127	1.009	432.097	433.106	9.127	0.15409
	180.	0.957	9.435	7.924	447.340	455.264	9.435	0.15680
	195.	1.037	9.964	14.859	432.098	446.957	9.964	0.15304
	210.	1.116	10.871	16.900	387.409	404.309	10.871	0.15321
	225.	1.196	11.512	16.148	316.319	332.467	11.512	0.15328
	240.	1.276	11.993	18.625	223.673	242.293	11.993	0.15347
	255.	1.356	11.835	21.934	115.783	187.717	11.835	0.15361
	270.	1.435	11.726	19.849	0.004	19.852	11.726	0.15369
	285.	1.515	11.604	16.121	0.0	16.121	11.604	0.15361
	300.	1.595	10.691	15.748	0.0	15.748	10.691	0.15319
	315.	1.675	9.430	13.398	0.0	13.398	9.430	0.14843
	330.	1.754	8.950	9.842	0.0	9.842	8.950	0.15386
	345.	1.834	8.895	3.402	0.0	3.402	8.895	0.16135
	360.	1.914	8.696	0.0	0.0	0.0	8.696	0.15474

TABLE XVII

SURFACE 5 HEAT FLUX; 900 MILE CIRCULAR POLAR ORBIT

	θ	T	Q_P	Q_{PR}	Q_S	Q_{solar}	Q_{IR}	F
	0.	0.0	0.0	0.0	0.000	0.000	0.0	0.0
	15.	0.080	0.0	0.0	0.0	0.0	0.0	0.0
	30.	0.159	0.0	0.0	0.0	0.0	0.0	0.0
	35.	0.186	0.0	0.0	0.0	0.0	0.0	0.0
SH	36.	0.191	0.0	0.0	0.0	0.0	0.0	0.0
SH	45.	0.239	0.0	0.0	0.0	0.0	0.0	0.0
SH	60.	0.319	0.0	0.0	0.0	0.0	0.0	0.0
SH	75.	0.399	0.0	0.0	0.0	0.0	0.0	0.0
SH	90.	0.478	0.0	0.0	0.0	0.0	0.0	0.0
SH	105.	0.558	0.0	0.0	0.0	0.0	0.0	0.0
SH	120.	0.638	0.0	0.0	0.0	0.0	0.0	0.0
SH	135.	0.718	0.0	0.0	0.0	0.0	0.0	0.0
SH	144.	0.766	0.0	0.0	0.0	0.0	0.0	0.0
	145.	0.771	0.0	0.0	0.0	0.0	0.0	0.0
	150.	0.797	0.0	0.0	0.0	0.0	0.0	0.0
	165.	0.877	0.0	0.0	0.0	0.0	0.0	0.0
	180.	0.957	0.0	0.0	0.0	0.0	0.0	0.0
	195.	1.037	0.0	0.0	115.778	115.778	0.0	0.0
	210.	1.116	0.0	0.0	223.668	223.668	0.0	0.0
	225.	1.196	0.0	0.0	316.315	316.315	0.0	0.0
	240.	1.276	0.0	0.0	387.406	387.406	0.0	0.0
	255.	1.356	0.0	0.0	432.097	432.097	0.0	0.0
	270.	1.435	0.0	0.0	447.340	447.340	0.0	0.0
	285.	1.515	0.0	0.0	432.098	432.098	0.0	0.0
	300.	1.595	0.0	0.0	387.410	387.410	0.0	0.0
	315.	1.675	0.0	0.0	316.320	316.320	0.0	0.0
	330.	1.754	0.0	0.0	223.674	223.674	0.0	0.0
	345.	1.834	0.0	0.0	115.785	115.785	0.0	0.0
	360.	1.914	0.0	0.0	0.005	0.005	0.0	0.0

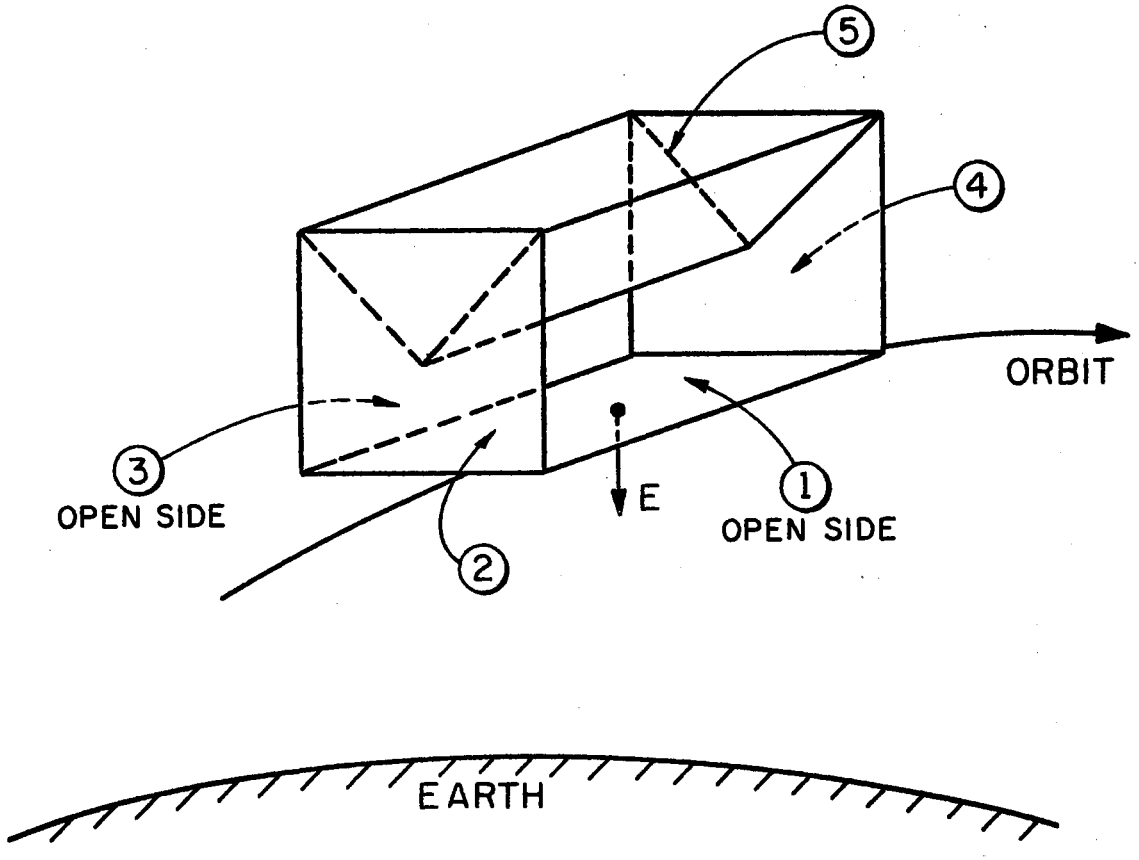

Figure 45. Surface Designations for Appendix B Tables

The sides receive direct energy from the earth, plus that specularly reflected from the opposite side and the reflector. This is expressed as

$$Q_{IR,6} = J_{e,IR} A_e (F_{e-6} + \rho_{\sigma,IR,15} F_{e-6(15)} + \rho_{\sigma,IR,9} F_{e-6(9)} \quad \text{(B-12)}$$

$$Q_{s,6} = J_{e,s} A_e (F_{e-6} + \rho_{\sigma,s,15} F_{e-6(15)} + \rho_{\sigma,s,9} F_{e-6(9)} \quad \text{(B-13)}$$

or, using reciprocity,

$$Q_{IR,6} = \frac{G_{0,IR}}{F_{0-e}} (A_6 F_{6-e} + A_{6(15)} \rho_{\sigma,IR,15} F_{6(15)-e} + A_{6(9)} \rho_{\sigma,IR,15} F_{6(9)-e}) \quad \text{(B-14)}$$

$$Q_{s,6} = \frac{G_{0,s}}{F_{0-e}} (A_6 F_{6-e} + A_{6(15)} \rho_{\sigma,s,15} F_{6(15)-e} + A_{6(9)} \rho_{\sigma,s,15} F_{6(9)-e}) . \quad \text{(B-15)}$$

Since the side surfaces are symmetrical with respect to their environmental energy inputs,

$$Q_{IR,9} = Q_{IR,6} \quad \text{(B-16)}$$

$$Q_{s,9} = Q_{s,6} . \quad \text{(B-17)}$$

The reflector receives direct input from the earth, plus that specularly reflected from each side. The reflected energy from both sides are equal. The environmental irradiation of the reflector is then given as

$$Q_{IR,15} = \frac{G_{0,IR}}{F_{0-e}} (A_{15} F_{15-e} + 2A_{15(6)} \rho_{\sigma,IR,6} F_{15(6)-e}) \quad \text{(B-18)}$$

$$Q_{s,15} = \frac{G_{0,s}}{F_{0-e}} (A_{15} F_{15-e} + 2A_{15(6)} \rho_{\sigma,s,6} F_{15(6)-e}) \quad \text{(B-19)}$$

The outside surfaces of the enclosure see only a direct view of the earth, and, therefore,

$$Q_{IR,8} = G_{2,IR} A_8 \alpha_{IR,8} \tag{B-20}$$

$$Q_{S,8} = G_{2,S} A_8 \alpha_{S,8} \tag{B-21}$$

where $G_{2,IR}$ is the value of the infrared flux taken from the tables for surface 2 of this appendix and $G_{2,S}$ is the value of the solar flux taken from the same tables. Similarly, for the opposite side,

$$Q_{IR,11} = G_{4,IR} A_{11} \alpha_{IR,11} \tag{B-22}$$

$$Q_{S,11} = G_{4,S} A_{11} \alpha_{S,11} . \tag{B-23}$$

The input to the enclosure top is taken from the surface 5 tables of this appendix and is expressed as

$$Q_{IR,14} = 0.0 \tag{B-24}$$

$$Q_{S,14} = G_{5,S} A_{14} \alpha_{S,14} . \tag{B-25}$$

The multiple shape factors are geometric shape factors used in specular-reflecting systems and are described by Wiebelt (17). They were determined by considering the appropriate blockage and partial views of the appropriate surfaces to the earth, as described by Figures 46 to 48. The values of these shape factors were determined by the computer program CONFAC II and are listed in Table XVIII (19).

The environmental heat fluxes were obtained from reference (18). The values tabulated in this appendix are also the orbital fluxes from direct and reflected solar and planetary irradiations on a plain surface element in a planetary-oriented circular polar orbit. Non-uniform radiosity of the earth, due to latitude and seasonal variations has been taken into account.

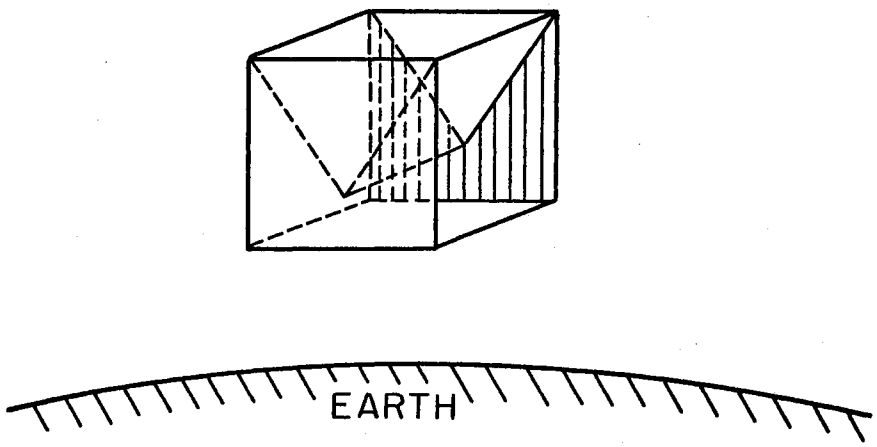

$F_{E\text{-}SIDE}$

$F_{E\text{-}6}$

$F_{E\text{-}9}$

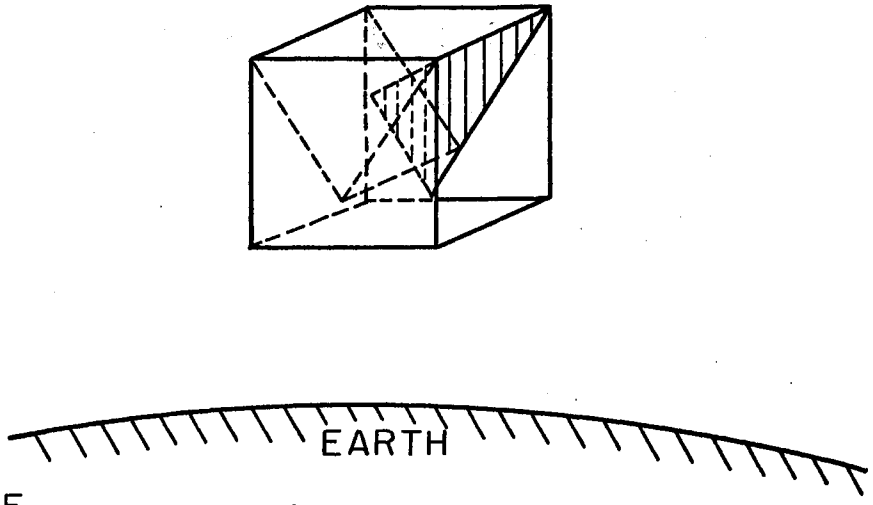

$F_{E\text{-}SIDE(REFLECTOR)}$

$F_{E\text{-}6(15)}$

$F_{E\text{-}9(15)}$

Figure 46. Shape Factor Enclosure Geometry

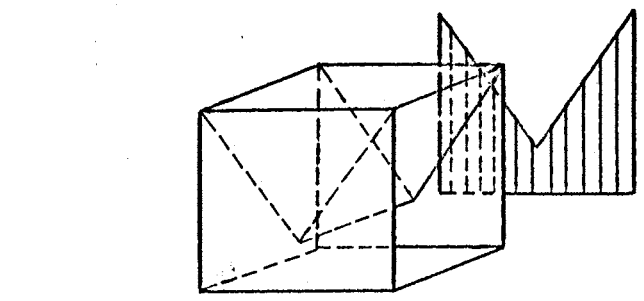

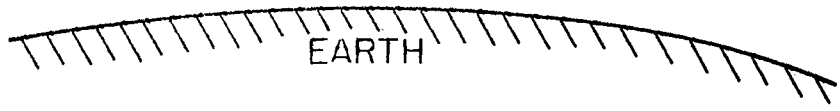

$F_{E\text{-}SIDE(SIDE)}$
$F_{E\text{-}6(9)}$
$F_{E\text{-}9(6)}$

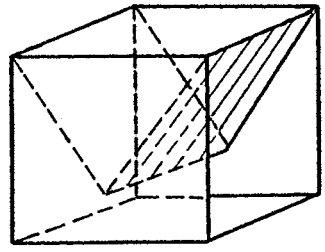

$F_{E\text{-}REFLECTOR}$
$F_{E\text{-}15}$

Figure 47. Shape Factor Enclosure Geometry

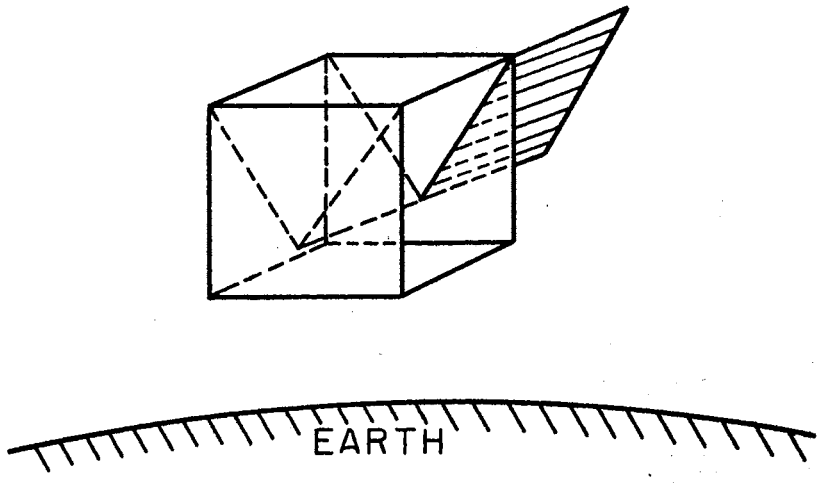

Figure 48. Shape Factor Enclosure Geometry

TABLE XVIII

SHAPE FACTORS FOR ENVIRONMENTAL ENERGY INPUTS

	300 s.m.	600 s.m.	900 s.m.
$F_{6-\bullet}$	.08612	.04485	.02897
$F_{6(15)-\bullet}$	.14074	.05004	.03880
$F_{\bullet-6(9)}$	.02677	.00553	.00514
$F_{15-\bullet}$	.28395	.22138	.14298
$F_{15(6)-\bullet}$	.11886	.03536	.02742

The heat fluxes presented in Tables VI-XVII are Q_P, the direct planetary irradiation, Q_{PR}, the reflected solar irradiation, and Q_S, the direct solar irradiation. Q_{solar} and Q_{IR} are the total energy fluxes in the solar and infrared spectra, respectively. All values of heat flux are in BTU/HR-FT^2. θ is the angular position in degrees and T is the orbital time in hours.

The position of the surfaces and the type of orbit are described in Figure 45. The sun's declination was assumed to be 0°; the vector E always points to the earth.

Heat fluxes are presented for 300, 600, and 900 statute-mile orbits, and the note "SH" found to the extreme left of each table indicates that the particular surface is in the earth's shadow. F represents the instantaneous geometric view factor of the surface to the earth. Average values of F were used in the analysis.

APPENDIX C

ANALYSIS TECHNIQUES BETWEEN SPECULAR-DIFFUSE REFLECTING SURFACES WITH BLOCKAGE

The radiant exchange between Lambertian surfaces is described in any standard heat transfer text. This exchange depends upon the geometric shape factor $dF_{dA_i - dA_j}$ between the two elemental surfaces which is given as

$$dF_{dA_i - dA_j} = \frac{\cos \theta_i \cos \theta_j \, dA_j}{\pi r^2} \tag{C-1}$$

or

$$F_{A_i - A_j} = \frac{1}{A_i} \int_{A_i} \int_{A_j} \frac{\cos \theta_i \cos \theta_j \, dA_i \, dA_j}{\pi r^2} . \tag{C-2}$$

The normal angles θ_i, θ_j and the length r are described in Figure 49a for the areas A_i and A_j. In case of blockage, as shown in Figure 49b, the shape factor from the elemental area dA_i to the area A_j' is determined where A_j' is the area as determined by

$$A_j' = A_j - A_j \cap A_k . \tag{C-3}$$

This is indicated in Figure 49c where A_j' is a function of the position of dA_i, assuming A_k and A_j are fixed.

The resulting geometric shape factor is solved by the approximation:

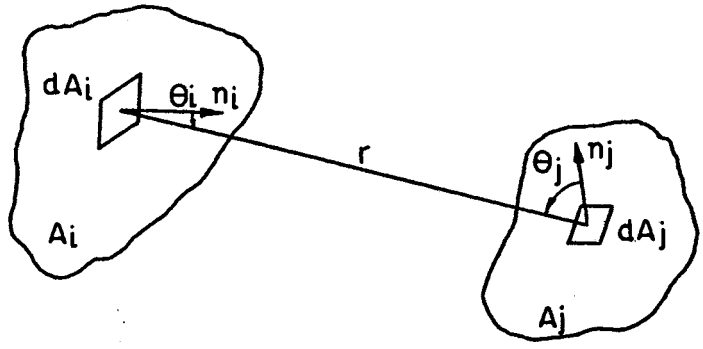

(a) SHAPE FACTOR GEOMETRY WITHOUT BLOCKAGE

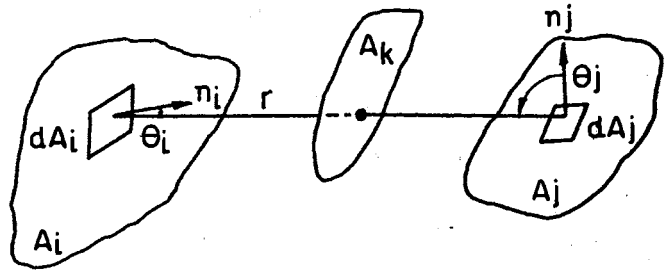

(b) SHAPE FACTOR GEOMETRY WITH BLOCKAGE

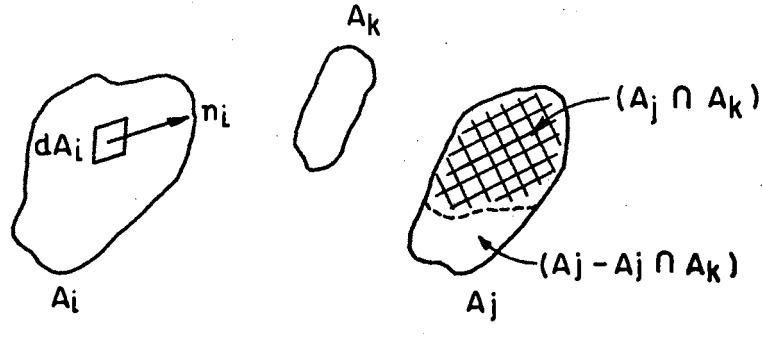

(c) INTERSECTED AREAS FOR BLOCKAGE

Figure 49. Shape Factor Geometry Logic

$$F_{dA_i - A'_j} = \sum_{\Delta A'_j} \left(\frac{\cos \theta_i \cos \theta_j \Delta A_j}{\pi r^2} \right) \tag{C-4}$$

or

$$F_{A_i - A'_j} = \frac{1}{A_i} \sum_{\Delta A_i} \sum_{\Delta A_j} \left(\frac{\cos \theta_i \cos \theta_j \Delta A_i \Delta A'_j}{\pi r^2} \right) . \tag{C-5}$$

This procedure was used to calculate the shape factors with blockage, utilizing the CONFAC II Computer Program. Since the exact solutions to many of these complicated shape factors are unavailable, the accuracy of the shape factor is felt to be no better than ±20 per cent at values of the shape factor = 0.10, and may be greater for smaller values.

When specular-diffuse reflecting surfaces are included in an enclosure, Holman (9) has shown that a radiosity network equivalent to a diffuse reflecting system can be used if the following modifications are made:

I. RADIATION SURFACE RESISTANCES

A. For diffusely reflecting surfaces

$$R_i = \frac{1 - \epsilon_i}{\epsilon_i A_i} \tag{C-6}$$

where the next radiant heat transfer from surface 1 is given as

$$q_i = \frac{E_{b_i} - J_i}{R_i} \tag{C-7}$$

B. For specular diffuse reflecting surfaces,

$$R_i = \frac{\rho_{\sigma,i}}{\epsilon_i A_i (1 - \rho_{\sigma,i})} \tag{C-8}$$

where the net radiant heat transfer from surface i is given as

$$q_i = \frac{E_{b_i} - \frac{J_i}{(1 - \rho\sigma, i)}}{R_i} \quad . \tag{C-9}$$

II. SPACE RADIATION RESISTANCE

A. Between diffusely reflecting surfaces within an enclosure containing other diffusely reflecting surfaces, as well as n specular-diffuse reflecting surfaces,

$$R_{ij} = [A_i (F_{i-j} + \sum_n \rho_{o,n} F_{i-j(n)} + \sum_m \sum_n \rho\sigma, m \rho\sigma, n F_{i-j(m,n)} + \ldots)]^{-1} \tag{C-10}$$

where the radiant energy transfer between the radiosity nodes i and j would be given as

$$\hat{q}_{i-j} = \frac{J_i - J_j}{R_{ij}} \quad . \tag{C-11}$$

B. Between a diffusely reflecting surface i and a specular-diffuse reflecting surface j within an enclosure with other surfaces of both types,

$$R^*_{ij} = [A_i (1 - \rho\sigma, j)(F_{i-j} + \sum_n \rho\sigma, n F_{i-j(n)} + \sum_m \sum_n \rho\sigma, m \rho\sigma, n F_{i-j(m,n)} + \ldots)]^{-1} \tag{C-12}$$

where the radiant energy transfer between the radiosity nodes i and j would be given as

$$\hat{q}_{i-j} = \frac{J_i - \frac{Jj}{(1 - \rho\sigma, j)}}{R^*_{ij}} \tag{C-13}$$

C. Between specular-diffuse reflecting surfaces within an enclosure of specular-diffuse reflecting and diffuse reflecting surfaces,

$$R_{ij}^{**} = [A_i (1 - \rho_{\sigma,i})(1 - \rho_{\sigma,j})(F_{i-j} + \sum_n \rho_{\sigma,n} F_{i-j(n)} + \sum \sum \rho_{\sigma,m} \rho_{o,n} F_{i-j(m,n)} + \ldots)]^{-1} \quad \text{(C-14)}$$

where the radiant energy transfer between the radiosity Nodes i and j are given as

$$\hat{q}_{i-j} = \frac{\frac{J_i}{(1 - \rho_{\sigma,i})} - \frac{J_j}{(1 - \rho_{\sigma,j})}}{R_{ij}^{**}} . \quad \text{(C-15)}$$

Following this general procedure, the radiation conductances of the analysis model are defined as follows:

$$R_{28} = \frac{1.0}{A_6 (1.0 - \rho_{6,\sigma}^{IR})(F_{6-1} + \rho_{9,\delta}^{IR} F_{6-1(9)} + \rho_{15,\sigma}^{IR} F_{6-1(15)})} \quad \text{(C-16)}$$

$$R_{29} = \frac{1.0}{A_9 (1.0 - \rho_{9,\sigma}^{IR})(F_{9-1} + \rho_{6,\delta}^{IR} F_{9-1(6)} + \rho_{15,\sigma}^{IR} F_{9-1(15)})} \quad \text{(C-17)}$$

$$R_{30} = \frac{1.0}{A_9 F_{9-15} (1.0 - \rho_{9,\sigma}^{IR})(1.0 - \rho_{15,\sigma}^{IR})} \quad \text{(C-18)}$$

$$R_{31} = \frac{1.0}{A_6 F_{6-15} (1.0 - \rho_{6,\sigma}^{IR})(1.0 - \rho_{15,\sigma}^{IR})} \quad \text{(C-19)}$$

$$R_{32} = \frac{\rho_{6,\delta}^{IR}}{\epsilon_6 A_6 (1.0 - \rho_{6,\sigma}^{IR})} \quad \text{(C-20)}$$

$$R_{33} = \frac{\rho_{15,\delta}^{IR}}{\epsilon_{15} A_{15} (1.0 - \rho_{15,\sigma}^{IR})} \quad \text{(C-21)}$$

$$R_{34} = \frac{\rho_{9,6}}{\epsilon_9 A_9 (1.0 - \rho_{9,\sigma})} \tag{C-22}$$

$$R_{35} = \frac{1.0}{A_1 (1.0 - \rho_{15,\sigma}) (F_{1-15} + \rho_{6,\sigma} F_{1-15(6)} + \rho_{9,\sigma} F_{1-15(9)})} . \tag{C-23}$$

The shape factors for these equations were determined, considering the geometries shown in Figure 50 and are presented for the 300, 600, and 900-mile orbit models in Table XIX.

To complete the heat inputs for the model, the view of each of the internal and external surfaces of the enclosure to space must be calculated. For surfaces 8 and 11, the shape factor to space is determined by

$$F_{8-\infty} = 1.0 - F_{8-e} \tag{C-24}$$

$$F_{11-\infty} = 1.0 - F_{11-e} \tag{C-25}$$

where F_{8-e} and F_{11-e} are given in the tables of this appendix for the proper orbit altitude, and are listed under the column "F" for the tables noted as "Surface 2".

The total flux for surfaces 8 and 11 is then given as:

$$Q_8 = -\sigma\epsilon_8 (1.0 - F_{8-e}) T_8^4 + Q_{IR,8} + Q_{s,8} \tag{C-26}$$

$$Q_{11} = -\sigma\epsilon_{11} (1.0 - F_{11-e}) T_{11}^4 + Q_{IR,11} + Q_{s,11} \tag{C-27}$$

where $Q_{IR,i}$ and $Q_{s,i}$ are determined in Appendix B.

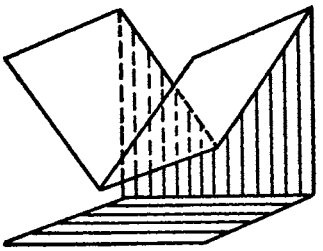

F_{6-1}

F_{9-1}

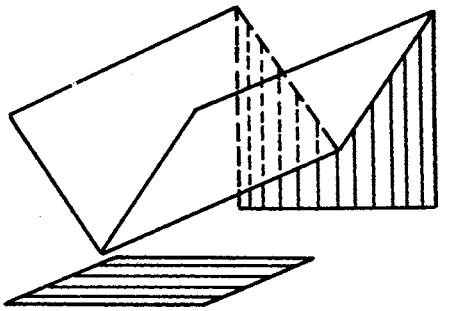

$F_{6-1(9)}$

$F_{9-1(6)}$

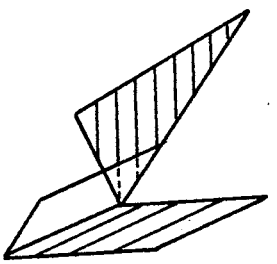

$F_{6-1(15)}$

$F_{9-1(15)}$

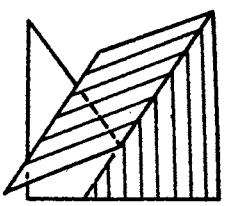

F_{9-15}

F_{6-15}

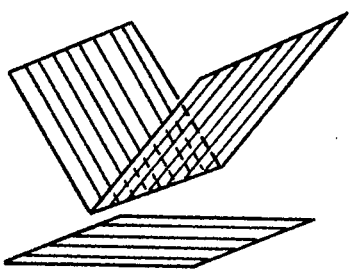

F_{1-15}

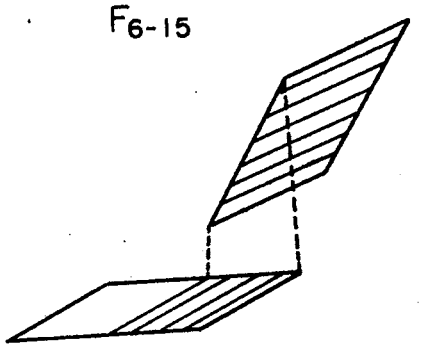

$F_{1-15(6)}$

$F_{1-15(9)}$

Figure 50. Shape Factor Enclosure Geometry

TABLE XIX

SHAPE FACTORS FOR INTERNAL RADIANT EXCHANGE

	300 s.m.	600 s.m.	900 s.m.
F_{6-1} F_{9-1}	0.148	0.164	0.164
$F_{6-1(9)}$ $F_{9-1(6)}$	0.0346	0.0520	0.0455
$F_{6-1(15)}$ $F_{9-1(15)}$	0.1175	0.0315	0.0293
F_{9-15} F_{6-15}	0.1658	0.1395	0.1267
F_{1-15}	0.1351	0.1250	0.1201
$F_{1-15(6)}$ $F_{1-15(9)}$	0.0557	0.0473	0.0430
$F_{1-6(9)}$ $F_{1-9(6)}$	0.02	0.02	0.02

The shape factors of the internal surface to space are calculated in the following manner:

$$F_{1-\infty} = 1.0 - F_{1-6(9)} - F_{1-9(6)} - F_{1-15(6)} - F_{1-15(9)} - F_{1-6(15)} - F_{1-9(15)} \quad \text{(C-28)}$$

$$F_{6-\infty} = 1.0 - F_{6-1} - F_{6-6(9)} - F_{6-9(15)} - F_{6-15(9)} - F_{6-1(9)} \quad \text{(C-29)}$$

$$F_{9-\infty} = 1.0 - F_{9-1} - F_{9-9(6)} - F_{9-6(15)} - F_{9-15(6)} - F_{9-1(6)} \quad \text{(C-30)}$$

$$F_{15-\infty} = 1.0 - F_{15-1} - F_{15-6(9)} - F_{15-9(6)} - F_{15-1(6)} - F_{15-1(9)} \cdot \quad \text{(C-31)}$$

Some of these shape factors have already been determined and are given in Table XIX. The rest were determined through consideration of the geometries shown in Figure 51 and are in Table XX.

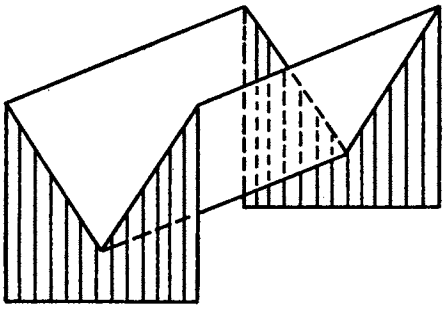

$F_{6\text{-}6(9)}$

$F_{9\text{-}9(6)}$

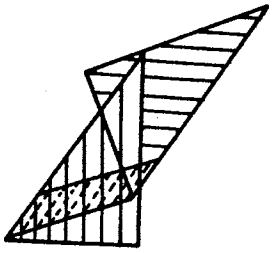

$F_{6\text{-}9(15)}$

$F_{9\text{-}6(15)}$

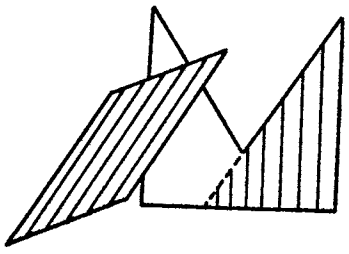

$F_{6\text{-}15(9)}$

$F_{9\text{-}15(6)}$

Figure 51. Shape Factor Enclosure Geometry

TABLE XX

INTERNAL AND SPACE SHAPE FACTORS

	300 s.m.	600 s.m.	900 s.m.
$F_{6-6(9)}$ $F_{9-9(6)}$	0.0327	0.0384	0.0406
$F_{6-9(15)}$ $F_{9-6(15)}$	0.2281	0.0539	0.0489
$F_{6-15(9)}$ $F_{9-15(6)}$	0.0162	0.0184	0.0175
F_{15-1}	0.0928	0.1249	0.1200
$F_{15-6(9)}$ $F_{15-9(6)}$	0.0064	0.0071	0.0077
$F_{15-1(6)}$ $F_{15-1(9)}$	0.0057	0.0473	0.0429
$F_{1-\infty}$	0.613	0.803	0.816
$F_{6-\infty}$ $F_{9-\infty}$	0.541	0.673	0.683
$F_{15-\infty}$	0.882	0.766	0.779

APPENDIX D

RESULTS OF THE COMPUTER ANALYSES

This appendix presents the results of the computer analyses for the optimization and the sensitivity checks in a tabular form. Each table presents the optimized parameters and the resulting radiator temperature (T1), side temperature (T2), and the reflector temperature (T3) in degree R. This information is always given in the column of numbers farthest to the left. The sensitivity of these parameters to various changes is presented by holding certain parameters fixed and varying one or more of the remaining parameters. Each column presents a set of variations of the parameters and the resulting temperatures. The tables are labeled as:

1. Preliminary Sensitivity Check; ±20 per cent.
2. Preliminary Sensitivity Check; ±40 per cent.
3. Sensitivity Check; Parameter Variation Equals .05, .10.
4. Sensitivity Check; Parameter Variation Equals .05.
5. Sensitivity Check; Final Analysis Model, Series "M".

The ±20 per cent and the ±40 per cent sensitivity checks represent the optimization considerations by varying the parameters ±20 per cent and ±40 per cent of their optimized values, respectively. In some cases, where the parameter constraints would be violated, both the positive and negative variations do not appear. Some constraint violations were allowed to occur in order to show the effect of that

constraint. The .05 and the .10 parameter variations were treated in a similar fashion. The Series "M" analysis presents the optimization and sensitivity check for the final analysis model.

The infrared flux and the solar flux are given for three steady-state orbital conditions. These fluxes are the power/area arriving at the enclosure opening and represent the high, the average, and the low heat inputs to the enclosure. The values Q1, Q2, and Q3 represent a parametric set of heat inputs to the radiator side and reflector, respectively, above that which is conducted through the insulation from an exterior temperature of 520° R.

Blank spaces in the tables are to be read by inserting the value of that parameter or temperature to the far left of the respective row.

TABLE XXI

PRELIMINARY SENSITIVITY CHECK; ±20 PER CENT

RUN # A10.1 to A10.3

INFRARED FLUX = 13.485
SOLAR FLUX = 9.344

Q1 = 0.0
Q2 = 0.0
Q3 = 0.0

P1	.246	.197	.295	.246																
P2	.05			.04	.06	.05														
P3	.33					.264	.396	.33												
P4	.17							.136	.204	.17										
P5	.854									.684	.854									
P6	.0458										.0366	.055	.0458							
P7	.47												.376	.47						
P8	.43													.344	.43					
P9	.854														.684	.854				
P10	.0458															.0366	.055	.0458		
P11	.47																	.376	.47	
P12	.43																		.344	
T1	125					126	124	125		129	125		126	125	132	125		127	125	1
T2	171		172							151	164	179	178	177	174	171	172	172	172	
T3	198														177	189	206	212	198	

TABLE XXII

PRELIMINARY SENSITIVITY CHECK; ±40 PER CENT

RUN # A10.1 to A10.3

INFRARED FLUX = 13.485
SOLAR FLUX = 9.344

Q1 = 0.0
Q2 = 0.0
Q3 = 0.0

P1	.246	.1485	.345	.246																
P2	.05			.03	.07	.05														
P3	.33					.198	.46	.33												
P4	.17							.102	.248	.170										
P5	.854									.512	.854									
P6	.0458										.0275	.0644	.0458							
P7	.47												.282	.47						
P8	.43													.258	.43					
P9	.854														.512	.854				
P10	.0458															.0275	.0644	.0458		
P11	.47																	.282	.50	.47
P12	.43																			.258
T1	125			124	125	127	123	126	124	133	125		127	126	138	125	124	130	124	127
T2	171	172	171	172			171	172	172	153	157	186	184	183	177	171	172	174	171	174
T3	198														181	180	215	223	193	222

TABLE XXIII

PRELIMINARY SENSITIVITY CHECK; ±20 PER CENT

RUN # A12.0

INFRARED FLUX = 13.485
SOLAR FLUX = 9.344

Q1 = .341
Q2 = 0.0
Q3 = 0.0

P1	.246	.197	.295	.246																
P2	.05			.04	.06	.05														
P3	.33					.264	.396	.33												
P4	.17							.136	.204	.17										
P5	.854									.684	.854									
P6	.0458										.0366	.055	.0458							
P7	.47												.376	.47						
P8	.43													.344	.43					
P9	.854														.684	.854				
P10	.0458															.0366	.055	.0458		
P11	.47																	.376	.47	
P12	.43																		.344	
T1	143			142	143		142	143	142	145	143				148	143	142	144	143	
T2	173		174	173						154	166	180		179	175	173	173	174	173	
T3	199														178	190	207	212	211	

TABLE XXIV

PRELIMINARY SENSITIVITY CHECK; ±40 PER CENT

RUN # A12.0

INFRARED FLUX = 13.485
SOLAR FLUX = 9.344

Q1 = .341
Q2 = 0.0
Q3 = 0.0

P1	.246	.1485	.345	.246																
P2	.05			.03	.07	.05														
P3	.33					.198	.46	.33												
P4	.17							.102	.248	.170										
P5	.854									.512	.854									
P6	.0458										.0275	.0644	.0458							
P7	.47												.282	.47						
P8	.43													.258	.43					
P9	.854														.512	.854				
P10	.0458															.0275	.0644	.0458		
P11	.47																	.282	.50	.47
P12	.43																			.258
T1	143	143		142	144		141	143	142	149	143		144	143	153	143	142	146	142	144
T2	173	174	173			174	173			155	159	187	185	184	178	173	173	175	173	176
T3	199														182	180	216	224	194	222

TABLE XXV

PRELIMINARY SENSITIVITY CHECK; ±20 PER CENT

RUN # A13.1 to A13.3

INFRARED FLUX = 13.485
SOLAR FLUX = 9.344

Q1 = 3.41
Q2 = 0.0
Q3 = 0.0

P1	.246	.197	.295	.246																
P2	.05			.04	.06	.05														
P3	.33					.264	.396	.33												
P4	.17							.136	.204	.17										
P5	.854									.684	.854									
P6	.0458										.0366	.055	.0458							
P7	.47												.376	.47						
P8	.43													.344	.43					
P9	.854														.684	.854				
P10	.0458															.0366	.055	.0458		
P11	.47																	.376	.47	
P12	.43																		.344	
T1	211			210	212	211				214	211				213	211		212	211	
T2	185	186		185						170	180	191		190	187	185		186	186	
T3	203														184	195	211	216	215	

TABLE XXVI

PRELIMINARY SENSITIVITY CHECK; ±40 PER CENT

RUN # A13.1 to A13.3

INFRARED FLUX = 13.485
SOLAR FLUX = 9.344

Q1 = 3.41
Q2 = 0.0
Q3 = 0.0

P1	.246	.1485	.345	.246																
P2	.05			.03	.07	.05														
P3	.33					.198	.46	.33												
P4	.17							.102	.248	.170										
P5	.854									.512	.854									
P6	.0458										.0275	.0644	.0458							
P7	.47												.282	.47						
P8	.43													.258	.43					
P9	.854														.512	.854				
P10	.0458															.0275	.0644	.0458		
P11	.47																	.282	.50	.47
P12	.43																			.258
T1	211	211	213	209	213	212	211			216	211		212	211	216	211		212	211	212
T2	185	186	185			186	185			172	174	198	195		189	185		187	185	187
T3	203														188	186	220	227	199	225

TABLE XXVII

PRELIMINARY SENSITIVITY CHECK; ±20 PER CENT

RUN # 1E1.0

INFRARED FLUX = 13.485
SOLAR FLUX = 9.344

Q1 = 0.0
Q2 = .341
Q3 = 0.0

P1	.288	.231	.346	.288																
P2	.05			.04	.06	.05														
P3	.33					.264	.396	.33												
P4	.17							.136	.204	.17										
P5	.854									.684	.854									
P6	.0458										.0366	.055	.0458							
P7	.47												.376	.47						
P8	.43													.344	.43					
P9	.854														.684	.854				
P10	.0458															.0366	.055	.0458		
P11	.47																	.376	.47	
P12	.43																		.344	
T1	132					133	131	132	131	135	132		133	132	138	132		134	132	
T2	206									170	195	216	210		207	206			205	
T3	200														179	191	208	213	200	

TABLE XXVIII

PRELIMINARY SENSITIVITY CHECK; ±40 PER CENT

RUN # 1E1.0

INFRARED FLUX = 13.485
SOLAR FLUX = 9.344

Q1 = 0.0
Q2 = .341
Q3 = 0.0

P1	.288	.173	.404	.288																
P2	.05			.03	.07	.05														
P3	.33					.198	.46	.33												
P4	.17							.102	.248	.170										
P5	.854									.512	.854									
P6	.0458										.0275	.0644	.0458							
P7	.47												.282	.47						
P8	.43													.258	.43					
P9	.854														.512	.854				
P10	.0458															.0275	.0644	.0458		
P11	.47																	.282	.50	.47
P12	.43																			.258
T1	132			131	133	134	130	133	131	139	132		134	133	144	132	132	136	131	134
T2	206		205	206						168	185	267	213		209	206	206	207	205	207
T3	200														183	181	217	225	195	229

TABLE XXIX

PRELIMINARY SENSITIVITY CHECK; ±20 PER CENT

RUN # D.1 to D.4

INFRARED FLUX = 13.485
SOLAR FLUX = 9.344

Q1 = 0.0
Q2 = 6.82
Q3 = 0.0

P1	.417	.334	.502	.417																
P2	.05			.04	.06	.05														
P3	.33					.264	.396	.33												
P4	.17							.136	.204	.17										
P5	.854									.684	.854									
P6	.0458										.0366	.055	.0458							
P7	.47												.376	.47						
P8	.43													.344	.43					
P9	.854														.684	.854				
P10	.0458															.0366	.055	.0458		
P11	.47																	.376	.47	
P12	.43																		.344	
T1	193						192	193		196	193	193			195	193				
T2	377									288	355	399	378	377	378	377				
T3	222														207	216	229	232		

TABLE XXX

PRELIMINARY SENSITIVITY CHECK; ±40 PER CENT

RUN # D.1 to D.4

INFRARED FLUX = 13.485
SOLAR FLUX = 9.344

Q1 = 0.0
Q2 = 6.82
Q3 = 0.0

P1	.417	.251	.584	.417																
P2	.05			.03	.07	.05														
P3	.33					.198	.46	.33												
P4	.17							.102	.248	.170										
P5	.854									.512	.854									
P6	.0458										.0275	.0644	.0458							
P7	.47												.282	.47						
P8	.43													.258	.43					
P9	.854														.512	.854				
P10	.0458															.0275	.0644	.0458		
P11	.47																	.282	.50	.47
P12	.43																			.258
T1	193	194		192	193		192	193	192	199	193				197	193		194	192	193
T2	377	378	376	377						372	332	423	378			377				
T3	222														210	209	236	241	219	240

TABLE XXXI

PRELIMINARY SENSITIVITY CHECK; ±20 PER CENT

RUN # F.1 to F.3

INFRARED FLUX = 13.485
SOLAR FLUX = 9.344

Q1 = 0.0
Q2 = 0.0
Q3 = .341

P1	.243	.194	.292	.243																
P2	.05			.04	.06	.05														
P3	.33					.264	.396	.33												
P4	.17							.136	.204	.17										
P5	.854									.684	.854									
P6	.0458										.0366	.055	.0458							
P7	.47												.376	.47						
P8	.43													.344	.43					
P9	.854														.684	.854				
P10	.0458															.0366	.055	.0458		
P11	.47																	.376	.47	
P12	.43																		.344	
T1	127					128	126	127		131	127		128		134	127		129	128	
T2	172	173								153	166	180	179		175	173		174		
T3	209														183	199	219	221	220	

TABLE XXXII

PRELIMINARY SENSITIVITY CHECK; ±40 PER CENT

RUN # F.1 to F.3

INFRARED FLUX = 13.485
SOLAR FLUX = 9.344

Q1 = 0.0
Q2 = 0.0
Q3 = .341

P1	.243	.146	.341	.243																
P2	.05			.03	.07	.05														
P3	.33					.198	.46	.33												
P4	.17							.102	.248	.170										
P5	.854									.512	.854									
P6	.0458										.0275	.0644	.0458							
P7	.47												.282	.47						
P8	.43													.258	.43					
P9	.854														.512	.854				
P10	.0458															.0275	.0644	.0458		
P11	.47																	.282	.50	.47
P12	.43																			.258
T1	127			126	128	129	125	128	126	135	127		129	128	140	127	126	132	126	129
T2	172	173								155	159	187	185	184	178	173	173	175	172	175
T3	209														185	189	229	232	205	230

TABLE XXXIII

PRELIMINARY SENSITIVITY CHECK; ±20 PER CENT

RUN # G.1 to G.3

INFRARED FLUX = 13.485
SOLAR FLUX = 9.344

Q1 = 0.0
Q2 = 0.0
Q3 = 3.41

P1	.243	.194	.292	.243																
P2	.05			.04	.06	.05														
P3	.33					.264	.396	.33												
P4	.17							.136	.204	.17										
P5	.854									.684	.854									
P6	.0458										.0366	.055	.0458							
P7	.47												.376	.47						
P8	.43													.344	.43					
P9	.854														.684	.854				
P10	.0458															.0366	.055	.0458		
P11	.47																	.376	.47	
P12	.43																		.344	
T1	142					143	141	142		145	142		143	143	147	142		144	143	
T2	182									165	176	188		187	183	182		183		
T3	270														217	255	284	276	275	

TABLE XXXIV

PRELIMINARY SENSITIVITY CHECK; ±40 PER CENT

RUN # G.1 to G.3

INFRARED FLUX = 13.485
SOLAR FLUX = 9.344

Q1 = 0.0
Q2 = 0.0
Q3 = 3.41

P1	.277	.166	.388	.277																
P2	.05			.03	.07	.05														
P3	.33					.198	.46	.33												
P4	.17							.102	.248	.170										
P5	.854									.512	.854									
P6	.0458										.0275	.0644	.0458							
P7	.47												.282	.47						
P8	.43													.258	.43					
P9	.854														.512	.854				
P10	.0458															.0275	.0644	.0458		
P11	.47																	.282	.50	.47
P12	.43																			.258
T1	142					143							143		152			145	141	144
T2	182										170	195	193	192	186	182		184	182	184
T3	270														211	239	300	281	268	280

TABLE XXXV

SENSITIVITY CHECK; PARAMETER VARIATION = .05, .10

RUN # IY.1

INFRARED FLUX = 28.536
SOLAR FLUX = 15.310

Q1 = 0.0
Q2 = 0.0
Q3 = 0.0

P1	.364	.404	.314	.264	.364															
P2	.05	.01	.10	.15	.05															
P3	.33				.28	.23	.38	.43	.33											
P4	.17				.22	.27	.12	.07	.17											
P5	.854								.804	.754	.854									
P6	.0458								.0958	.1458	.0458									
P7	.854										.804	.754	.854							
P8	.0458										.0958	.1458	.0458							
P9	.854												.804	.754	.854					
P10	.0458												.0958	.1458	.0458					
P11	.854														.804	.754				
P12	.0458														.0958	.1458				
T1	131	129	132	133	131					132	131	132		133	132	134				
T2	192								207	215	192					191				
T3	232										231		254	265	232					

TABLE XXXVI

SENSITIVITY CHECK; PARAMETER VARIATION = .05, .10

RUN # IY.2

INFRARED FLUX = 28.536
SOLAR FLUX = 15.310

Q1 = .341
Q2 = 0.0
Q3 = 0.0

P1	.243	.283	.203	.143	.243															
P2	.05	.01	.10	.15	.05															
P3	.33				.28	.23	.38	.43	.33											
P4	.17				.22	.27	.12	.07	.17											
P5	.854								.804	.754	.854									
P6	.0458								.0958	.1458	.0458									
P7	.854										.804	.754	.854							
P8	.0458										.0958	.1458	.0458							
P9	.854												.804	.754	.854					
P10	.0458												.0958	.1458	.0458					
P11	.854														.804	.754				
P12	.0458														.0958	.1458				
T1	147	145	149	150	147				148		147		148	149	148	149				
T2	193								208	216	193			194	193					
T3	232									233	232		254	265	232					

TABLE XXXVII

SENSITIVITY CHECK; PARAMETER VARIATION = .05, .10

RUN # IY.3

INFRARED FLUX = 28.536
SOLAR FLUX = 15.310

Q1 = 3.41
Q2 = 0.0
Q3 = 0.0

P1	.243	.283	.203	.143	.243															
P2	.05	.01	.10	.15	.05															
P3	.33				.28	.23	.38	.43	.33											
P4	.17				.22	.27	.12	.07	.17											
P5	.854								.804	.754	.854									
P6	.0458								.0958	.1458	.0458									
P7	.854										.804	.754	.854							
P8	.0458										.0958	.1458	.0458							
P9	.854												.804	.754	.854					
P10	.0458												.0958	.1458	.0458					
P11	.854														.804	.754				
P12	.0458														.0958	.1458				
T1	213	209	217	220	213					214	213									
T2	202			203	202				216	223	202			203	202					
T3	235	205	235	236	235				236		235		257	267	235					

TABLE XXXVIII

SENSITIVITY CHECK; PARAMETER VARIATION = .05, .10

RUN # IY.4

INFRARED FLUX = 28.536
SOLAR FLUX = 15.310

Q1 = 0.0
Q2 = .341
Q3 = 0.0

P1	.405	.445	.355	.305	.405															
P2	.05	.01	.10	.15	.05															
P3	.33				.28	.23	.38	.43	.33											
P4	.17				.22	.27	.12	.07	.17											
P5	.854								.804	.754	.854									
P6	.0458								.0958	.1458	.0458									
P7	.854										.804	.754	.854							
P8	.0458										.0958	.1458	.0458							
P9	.854												.804	.754	.854					
P10	.0458												.0958	.1458	.0458					
P11	.854														.804	.754				
P12	.0458														.0958	.1458				
T1	137	135	138	139	137				138		137	138		139	138	140				
T2	219								238	247	219									
T3	233												255	265	233					

TABLE XXXIX

SENSITIVITY CHECK; PARAMETER VARIATION = .05, .10

RUN # IY.5

INFRARED FLUX = 28.536
SOLAR FLUX = 15.310

Q1 = 0.0
Q2 = 3.41
Q3 = 0.0

P1	.415	.455	.365	.315	.415															
P2	.05	.01	.10	.15	.05															
P3	.33				.28	.23	.38	.43	.33											
P4	.17				.22	.27	.12	.07	.17											
P5	.854								.804	.754	.854									
P6	.0458								.0958	.1458	.0458									
P7	.854										.804	.754	.854							
P8	.0458										.0958	.1458	.0458							
P9	.854												.804	.754	.854					
P10	.0458												.0958	.1458	.0458					
P11	.854														.804	.754				
P12	.0458														.0958	.1458				
T1	171	170	172	173	171				172	173	171	172				173				
T2	323		324						355	370	323			324	323					
T3	241										240		261	271	241					

TABLE XL

SENSITIVITY CHECK; PARAMETER VARIATION = .05, .10

RUN # IY.7

INFRARED FLUX = 28.536
SOLAR FLUX = 15.310

Q1 = 0.0
Q2 = 0.0
Q3 = 3.41

P1	.41	.45	.36	.31	.41															
P2	.05	.01	.10	.15	.05															
P3	.33				.28	.23	.38	.43	.33											
P4	.17				.22	.27	.12	.07	.17											
P5	.854								.804	.754	.854									
P6	.0458								.0958	.1458	.0458									
P7	.854										.804	.754	.854							
P8	.0458										.0958	.1458	.0458							
P9	.854												.804	.754	.854					
P10	.0458												.0958	.1458	.0458					
P11	.854														.804	.754				
P12	.0458														.0958	.1458				
T1	146	145	147	148	146				147		146	147	146	148	147	149				
T2	199								214	221	199		200		199					
T3	285			286	285					286	285		313	326	285					

TABLE XLI

SENSITIVITY CHECK; PARAMETER VARIATION = .05, .10

RUN # AX.1

INFRARED FLUX = 13.485
SOLAR FLUX = 9.344

Q1 = 0.0
Q2 = 0.0
Q3 = 0.0

P1	.34	.38	.29	.24	.34															
P2	.05	.01	.10	.15	.05															
P3	.33				.28	.23	.38	.43	.33											
P4	.17				.22	.27	.12	.07	.17											
P5	.854								.804	.754	.854									
P6	.0458								.0958	.1458	.0458									
P7	.854										.804	.754	.854							
P8	.0458										.0958	.1458	.0458							
P9	.854												.804	.754	.854					
P10	.0458												.0958	.1458	.0458					
P11	.854														.804	.754				
P12	.0458														.0958	.1458				
T1	118	117	119	120	118					120	118		119	121	119					
T2	171	172							186	192	172			173	172					
T3	199												218	227	199					

TABLE XLII

SENSITIVITY CHECK; PARAMETER VARIATION = .05, .10

RUN # AX.2

INFRARED FLUX = 13.485
SOLAR FLUX = 9.344

Q1 = .341
Q2 = 0.0
Q3 = 0.0

P1	.243	.283	.193	.143	.243															
P2	.05	.01	.10	.15	.05															
P3	.33				.28	.23	.38	.43	.33											
P4	.17				.22	.27	.12	.07	.17											
P5	.854								.804	.754	.854									
P6	.0458								.0958	.1458	.0458									
P7	.854										.804	.754	.854							
P8	.0458										.0958	.1458	.0458							
P9	.854												.804	.754	.854					
P10	.0458												.0958	.1458	.0458					
P11	.854														.804	.754				
P12	.0458														.0958	.1458				
T1	138	136	140	142	138				139	140	138		139	140	139					
T2	173	174							187	194	174			175	174					
T3	200												218	227	200					

TABLE XLIII

SENSITIVITY CHECK; PARAMETER VARIATION = .05, .10

RUN # AX.3

INFRARED FLUX = 13.485
SOLAR FLUX = 9.344

Q1 = 3.41
Q2 = 0.0
Q3 = 0.0

P1	.243	.283	.193	.143	.243															
P2	.05	.01	.10	.15	.05															
P3	.33				.28	.23	.38	.43	.33											
P4	.17				.22	.27	.12	.07	.17											
P5	.854								.804	.754	.854									
P6	.0458								.0958	.1458	.0458									
P7	.854										.804	.754	.854							
P8	.0458										.0958	.1458	.0458							
P9	.854												.804	.754	.854					
P10	.0458												.0958	.1458	.0458					
P11	.854														.804	.754				
P12	.0458														.0958	.1458				
T1	210	205	214	218	210					211	210			211	210					
T2	186								198	204	186									
T3	204								205		204		222	231	205					

TABLE XLIV

SENSITIVITY CHECK; PARAMETER VARIATION = .05, .10

RUN # AX.4

INFRARED FLUX = 13.485
SOLAR FLUX = 9.344

Q1 = 0.0
Q2 = .341
Q3 = 0.0

P1	.395	.435	.345	.295	.395															
P2	.05	.01	.10	.15	.05															
P3	.33				.28	.23	.38	.43	.33											
P4	.17				.22	.27	.12	.07	.17											
P5	.854								.804	.754	.854									
P6	.0458								.0958	.1458	.0458									
P7	.854										.804	.754	.854							
P8	.0458										.0958	.1458	.0458							
P9	.854												.804	.754	.854					
P10	.0458												.0958	.1458	.0458					
P11	.854														.804	.754				
P12	.0458														.0958	.1458				
T1	126	125	127	129	126				127	128	126		127	128	127					
T2	206								224	233	206									
T3	201											200	219	228	201					

TABLE XLV

SENSITIVITY CHECK; PARAMETER VARIATION = .05, .10

RUN # AX.5

INFRARED FLUX = 13.485
SOLAR FLUX = 9.344

Q1 = 0.0
Q2 = 3.41
Q3 = 0.0

P1	.417	.457	.367	.317	.417															
P2	.05	.01	.10	.15	.05															
P3	.33				.28	.23	.38	.43	.33											
P4	.17				.22	.27	.12	.07	.17											
P5	.854								.804	.754	.854									
P6	.0458								.0958	.1458	.0458									
P7	.854										.804	.754	.854							
P8	.0458										.0958	.1458	.0458							
P9	.854												.804	.754	.854					
P10	.0458												.0958	.1458	.0458					
P11	.854														.804	.754				
P12	.0458														.0958	.1458				
T1	166	165	167	168	166				167	168	166		167		166					
T2	320								351	366	320									
T3	213											212	229	237	213					

TABLE XLVI

SENSITIVITY CHECK; PARAMETER VARIATION = .05, .10

RUN # AX.6

INFRARED FLUX = 13.485
SOLAR FLUX = 9.344

Q1 = 0.0
Q2 = 0.0
Q3 = .341

P1	.345	.385	.295	.245	.345															
P2	.05	.01	.10	.15	.05															
P3	.33				.28	.23	.38	.43	.33											
P4	.17				.22	.27	.12	.07	.17											
P5	.854								.804	.754	.854									
P6	.0458								.0958	.1458	.0458									
P7	.854										.804	.754	.854							
P8	.0458										.0958	.1458	.0458							
P9	.854												.804	.754	.854					
P10	.0458												.0958	.1458	.0458					
P11	.854														.804	.754				
P12	.0458														.0958	.1458				
T1	120	119	122	123	120				121	122	121		122	123	121					
T2	173								187	193	173		174							
T3	210												230	239	210					

TABLE XLVII

SENSITIVITY CHECK; PARAMETER VARIATION = .05, .10

RUN # AX.7

INFRARED FLUX = 13.485
SOLAR FLUX = 9.344

Q1 = 0.0
Q2 = 0.0
Q3 = 3.41

P1	.405	.445	.355	.305	.405															
P2	.05	.01	.10	.15	.05															
P3	.33				.28	.23	.38	.43	.33											
P4	.17				.22	.27	.12	.07	.17											
P5	.854								.804	.754	.854									
P6	.0458								.0958	.1458	.0458									
P7	.854										.804	.754	.854							
P8	.0458										.0958	.1458	.0458							
P9	.854												.804	.754	.854					
P10	.0458												.0958	.1458	.0458					
P11	.854														.804	.754				
P12	.0458														.0958	.1458				
T1	137	136	138	139	137				138	139	138			139	138					
T2	182	183							195	201	183			184	183					
T3	270												296	309	270					

TABLE XLVIII

SENSITIVITY CHECK; PARAMETER VARIATION = .05, .10

RUN # RX.1

INFRARED FLUX = 11.145
SOLAR FLUX = .001

Q1 = 0.0
Q2 = 0.0
Q3 = 0.0

P1	.307	.347	.257	.207	.307															
P2	.05	.01	.10	.15	.05															
P3	.33				.28	.23	.38	.43	.33											
P4	.17				.22	.27	.12	.07	.17											
P5	.854								.804	.754	.854									
P6	.0458								.0958	.1458	.0458									
P7	.854										.804	.754	.854							
P8	.0458										.0958	.1458	.0458							
P9	.854												.804	.754	.854					
P10	.0458												.0958	.1458	.0458					
P11	.854														.804	.754				
P12	.0458														.0958	.1458				
T1	110	108	111	112	109				110	111	109		111	112	109					
T2	157	158							171	177	158		159		158					
T3	173												189	196	173					

TABLE XLX

SENSITIVITY CHECK; PARAMETER VARIATION = .05, .10

RUN # RX.2

INFRARED FLUX = 11.145
SOLAR FLUX = .001

Q1 = .341
Q2 = 0.0
Q3 = 0.0

P1	.243	.283	.203	.143	.243															
P2	.05	.01	.10	.15	.05															
P3	.33				.28	.23	.38	.43	.33											
P4	.17				.22	.27	.12	.07	.17											
P5	.854								.804	.754	.854									
P6	.0458								.0958	.1458	.0458									
P7	.854										.804	.754	.854							
P8	.0458										.0958	.1458	.0458							
P9	.854												.804	.754	.854					
P10	.0458												.0958	.1458	.0458					
P11	.854														.804	.754				
P12	.0458														.0958	.1458				
T1	133	131	135	137	133				134		133		134	135	133					
T2	160	161							173	179	161									
T3	174												189	197	174					

TABLE L

SENSITIVITY CHECK; PARAMETER VARIATION = .05, .10

RUN # RX.3

INFRARED FLUX = 11.145
SOLAR FLUX = .001

Q1 = 3.41
Q2 = 0.0
Q3 = 0.0

P1	.243	.283	.203	.143	.243															
P2	.05	.01	.10	.15	.05															
P3	.33				.28	.23	.38	.43	.33											
P4	.17				.22	.27	.12	.07	.17											
P5	.854								.804	.754	.854									
P6	.0458								.0958	.1458	.0458									
P7	.854										.804	.754	.854							
P8	.0458										.0958	.1458	.0458							
P9	.854												.804	.754	.854					
P10	.0458												.0958	.1458	.0458					
P11	.854														.804	.754				
P12	.0458														.0958	.1458				
T1	208	204	213	216	208				209	210	208		209		208					
T2	175		176		175				186	191	175		176		175					
T3	181												195	202	181					

TABLE LI

SENSITIVITY CHECK; PARAMETER VARIATION = .05, .10

RUN # RX.4

INFRARED FLUX = 11.145
SOLAR FLUX = .001

Q1 = 0.0
Q2 = .341
Q3 = 0.0

P1	.377	.417	.327	.277	.377															
P2	.05	.01	.10	.15	.05															
P3	.33				.28	.23	.38	.43	.33											
P4	.17				.22	.27	.12	.07	.17											
P5	.854								.804	.754	.854									
P6	.0458								.0958	.1458	.0458									
P7	.854										.804	.754	.854							
P8	.0458										.0958	.1458	.0458							
P9	.854												.804	.754	.854					
P10	.0458												.0958	.1458	.0458					
P11	.854														.804	.754				
P12	.0458														.0958	.1458				
T1	119	118	121	122	119				120	121	119		120	121	119					
T2	198								215	224	198									
T3	175			176	175				176		175		191	198	175					

TABLE LII

SENSITIVITY CHECK; PARAMETER VARIATION = .05, .10

RUN # RX.5

INFRARED FLUX = 11.145
SOLAR FLUX = .001

Q1 = 0.0
Q2 = 3.41
Q3 = 0.0

P1	.417	.457	.367	.317	.417															
P2	.05	.01	.10	.15	.05															
P3	.33				.28	.23	.38	.43	.33											
P4	.17				.22	.27	.12	.07	.17											
P5	.854								.804	.754	.854									
P6	.0458								.0958	.1458	.0458									
P7	.854										.804	.754	.854							
P8	.0458										.0958	.1458	.0458							
P9	.854												.804	.754	.854					
P10	.0458												.0958	.1458	.0458					
P11	.854														.804	.754				
P12	.0458														.0958	.1458				
T1	163	162	164	165	163				164	165	163		164		163					
T2	318	317	318						348	363	318									
T3	192								193		192		205	212	192					

TABLE LIII

SENSITIVITY CHECK; PARAMETER VARIATION = .05, .10

RUN # RX.6

INFRARED FLUX = 11.145
SOLAR FLUX = .001

Q1 = 0.0
Q2 = 0.0
Q3 = .341

P1	.319	.359	.269	.219	.319															
P2	.05	.01	.10	.15	.05															
P3	.33				.28	.23	.38	.43	.33											
P4	.17				.22	.27	.12	.07	.17											
P5	.854								.804	.754	.854									
P6	.0458								.0958	.1458	.0458									
P7	.854										.804	.754	.854							
P8	.0458										.0958	.1458	.0458							
P9	.854												.804	.754	.854					
P10	.0458												.0958	.1458	.0458					
P11	.854														.804	.754				
P12	.0458														.0958	.1458				
T1	113	111	114	115	112				113	114	112		114	115	112					
T2	159	160							172	178	160			161						
T3	189	188		189	188					189			206	214	188					

TABLE LIV

SENSITIVITY CHECK; PARAMETER VARIATION = .05, .10

RUN # RX.7

INFRARED FLUX = 11.145
SOLAR FLUX = .001

Q1 = 0.0
Q2 = 0.0
Q3 = 3.41

P1	.389	.429	.339	.289	.389															
P2	.05	.01	.10	.15	.05															
P3	.33				.28	.23	.38	.43	.33											
P4	.17				.22	.27	.12	.07	.17											
P5	.854								.804	.754	.854									
P6	.0458								.0958	.1458	.0458									
P7	.854										.804	.754	.854							
P8	.0458										.0958	.1458	.0458							
P9	.854												.804	.754	.854					
P10	.0458												.0958	.1458	.0458					
P11	.854														.804	.754				
P12	.0458														.0958	.1458				
T1	132	131	133	134	132				133	134	132		133	134	132					
T2	171	172							183	188	172			173	172					
T3	261	260	261										286	298	261					

TABLE LV

SENSITIVITY CHECK; PARAMETER VARIATION = .05

RUN # L.7 to L.8

INFRARED FLUX = 13.485
SOLAR FLUX = 9.344

Q1 = 0.0
Q2 = 0.0
Q3 = 0.0

P1	.169	.019	.219	.169																
P2	.011			.061	.011															
P3	.505				.455	.555	.505													
P4	.446						.396	.496	.446											
P5	.889								.839	.889										
P6	.05																			
P7	.887									.837	.887									
P8	.05																			
P9	.889										.839	.889								
P10	.05																			
P11	.887											.837								
P12	.05																			
T1	111	112	111	113	112	111	112	111	113		115	114								
T2	190								166	196	189	190								
T3	215	216	215								192	229								

TABLE LVI

SENSITIVITY CHECK; PARAMETER VARIATION = .05

RUN # L.4 to L.5

INFRARED FLUX = 13.485
SOLAR FLUX = 9.344

Q1 = .341
Q2 = 0.0
Q3 = 0.0

P1	.1475	.0975	.1975	.1475																
P2	.012			.062	.012															
P3	.5535				.5035	.6035	.5535													
P4	.373						.346	.446	.396											
P5	.889								.839	.889										
P6	.05																			
P7	.887									.837	.887									
P8	.05																			
P9	.889										.839	.889								
P10	.05																			
P11	.887											.837								
P12	.05																			
T1	133			135	133				134	133	135	134								
T2	191	192	191	192	191				169	197	191	192								
T3	216								215	216	192	229								

TABLE LVII

SENSITIVITY CHECK; PARAMETER VARIATION = .05

RUN # L.1 to L.3

INFRARED FLUX = 13.485
SOLAR FLUX = 9.344

Q1 = 3.41
Q2 = 0.0
Q3 = 0.0

P1	.093	.043	.143	.093																
P2	.0107			.0607	.0107															
P3	.196				.146	.246	.196													
P4	.373						.323	.423	.373											
P5	.889								.839	.889										
P6	.05																			
P7	.887									.837	.887									
P8	.05																			
P9	.889										.839	.889								
P10	.05																			
P11	.887											.837								
P12	.05																			
T1	204			208	204				205	204	205	204								
T2	202								182	207	201	202								
T3	220										198	232								

TABLE LVIII

SENSITIVITY CHECK; PARAMETER VARIATION = .05

RUN # L.9 to L.10

INFRARED FLUX = 13.485
SOLAR FLUX = 9.344

Q1 = 0.0
Q2 = .341
Q3 = 0.0

P1	.1645	.1145	.2145	.1645																
P2	.011			.061	.011															
P3	.503				.453	.553	.503													
P4	.448						.398	.498	.448											
P5	.889								.839	.889										
P6	.05																			
P7	.887									.837	.887									
P8	.05																			
P9	.889										.839	.889								
P10	.05																			
P11	.887											.837								
P12	.05																			
T1	121			122							124	123								
T2	237	238	237	238	237				201	241	237	238								
T3	217										194	230								

TABLE LVIX

SENSITIVITY CHECK; PARAMETER VARIATION = .05

RUN # L.11 to L.12

INFRARED FLUX = 13.485
SOLAR FLUX = 9.344

Q1 = 0.0
Q2 = 3.41
Q3 = 0.0

P1	.172	.122	.222	.172																
P2	.011			.061	.011															
P3	.446				.396	.496	.446													
P4	.433						.383	.483	.433											
P5	.889								.839	.889										
P6	.05																			
P7	.887									.837	.887									
P8	.05																			
P9	.889										.839	.889								
P10	.05																			
P11	.887											.837								
P12	.05																			
T1	165	166	165	166	165				166											
T2	383		382	383					313	383										
T3	228								227	229	206	239								

TABLE LX

SENSITIVITY CHECK; PARAMETER VARIATION = .05

RUN # L.13 to L.14

INFRARED FLUX = 13.485
SOLAR FLUX = 9.344

Q1 = 0.0
Q2 = 0.0
Q3 = .341

P1	.162	.112	.212	.162																
P2	.011			.061	.011															
P3	.496				.446	.546	.496													
P4	.449						.399	.499	.449											
P5	.889								.839	.889										
P6	.05																			
P7	.887									.837	.887									
P8	.05																			
P9	.889										.839	.889								
P10	.05																			
P11	.887											.837								
P12	.05																			
T1	114	115	114	115	114				116	115	117	116								
T2	191								168	197	190	192								
T3	232	233							232	233	203	243								

TABLE LXI

SENSITIVITY CHECK; PARAMETER VARIATION = .05

RUN # L.15

INFRARED FLUX = 13.485
SOLAR FLUX = 9.344

Q1 = 0.0
Q2 = 0.0
Q3 = 3.41

P1	.168	.118	.218	.168																
P2	.011			.061	.011															
P3	.496				.446	.546	.496													
P4	.446						.496	.396	.446											
P5	.889								.839	.889										
P6	.05																			
P7	.887									.837	.887									
P8	.05																			
P9	.889										.839	.889								
P10	.05																			
P11	.887											.837								
P12	.05																			
T1	133	134	133	134	133				135	134	135									
T2	199	200							178	205	199	200								
T3	316										263	321								

TABLE LXII

SENSITIVITY CHECK; FINAL ANALYSIS MODEL, SERIES "M"

RUN # M.1

INFRARED FLUX = 13.485
SOLAR FLUX = 9.344

Q1 = 0.0
Q2 = 0.0
Q3 = 0.0

P1	.245	.195	.145	.245																
P2	.001	.051	.101	.001																
P3	.481			.431	.531	.481														
P4	.471			.521	.421	.471														
P5	.889					.839	.789	.889												
P6	.05					.100	.150	.050												
P7	.887							.837	.787	.887										
P8	.05							.100	.150	.050										
P9	.889									.839	.789	.889								
P10	.05									.100	.150	.050								
P11	.887											.837								
P12	.05											.100								
T1	111	112	113	111		112	113	111		113	115	111								
T2	190					202	207	189	190											
T3	216	215				216	215			231	237	215								

TABLE LXIII

SENSITIVITY CHECK; FINAL ANALYSIS MODEL, SERIES "M"

RUN # M.2

INFRARED FLUX = 13.485
SOLAR FLUX = 9.344

Q1 = .341
Q2 = 0.0
Q3 = 0.0

P1	.245	.195	.145	.245																
P2	.001	.051	.101	.001																
P3	.481			.431	.531	.481														
P4	.471			.521	.421	.471														
P5	.889					.839	.789	.889												
P6	.05					.100	.150	.050												
P7	.887							.837	.787	.887										
P8	.05							.100	.150	.050										
P9	.889									.839	.789	.889								
P10	.05									.100	.150	.050								
P11	.887											.837								
P12	.05											.100								
T1	132	134	136	132		133		132		133	134	132								
T2	191					203	208	191		192		191								
T3	216								215	231	237	216								

TABLE LXIV

SENSITIVITY CHECK; FINAL ANALYSIS MODEL, SERIES "M"

RUN # M.3

INFRARED FLUX = 13.485
SOLAR FLUX = 9.344

Q1 = 3.41
Q2 = 0.0
Q3 = 0.0

P1	.245	.195	.145	.245																
P2	.001	.051	.101	.001																
P3	.481			.431	.531	.481														
P4	.471			.521	.421	.471														
P5	.889					.839	.789	.889												
P6	.05					.100	.150	.050												
P7	.887							.837	.787	.887										
P8	.05							.100	.150	.050										
P9	.889									.839	.789	.889								
P10	.05									.100	.150	.050								
P11	.887											.837								
P12	.05											.100								
T1	203	208	212	203		204		203			204	203								
T2	200	202		201		212	217	201		202		201								
T3	220							219		234	240	220								

TABLE LXV

SENSITIVITY CHECK; FINAL ANALYSIS MODEL, SERIES "M"

RUN # M.4

INFRARED FLUX = 13.485
SOLAR FLUX = 9.344

Q1 = 0.0
Q2 = .341
Q3 = 0.0

P1	.245	.195	.145	.245																
P2	.001	.051	.101	.001																
P3	.481			.431	.531	.481														
P4	.471			.521	.421	.471														
P5	.889					.839	.789	.889												
P6	.05					.100	.150	.050												
P7	.887							.837	.787	.887										
P8	.05							.100	.150	.050										
P9	.889									.839	.789	.889								
P10	.05									.100	.150	.050								
P11	.887											.837								
P12	.05											.100								
T1	121	122	123	121			122	121		122	123	121								
T2	237		238	237		254	261	237		238		237								
T3	217					218		217		233	239	217								

TABLE LXVI

SENSITIVITY CHECK; FINAL ANALYSIS MODEL, SERIES "M"

RUN # M.5

INFRARED FLUX = 13.485
SOLAR FLUX = 9.344

Q1 = 0.0
Q2 = 3.41
Q3 = 0.0

P1	.245	.195	.145	.245																
P2	.001	.051	.101	.001																
P3	.481			.431	.531	.481														
P4	.471			.521	.421	.471														
P5	.889					.839	.789	.889												
P6	.05					.100	.150	.050												
P7	.887							.837	.787	.887										
P8	.05							.100	.150	.050										
P9	.889									.839	.789	.889								
P10	.05									.100	.150	.050								
P11	.887											.837								
P12	.05											.100								
T1	165	166		165		166		165			166	165								
T2	382	383		382		411	424	382		383		382								
T3	228					229		228		243	248	228								

TABLE LXVII

SENSITIVITY CHECK; FINAL ANALYSIS MODEL, SERIES "M"

RUN # M.6

INFRARED FLUX = 13.485
SOLAR FLUX = 9.344

Q1 = 0.0
Q2 = 0.0
Q3 = .341

P1	.245	.195	.145	.245																
P2	.001	.051	.101	.001																
P3	.481			.431	.531	.481														
P4	.471			.521	.421	.471														
P5	.889					.839	.789	.889												
P6	.05					.100	.150	.050												
P7	.887							.837	.787	.887										
P8	.05							.100	.150	.050										
P9	.889									.839	.789	.889								
P10	.05									.100	.150	.050								
P11	.887											.837								
P12	.05											.100								
T1	114	115	116	114		115	116	114		115	117	114								
T2	191					203	208	191				191								
T3	233							232		250	256	233								

TABLE LXVIII

SENSITIVITY CHECK; FINAL ANALYSIS MODEL, SERIES "M"

RUN # M.7

INFRARED FLUX = 13.485
SOLAR FLUX = 9.344

Q1 = 0.0
Q2 = 0.0
Q3 = 3.41

P1	.245	.195	.145	.245																
P2	.001	.051	.101	.001																
P3	.481			.431	.531	.481														
P4	.471			.521	.421	.471														
P5	.889					.839	.789	.889												
P6	.05					.100	.150	.050												
P7	.887							.837	.787	.887										
P8	.05							.100	.150	.050										
P9	.889									.839	.789	.889								
P10	.05									.100	.150	.050								
P11	.887											.837								
P12	.05											.100								
T1	133	134	135	133		134	135	133		134	135	133								
T2	198	200				211	217	200		201		200								
T3	316									340	348	316								

TABLE LXIX

SENSITIVITY CHECK; FINAL ANALYSIS MODEL, SERIES "M"

RUN # M.8

INFRARED FLUX = 11.145
SOLAR FLUX = .001

Q1 = 0.0
Q2 = 0.0
Q3 = 0.0

P1	.245	.195	.145	.245																
P2	.001	.051	.101	.001																
P3	.481			.431	.531	.481														
P4	.471			.521	.421	.471														
P5	.889					.839	.789	.889												
P6	.05					.100	.150	.050												
P7	.887							.837	.787	.887										
P8	.05							.100	.150	.050										
P9	.889									.839	.789	.889								
P10	.05									.100	.150	.050								
P11	.887											.837								
P12	.05											.100								
T1	105	106	108	105		106	107	105		107	109	105								
T2	177		178	177		188	193	177		178		177								
T3	189									202	207	189								

TABLE LXX

SENSITIVITY CHECK; FINAL ANALYSIS MODEL, SERIES "M"

RUN # M.9

INFRARED FLUX = 11.145
SOLAR FLUX = .001

Q1 = .341
Q2 = 0.0
Q3 = 0.0

P1	.245	.195	.145	.245																
P2	.001	.051	.101	.001																
P3	.481			.431	.531	.481														
P4	.471			.521	.421	.471														
P5	.889					.839	.789	.889												
P6	.05					.100	.150	.050												
P7	.887							.837	.787	.887										
P8	.05							.100	.150	.050										
P9	.889									.839	.789	.889								
P10	.05									.100	.150	.050								
P11	.887											.837								
P12	.05											.100								
T1	129	131	133	129			130	129		130	131	129								
T2	179	180				190	195	180												
T3	189									202	208	189								

TABLE LXXI

SENSITIVITY CHECK; FINAL ANALYSIS MODEL, SERIES "M"

RUN # M.10

INFRARED FLUX = 11.145
SOLAR FLUX = .001

Q1 = 3.41
Q2 = 0.0
Q3 = 0.0

P1	.245	.195	.145	.245																
P2	.001	.051	.101	.001																
P3	.481			.431	.531	.481														
P4	.471			.521	.421	.471														
P5	.889					.839	.789	.889												
P6	.05					.100	.150	.050												
P7	.887							.837	.787	.887										
P8	.05							.100	.150	.050										
P9	.889									.839	.789	.889								
P10	.05									.100	.150	.050								
P11	.887											.837								
P12	.05											.100								
T1	202	207	211	202		203		202			203	202								
T2	191	192		191		201	206	191		192		191								
T3	195									207	212	195								

TABLE LXXII

SENSITIVITY CHECK; FINAL ANALYSIS MODEL, SERIES "M"

RUN # M.11

INFRARED FLUX = 11.145
SOLAR FLUX = .001

Q1 = 0.0
Q2 = .341
Q3 = 0.0

P1	.245	.195	.145	.245																
P2	.001	.051	.101	.001																
P3	.481			.431	.531	.481														
P4	.471			.521	.421	.471														
P5	.889					.839	.789	.889												
P6	.05					.100	.150	.050												
P7	.887							.837	.787	.887										
P8	.05							.100	.150	.050										
P9	.889									.839	.789	.889								
P10	.05									.100	.150	.050								
P11	.887											.837								
P12	.05											.100								
T1	116	117	119	116		117	118	116		117	119	116								
T2	231					247	254	231												
T3	192									205	210	192								

TABLE LXXIII

SENSITIVITY CHECK; FINAL ANALYSIS MODEL, SERIES "M"

RUN # M.12

INFRARED FLUX = 11.145
SOLAR FLUX = .001

Q1 = 0.0
Q2 = 3.41
Q3 = 0.0

P1	.245	.195	.145	.245																
P2	.001	.051	.101	.001																
P3	.481			.431	.531	.481														
P4	.471			.521	.421	.471														
P5	.889					.839	.789	.889												
P6	.05					.100	.150	.050												
P7	.887							.837	.787	.887										
P8	.05							.100	.150	.050										
P9	.889									.839	.789	.889								
P10	.05									.100	.150	.050								
P11	.887											.837								
P12	.05											.100								
T1	163	164	165	163		164	165	163			164	163								
T2	381					410	422	381												
T3	207						208	207		219	223	207								

TABLE LXXIV

SENSITIVITY CHECK; FINAL ANALYSIS MODEL, SERIES "M"

RUN # M.13

INFRARED FLUX = 11.145
SOLAR FLUX = .001

Q1 = 0.0
Q2 = 0.0
Q3 = .341

P1	.245	.195	.145	.245																
P2	.001	.051	.101	.001																
P3	.481			.431	.531	.481														
P4	.471			.521	.421	.471														
P5	.889					.839	.789	.889												
P6	.05					.100	.150	.050												
P7	.887							.837	.787	.887										
P8	.05							.100	.150	.050										
P9	.889									.839	.789	.889								
P10	.05									.100	.150	.050								
P11	.887											.837								
P12	.05											.100								
T1	108	110	111	108		109	110	108		110	112	108								
T2	178	179	180	179		191	195	179		180		179								
T3	212									228	233	212								

TABLE LXXV

SENSITIVITY CHECK; FINAL ANALYSIS MODEL, SERIES "M"

RUN # M.14

INFRARED FLUX = 11.145
SOLAR FLUX = .001

Q1 = 0.0
Q2 = 0.0
Q3 = 3.41

P1	.245	.195	.145	.245																
P2	.001	.051	.101	.001																
P3	.481			.431	.531	.481														
P4	.471			.521	.421	.471														
P5	.889					.839	.789	.889												
P6	.05					.100	.150	.050												
P7	.887							.837	.787	.887										
P8	.05							.100	.150	.050										
P9	.889									.839	.789	.889								
P10	.05									.100	.150	.050								
P11	.887											.837								
P12	.05											.100								
T1	130	131		130		131		130		131	132	130								
T2	189	190				201	206	190		191	192	190								
T3	309									332	339	309								

TABLE LXXVI

SENSITIVITY CHECK; FINAL ANALYSIS MODEL, SERIES "M"

RUN # M.15

INFRARED FLUX = 28.536
SOLAR FLUX = 15.310

Q1 = 0.0
Q2 = 0.0
Q3 = 0.0

P1	.245	.195	.145	.245																
P2	.001	.051	.101	.001																
P3	.481			.431	.531	.481														
P4	.471			.521	.421	.471														
P5	.889					.839	.789	.889												
P6	.05					.100	.150	.050												
P7	.887							.837	.787	.887										
P8	.05							.100	.150	.050										
P9	.889									.839	.789	.889								
P10	.05									.100	.150	.050								
P11	.887											.837								
P12	.05											.100								
T1	120	121	122	120		121	122	120		121	123	120								
T2	207	208				221	227	208			209	208								
T3	250								249	267	274	250								

TABLE LXXVII

SENSITIVITY CHECK; FINAL ANALYSIS MODEL, SERIES "M"

RUN # M.16

INFRARED FLUX = 28.536
SOLAR FLUX = 15.310

Q1 = .341
Q2 = 0.0
Q3 = 0.0

P1	.245	.195	.145	.245																	
P2	.001	.051	.101	.001																	
P3	.481			.431	.531	.481															
P4	.471			.521	.421	.471															
P5	.889					.839	.789	.889													
P6	.05					.100	.150	.050													
P7	.887							.837	.787	.887											
P8	.05							.100	.150	.050											
P9	.889									.839	.789	.889									
P10	.05									.100	.150	.050									
P11	.887											.837									
P12	.05											.100									
T1	138	140	142	138			139	138		139	140	138									
T2	208	209				222	229	209			210	209									
T3	250							249		268	275	250									

TABLE LXXVIII

SENSITIVITY CHECK; FINAL ANALYSIS MODEL, SERIES "M"

RUN # M.17

INFRARED FLUX = 28.536
SOLAR FLUX = 15.310

Q1 = 3.41
Q2 = 0.0
Q3 = 0.0

P1	.245	.195	.145	.245																
P2	.001	.051	.101	.001																
P3	.481			.431	.531	.481														
P4	.471			.521	.421	.471														
P5	.889					.839	.789	.889												
P6	.05					.100	.150	.050												
P7	.887							.837	.787	.887										
P8	.05							.100	.150	.050										
P9	.889									.839	.789	.889								
P10	.05									.100	.150	.050								
P11	.887											.837								
P12	.05											.100								
T1	205	209	213	205			206	205		205	206	205								
T2	217		218	217		230	236	217		218		217								
T3	252									270	276	252								

TABLE LXXIX

SENSITIVITY CHECK; FINAL ANALYSIS MODEL, SERIES "M"

RUN # M.18

INFRARED FLUX = 28.536
SOLAR FLUX = 15.310

Q1 = 0.0
Q2 = .341
Q3 = 0.0

P1	.245	.195	.145	.245																
P2	.001	.051	.101	.001																
P3	.481			.431	.531	.481														
P4	.471			.521	.421	.471														
P5	.889					.839	.789	.889												
P6	.05					.100	.150	.050												
P7	.887							.837	.787	.887										
P8	.05							.100	.150	.050										
P9	.889									.839	.789	.889								
P10	.05									.100	.150	.050								
P11	.887											.837								
P12	.05											.100								
T1	128	129	130	128		129	130	128		129	130	128								
T2	248					265	273	248		248	249	248								
T3	251							250		269	275	251								

TABLE LXXX

SENSITIVITY CHECK; FINAL ANALYSIS MODEL, SERIES "M"

RUN # M.19

INFRARED FLUX = 28.536
SOLAR FLUX = 15.310

Q1 = 0.0
Q2 = 3.41
Q3 = 0.0

P1	.245	.195	.145	.245																
P2	.001	.051	.101	.001																
P3	.481			.431	.531	.481														
P4	.471			.521	.421	.471														
P5	.889					.839	.789	.889												
P6	.05					.100	.150	.050												
P7	.887							.837	.787	.887										
P8	.05							.100	.150	.050										
P9	.889									.839	.789	.889								
P10	.05									.100	.150	.050								
P11	.887											.837								
P12	.05											.100								
T1	168	169				169		168			169	168								
T2	385		386			414	427	385												
T3	258			259	258		259	258	257	276	282	258								

TABLE LXXXI

SENSITIVITY CHECK; FINAL ANALYSIS MODEL, SERIES "M"

RUN # M.20

INFRARED FLUX = 28.536
SOLAR FLUX = 15.310

Q1 = 0.0
Q2 = 0.0
Q3 = .341

P1	.245	.195	.145	.245																
P2	.001	.051	.101	.001																
P3	.481			.431	.531	.481														
P4	.471			.521	.421	.471														
P5	.889					.839	.789	.889												
P6	.05					.100	.150	.050												
P7	.887							.837	.787	.887										
P8	.05							.100	.150	.050										
P9	.889									.839	.789	.889								
P10	.05									.100	.150	.050								
P11	.887											.837								
P12	.05											.100								
T1	122	123	124	122		123	124	122		124	125	122								
T2	208	209				222	228	209			210	209								
T3	261									281	287	261								

TABLE LXXXII

SENSITIVITY CHECK; FINAL ANALYSIS MODEL, SERIES "M"

RUN # M.21

INFRARED FLUX = 28.536
SOLAR FLUX = 15.310

Q1 = 0.0
Q2 = 0.0
Q3 = 3.41

P1	.245	.195	.145	.245																
P2	.001	.051	.101	.001																
P3	.481			.431	.531	.481														
P4	.471			.521	.421	.471														
P5	.889					.839	.789	.889												
P6	.05					.100	.150	.050												
P7	.887							.837	.787	.887										
P8	.05							.100	.150	.050										
P9	.889									.839	.789	.889								
P10	.05									.100	.150	.050								
P11	.887											.837								
P12	.05											.100								
T1	139		140	139			140	139		140	141	139								
T2	215			216		229	234	216			217	215								
T3	329						330	329		354	362	329								

VITA

Victor John Anselmo

Candidate for the Degree of

Doctor of Philosophy

Thesis: AN OPTIMUM RADIATION CRYOSTAT FOR INFRARED DETECTOR COOLING ON EARTH ORBITING SATELLITES

Major Field: Engineering

Biographical:

Personal Data: Born in Brooklyn, New York, August 21, 1940, the son of Peter J. and Helen T. Anselmo.

Education: Graduated from the University of Maryland with a Bachelor of Science degree in Aeronautical Engineering in 1963; graduated from Southern Methodist University with a Master of Science degree in Engineering in 1966; completed requirements for the Doctor of Philosophy degree in Mechanical Engineering, May, 1971.

Professional Experience: Employed by General Dynamics in Fort Worth, Texas, as an Aerothermodynamics engineer from 1963 to 1966; employed as a full-time consultant to Bendix Aerospace Systems in Ann Arbor, Michigan, and to Ball Brothers Research Corporation in Boulder, Colorado, from 1966 to 1967; employed by Oklahoma State University as a Research Associate from 1967 to 1970; presently employed as Senior Engineer at the California Institute of Technology Jet Propulsion Laboratory in Pasadena, California.